An Oxygen Reduction Reaction Kinetic Model for Proton Exchange Membrane Fuel Cells Based on Free Energies of Activation and Adsorption

by

Elena Ezquerra Silva

A thesis submitted in partial fulfillment of the requirements for the degree of

Master of Science

Department of Mechanical Engineering

University of Alberta

Abstract

Polymer electrolyte membrane fuel cells (PEMFCs) are a promising alternative technology to internal combustion engines used on vehicles. However, improvements on durability and performance are needed in order to boost the commercialization of this technology. The oxygen reduction reaction (ORR) is the greatest source of voltage losses, and several studies have identified that the catalyst degradation on the cathode is the main contributor to the loss of electrochemical surface area (ECSA). Therefore, understanding degradation pathways in the ORR kinetics and the activity of the catalyst layer (CL) are a priority for improving the performance and durability of PEMFC.

Three well-known phenomena occur in the oxygen electrochemistry on platinum catalyst: i) oxygen reduction reaction (ORR), ii) platinum oxide growth and iii) peroxide formation. Many of the elementary steps are common to the three reaction pathways, even though, the kinetics of these mechanisms are usually modelled separately. This MSc thesis first analyzes and studies novel unified micro kinetic models on ORR available in the literature. Then, it derives and implements a new ORR kinetic model that depends only on the activation and adsorption energies. Kinetic parameters were estimated by fitting the model to Pt electrode experimental data. Comparison between experimental data and proposed model as well as other models show that the model is able to capture key steady state characteristics of the ORR, and some transient trends.

Keywords: Oxygen reduction reaction (ORR), Kinetic model, Proton exchange membrane fuel cells (PEMFCs)

Dedicated to my family

Acknowledgements

Table of Contents

List of Tables

List of Figures

Nomenclature

Constants

F Faraday constant, ≈ 96485 C/mol

j^* reference pre-factor

R universal gas constant, ≈ 8.314 J/(mol·K)

Greek Letters

α charge-transfer coefficient

β symmetry factor

ΔG^{0*} Gibbs free energy of activation

ΔG^0 Gibbs free energy of adsorption

η overpotential, $\eta = E - E^0$, V

ω Temkin term

θ coverage fraction

Latin

a activity

A' reaction dependent pre-exponential factor

b Tafel slope, V

C concentration

E cell voltage, V

E^0 theoretical equilibrium potential, V

i current density

i_0 exchange current density

j individual current density

k reaction rate constant, m/s

M molar mass, g/mol

T temperature, K

t time, s

Subscripts and Superscripts

AA   associative adsorption

DA   dissociative adsorption

DT   dissociative transition

e^- electron

H^+ hydrogen proton

H_2 hydrogen

H_2O water

H_2O_2 peroxide

O_2 oxygen

RA   reductive adsorption

RD   reductive desorption

RT   reductive transition

SUB   subsurface place exchange

$OPt_{(sub)}$ subsurface exchange species

$OPtO_{(sub)}$ subsurface adsorbed species O_{ex}

$OPtOH_{(sub)}$ subsurface adsorbed species OH_{ex}

$PtO_2H_{(ads)}$ adsorbed specie O_2H

$PtO_{(ads)}$ adsorbed specie O

$PtOH_{(ads)}$ adsorbed specie OH

RD_{ex} reductive desorption place exchange

RT_{ex} reductive transition place exchange

Chapter 1

Introduction

1.1 Motivation

Growing concerns over the negative impacts of climate change are forcing governments world-wide to set targets for reducing green house gas (GHG) emissions. In the Paris Agreement, many countries committed to reduce by 50 % their GHGs by 2030 and achieve net zero emissions by 2050 [6]. Transitioning to a net zero world means completely transforming the way humankind produces, consumes and moves energy. since the energy sector is responsible of most of the GHG emissions emitted today.

The development of technologies that allow the production and consumption of clean energy and the wide implementation of sustainable energy pathways are crucial for achieving a net zero future. Among these technologies and energy pathways, hydrogen is a promising alternative to the current fossil fuels. Hydrogen is a very convenient energy carrier given that it has a high energy density, is easy to storage and can be produced from several sources [7]. Hydrogen fuel cells are a clean alternative to internal combustion engines for heavy-duty and mid-range automotive applications. In a hydrogen proton exchange membrane (PEM) fuel cell, the hydrogen and oxygen chemical energy is converted to electric power through an electrochemical reaction. This electric current can feed an electric motor, or be stored in batteries. The only by product of the reaction is water vapour [3] and there are no GHG emissions.

Battery electric vehicles (BEVs) are another zero-emission alternative to the internal combustion engine vehicles (ICEVs). Both BEVs and hydrogen fuel cell electric vehicles (HFCEVs) have advantages and disadvantages. According to the IEA, the average driving range of a small EVs in 2019 was 336 km [8], while the average driving range of a HFCEV in 2017 was 643 km, according to the DOE. The driving range of a fuel cell vehicle doubles

the driving range of a battery vehicle and is similar to the driving range of a internal combustion engine vehicle [9]. In addition, refuelling a hydrogen tank takes only 5-10 minutes while recharging a battery can take several hours [10]. In terms of efficiency, however, BEVs are more efficient, even though the well-to-wheel efficiency depends on the energy pathway used to produce the electricity or hydrogen [11]. The cost of HFCEVs is however still higher than BEVs, a Toyota Mirai 2022 estimated cost is approx. $50,000 while EVs range between $30,000 - $40,000. Overall, it is likely that FCEVs will dominate the heavy-duty and long range vehicle market while small and medium range vehicles will be BEV.

HFCEVs are however still an expensive alternative to ICEVs. The power generation source in the vehicle, i.e., the fuel cell stack, needs more development in order to reduce its cost and increase its efficiency and durability. The main source of energy losses occurs during the oxygen reduction reaction (ORR), which requires a strong catalytic agent to take place, such as, platinum catalysts. The greatest cost contributor to the fuel cell stack is the membrane electrode assembly (MEA), and inside of it the most expensive component is the platinum catalyst, which could represent up to 41% of the total FC stack mass production, i.e., 500,000 units/year cost [12]. The degradation in PEMFCs is typically dominated by the degradation of the membrane due to various mechanisms depending on the operating conditions [13]. Among these mechanisms we can find the oxygen reduction reaction (ORR), the oxide growth and the peroxide formation. By studying these mechanisms, a better understanding of the complex platinum dissolution in PEMFCs can be achieved [14].

Therefore, optimization of utilization and lifetime of the expensive platinum catalyst used in PEM fuel cells are crucial research areas for making this technology achieve full scale commercialization as an alternative to internal combustion engines. Based on all of this, this work is focused on understanding the kinetics of the oxygen reduction reaction on Pt catalyst used in PEMFCs.

The overall objective of this thesis is to understand the reaction kinetics of the ORR in PEMFCs and propose a new numerical model capable of predicting steady and transient results of the performance at different operating conditions. The reason why this work uses numerical modelling tools is because of the multi-step, multi-species nature of the ORR which necessitates of complex models to understand the interaction between species and electrical potentials. The developed ORR kinetic model can then be used to estimate the performance of fuel cells thereby decreasing the design-cycle needed to produce cost-effective and durable stacks.

1.2 Fuel cell background

William Grove discovered the operating principle of a fuel cell in 1839 [15]. A fuel cell is an electrochemical device that converts the chemical energy of hydrogen or another fuel to electrical energy and heat in a clean and efficient way [12].

Unlike batteries, the energy supply in a fuel cell is external and can be replenished by re-fueling the external tank, the same as in an internal combustion engine. Generally, fuel cells use gaseous or liquid fuels, such a natural gas, methanol. Hydrogen fuel cells uses hydrogen as fuel and oxygen in air as oxidant [16]. In comparison to heat engines, the energy conversion in fuel cells is direct and simple and it is not limited by the thermodynamic Carnot efficiency.

Fuel cells are a promising technology for the transportation, power generation and energy storage sectors because of their high energy density and efficiency and low environmental impact [3]. They can be used in very small devices producing only a few watts of electricity, or in large power plants producing megawatts. Fuel cells are classified according to the electrolyte, fuel and reactant they use [15]. In this work, the fuel cell type under study is the hydrogen proton exchange membrane fuel cell (PEMFC).

1.2.1 PEM Fuel Cells

Proton exchange membrane fuel cells (PEMFCs) are electrochemical devices capable of converting directly the chemical energy of hydrogen and oxygen molecules into electricity. They operate using hydrogen as fuel at low temperatures and, they can continuously power an electric motor producing only water and heat. The overall electrochemical reaction that takes place in this device is the following:

$$O_2 + 2\,H_2 \rightleftharpoons 2\,H_2O \tag{1.1}$$

By splitting this process into two half cell electrochemical reactions, the electrons produced can be extracted. These two reactions are the hydrogen oxidation reaction (HOR) and the oxygen reduction reaction (ORR). On the anode, the HOR takes place where the hydrogen is the reactant that is oxidized and releases hydrogen protons and electrons,

$$2\,H_2 \rightleftharpoons 4\,H^+ + 4\,e^- \tag{1.2}$$
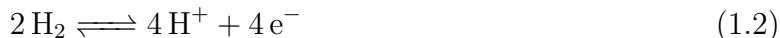
On the other cathode, the ORR takes place where oxygen is reduced to form water,

$$O_2 + 4\,H^+ + 4\,e^- \rightleftharpoons 2\,H_2O \tag{1.3}$$

For ensuring a favorable scenario where this reaction can take place, the following conditions need to be met:

1. the reactants, i.e. the hydrogen and oxygen, need to reach the reaction sites in the anode and cathode, respectively.

2. the protons and electrons released from the HOR need to be able to travel from the anode to the cathode, so that the ORR can take place.

3. the water produced from this reaction needs to be removed from the system, or else it will flood the electrodes and the mass transport of reactants will be hampered.

Figure 1.1 shows an schematic representation of the structure of a PEM fuel cell. This device is composed of layers that work together to officially transport reactants and products. Each individual layer plays different roles in the performance of the cell.
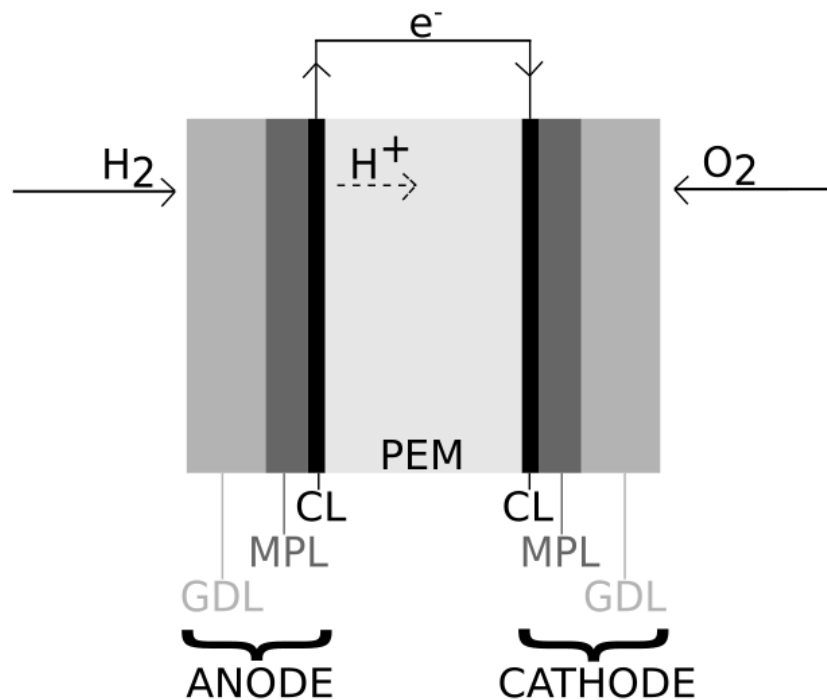
Figure 1.1 – Basic schematic representation of a PEM fuel cell.

The catalyst layer (CL) in a PEMFC is where the catalyst particles are located, therefore where the reactions take place. The fuel cell has two catalyst layers, the anode and cathode CLs where both half cell reactions occur separately. These layers transport the reactants, electrons and protons through their respective phases inside porous composite media to

available reaction sites. Usually these layers are made of platinum nanoparticles that are supported by carbon for a higher surface layer and an ion-conducting polymer, called Nafion.

Both electrodes are separated by a polymer electrolyte membrane (PEM), an impermeable layer that only allows the transport of protons and prevents the reactants from crossing from anode to cathode or vice-versa. It also prevents the electrons from passing through the membrane, therefore they have to travel through an external circuit, and that electron current produced can be used in a load.

The micro-porous layer (MPL) is a hydrophobic porous material that is electronically conductive. The main function of this layer is to remove the produced water from the reactions that take place in the catalyst layer. The gas diffusion layer (GDL), which is usually made of carbon fibers, is in charge of diffusing the reactant gases, facilitating the supply of reactants to the CLs. All these layers assembled together compose the membrane electrode assembly (MEA) of a PEMFC.

This work is focused in studying the ORR that takes place in the cathode catalyst layer (CCL) for the following reasons:

- the reaction mechanism and the intermediate species formed in the CCL are not yet fully understood [17, 18].

- the major performance losses in a PEMFC are attributed to the cathode [19, 20].

- understanding the Pt degradation in the cathode is crucial for improving the durability of PEMFC [21].

- reducing the Pt loading in the catalyst and optimizing its usage is essential for reducing the production cost of the fuel cells [12].

1.2.2 Catalyst layer performance

The performance of a PEMFC is usually evaluated using a steady state polarization curve as shown in Figure 1.2. The cell potential decreases when current generation increases due to several reversible and irreversible losses. At open cell voltage, hydrogen crosses the membrane and reacts in the cathode reducing the open circuit voltage of the cell. At low current density, the cell voltage is reduced due to activation losses, i.e., voltage losses necessary to drive the electrochemical reaction forward, mainly the slow ORR kinetics. Then, at medium current densities, ohmic losses occur due to the finite conductivity of the electrolyte. Finally,

at high current densities, the mass transport losses limit the amount of reactant that can be consumed.
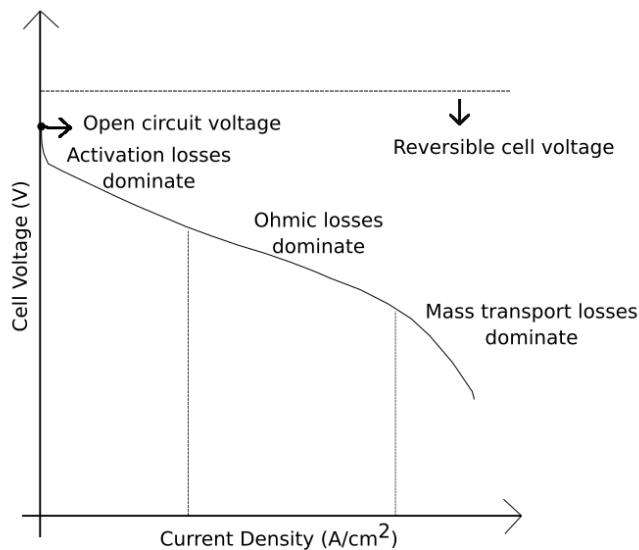
Figure 1.2 – Typical steady state polarization curve.

For improving the overall performance of a fuel cell, specific areas of the operation of a cell need to be assessed for addressing certain type of losses. In the past years, many researchers have been trying to identify experimentally which factors affect mostly the performance of a cell [22, 23], and some of them have been developing modeling tools that analyze changes in the PEM polarization response to determine if the performance degradation was related to transport or kinetic losses [24]. Given that the major losses in a fuel cell are attributed to the kinetic losses [25], and by understanding the activation losses, the catalyst use can be reduced [26], this work is focused on studying the ORR kinetics of PEMFCs.

Another significant area for improvement in the development of PEMFCs is the durability. The lifetime of the proton exchange membrane fuel cell is directly related to the durability of some of its components, i.e., catalyst layers, and one of the major aspects that affects the durability of the cell is the catalytic decay [27]. Over the past years, several mechanisms that contribute to the cathode catalytic decay have been proposed, among these are the catalyst particle sintering, the Pt dissolution and the cathode support corrosion [28]. Darling and Meyers proposed a kinetic model of platinum dissolution in PEMFCs and they considered three electrochemical reactions: platinum dissolution, platinum oxide film formation and chemical dissolution of platinum oxide [29]. That is why an important aspect of the catalyst performance that is under study is the oxide film formation and reduction. This phenomena

6

is studied experimentally during cyclic voltammetry (CV) tests in absence of oxygen [3]. This CV technique sweeps back and forth the potential between maximum and minimum voltage limits while recording the current [30]. The voltage sweep is ramped linearly with time and the plot of the current versus voltage is called a cyclic voltammogram as shown in Figure 1.3.
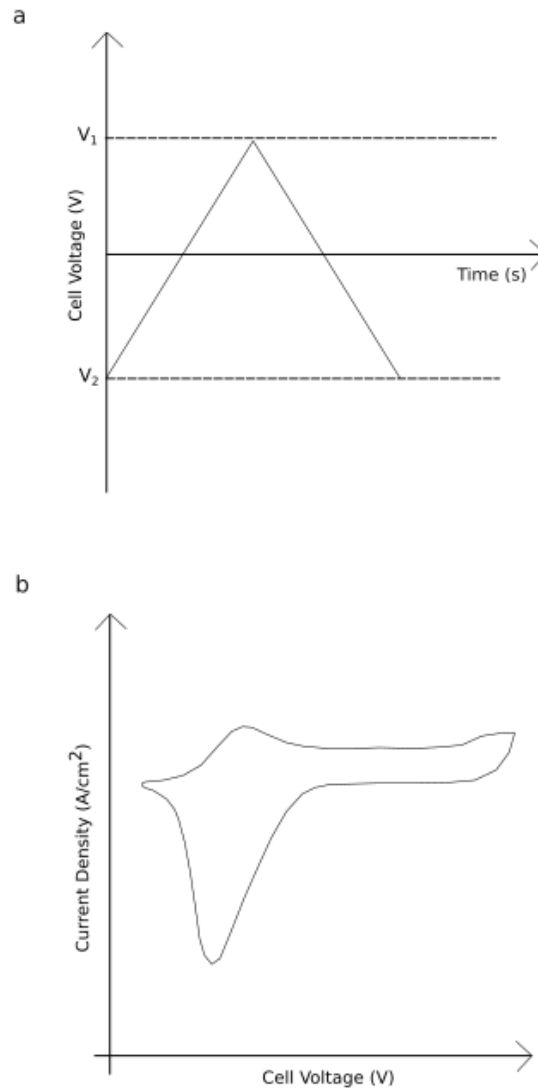
Figure 1.3 – (a) Schematic of voltage sweep; (b) typical cyclic voltammogram (extracted from O'Hayre et al. [3]).

1.2.3 Electrochemical reactions

This section has been cited from the lecture notes from Dr. Marc Secanell's course MEC E 645 - Transport and Kinetic Processes in Electrochemical Systems, taught at the University of Alberta.

For a reaction to occur the reacting molecules must meet three conditions:

1. Collide with one another.

2. Collide with one another with sufficient energy.

3. Collide in an orientation that can lead to rearrangements of the atoms.

Based on these arguments, the rate constants, k, of most solution-phase reactions follow Arrhenius equation:

$$k = A' \exp \left(-\frac{\triangle G}{RT} \right) \tag{1.4}$$

where $\triangle G$ is known as the standard free energy of activation, and A' is a reaction dependent pre-exponential factor.

One electron transfer reaction

The simplest possible electrode process considered is when a oxidant species O is reduced to species R: $O + e^- \underset{k_b}{\overset{k_f}{\rightleftharpoons}} R$.

If a potential lower than the Nernst potential (E^0) is applied, the activation energy barriers will change as given by:

$$\triangle G_a = \triangle G_a^0 + (\alpha - 1)F(E - E^0), \tag{1.5}$$

$$\triangle G_c = \triangle G_c^0 + \alpha F(E - E^0) \tag{1.6}$$

where $\triangle G_a$ and $\triangle G_c$ are the oxidation and reduction free energy barriers, respectively, and α is the transfer coefficient. In general, oxidation reactions are favoured by making the electrode potential positive and reductions are favoured by making the electrode potential more negative.

8

Therefore, the potential dependent reaction rate constants can be written in terms of the standard free energy following an Arrhenius eq. such that,

$$k_f = A_f \exp\left(-\frac{\Delta G_c}{RT}\right)$$
$$= \underbrace{A_f \exp\left(-\frac{\Delta G_c^0}{RT}\right)}_{\text{rate constant, } k_f^0(T)} \exp\left(-\frac{\alpha F}{RT}(E - E^0)\right) \tag{1.7}$$

and

$$k_b = \underbrace{A_b \exp\left(-\frac{\Delta G_a^0}{RT}\right)}_{\text{rate constant, } k_b^0(T)} \exp\left(\frac{(1-\alpha)F}{RT}(E - E^0)\right) \tag{1.8}$$

where subscripts f and b denote the forward and backward reactions, respectively.

The reaction rate constants can be defined per unit area of the electrode surface as:

$$v_f = k_f C_O = -\frac{I_c}{nFA} = -\frac{i_c}{nF} \tag{1.9}$$

$$v_b = k_b C_R = \frac{i_a}{nF} \tag{1.10}$$

where C_O and C_R are the concentrations of the oxidizing and reduced species at the surface of the electrode, n is the number of electrons per mole of O, I is the current produced, A is the area of the electrode and i is the current density (I/A).

The net reaction rate will be given by:

$$v_{net} = v_f - v_b = k_f C_O - k_b C_R = -\frac{i_c}{nF} + \frac{i_a}{nF} = -\frac{i}{nF} \tag{1.11}$$

At equilibrium potential, where the applied potential E is equal to E^0, the net reaction is equal to zero and C_O will equal C_R and the surface concentration will be equal to the bulk concentration, far from the surface of the electrode. The bulk concentration is denoted as C_O^0 and C_R^0. The forward and backward reaction rates will therefore be equal and

$$r_{net} = 0 = k_f C_O^0 - k_b C_R^0 \Rightarrow k_f \cancel{C_O^0} = k_b \cancel{C_R^0}$$
$$\Rightarrow k_f = k_b$$

Thus, at equilibrium under $C_O^0 = C_R^0$, there is a potential E^0 where the forward and backward reaction rates are the same. The rate constant at E^0 is known as the standard rate constant, k_0. Then the current produced by the reaction will be:

$$i = -F(v_f - v_b) = -Fk_0 \left(C_O \exp\left(-\frac{\alpha F}{RT}(E - E^0) \right) - C_R \exp\left(\frac{(1-\alpha)F}{RT}(E - E^0) \right) \right)$$

This equation is known as the Butler-Volmer (BV) equation. This is used as the first approximation to predict the current of an electrochemical reaction.

Multi-step reactions

Multi-step reactions are very common in the electrochemical field because most electrode reactions involve more than one electron transfer. Usually a reaction that involves more than one electron transfer, is constituted by several elementary reactions, also called individual reactions or steps. An example of it is the following reaction,

$$2H^+ + 2e^- \rightleftharpoons H_2$$

In this reaction, hydrogen might involve first adsorption of H^+ to the surface and then, recombination of two adsorbed H^+ to form H_2. In order to analyse reactions involving several elementary reactions (one-electron transfer), we will need to take into account:

- the potential dependencies of all steps and

- the surface concentration of all intermediate components in order to estimate the relationship between current density and voltage.

Adsorbed species at the surface of the catalyst are given by their fractional coverage, i.e.,

$$\theta = \frac{\text{number of adsorbed molecules}}{\text{number of available sites on clean catalyst surface}} < 1$$

Using fractional coverages, the rate of each reaction can be written as a function of concentrations and coverages. For example, assume that the hydrogen reduction reaction proceeds according to the following three steps:

$$\underset{\sigma}{Pt} + H^+(aq) + e^- \underset{k_{-1}}{\overset{k_1}{\rightleftharpoons}} \underset{\theta}{PtH}(ads) \; (\text{Volmer}) \tag{1.12}$$

$$\underset{\theta}{PtH}(ads) + H^+(aq) + e^- \underset{k_{-2}}{\overset{k_2}{\rightleftharpoons}} \underset{\sigma}{Pt} + H_2(g) \; (\text{Heyrowsky}) \tag{1.13}$$

$$2 \underset{\theta^2}{PtH}(ads)) \underset{k_{-3}}{\overset{k_3}{\rightleftharpoons}} 2 \underset{\sigma^2}{Pt} + H_2(g) \; (\text{Tafel}) \tag{1.14}$$

10
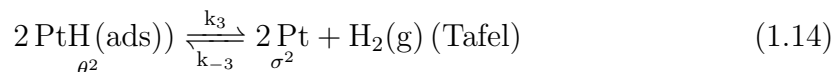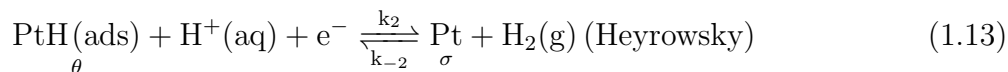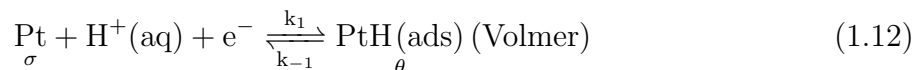
In this case PtH(ads) is the only adsorbed species. The surface of Pt is given by $\sigma = 1 - \theta$. Steps 1 to 3 correspond to the Volmer, Heyrowsky and Tafel reactions, respectively. The individual rate of each reaction can be expressed like the following reaction for step 1,

$$r_1 = k_1 \sigma C_{\text{H}^+} - k_{-1}\theta \tag{1.15}$$

$$= k_1(1 - \theta)C_{\text{H}^+} - k_{-1}\theta \tag{1.16}$$

where

$$k_1 = k_1^0 exp\left(-\frac{\beta_1 F(E - E^0)}{RT}\right) \tag{1.17}$$

$$k_{-1} = k_{-1}^0 exp\left(-\frac{(1 - \beta_1)F(E - E^0)}{RT}\right) \tag{1.18}$$

and the overpotential $\eta = (E - E^0)$.

Considering all steps, which produce or consume electrons, the current density in $[A/cm^2]$ produced by the electrode can be expressed as,

$$i = F(-r_1 - r_2) \tag{1.19}$$

and for each species involved in the reaction, the production rates can be written as,

$$\Gamma\frac{d\theta}{dt} = r_1 - r_2 - 2r_3 \tag{1.20}$$

Then, for a given overpotential $\eta = (E - E^0)$, the steady-state current can be obtained following these steps:

1. At steady-state $\frac{d\theta_i}{dt} = 0$, so the equation above, being equal to zero, can be solved to obtain all coverages.

2. Substitute θ_i into the eq. for i ((1.19)) to find the steady-state current.

1.3   Literature Review

This work is mainly focused in understanding the kinetics of the oxygen reduction reaction (ORR) and developing and implementing a novel micro kinetic model because, as explained in section 1.2.2, the major losses in a PEMFC are due to activation losses and the ORR is a complex reaction that needs to be better studied for improving the use of Pt catalyst and reducing PEMFCs losses. In section 1.3.1, an exhaustive research on the fundamentals of the

ORR kinetics is presented. A literature review of numerical models are presented in section 1.3.2 with a focus on how the ORR kinetics are being simulated. Experimental work that shows the complexity of the reaction and quantum mechanical studies on the elementary reactions that are assumed to be part of the ORR mechanism is presented in section 1.3.3.

1.3.1 ORR kinetics

A major challenge in the research and development of PEMFC is understanding and improving the sluggish rate of the ORR kinetics at the cathode [17]. Despite decades of research, there is no consensus on the individual elementary reactions that conform the overall mechanism [31]. Not all intermediate species adsorbed during this mechanism are fully identified and there are different approaches that are used for modeling the reaction kinetics.

Reaction Mechanisms

It is well known that the overall mechanism for the ORR can follow two paths, the direct four-electron transfer mechanism (see eq. (1.21)) or the series two-electron transfer mechanism (see eq. (1.22)-(1.24)):

- Four electron transfer path:

$$O_2 + 4\,H^+ + 4\,e^- \rightleftharpoons 2\,H_2O \tag{1.21}$$

- Two electron transfer path:

$$O_2 + 2\,H^+ + 2\,e^- \rightleftharpoons H_2O_2 \tag{1.22}$$
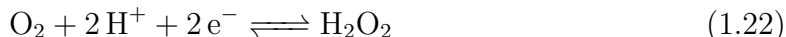
Followed by either one of the following reactions:

$$H_2O_2 + 2\,H^+ + 2\,e^- \rightleftharpoons 2\,H_2O \tag{1.23}$$

$$2\,H_2O_2 \rightleftharpoons 2\,H_2O + O_2 \tag{1.24}$$

The four-electron transfer path has been recognized as the favoured pathway [32] specially at high cell potentials because the formation of peroxide species, known to contribute to membrane degradation, only happens at very low cell potentials [33].

The peroxide pathway is still an active area of research, and even though some authors agree that the peroxide formation is insignificant [34, 35], the effect on ORR is an ongoing debate and it is considered in this work because it can lead to the degradation of the Nafion membrane [5, 36].

The direct four-electron transfer mechanism has been the main focus of ORR kinetics in the past decades, and has been studied in acidic and alkaline media as shown in the following references [37–41]. Wroblowa et al. [40] proposed one of the earliest mechanisms for the ORR kinetics, suggesting the following reaction mechanism:

$$O_2 + Pt + H^+ + e^- \rightleftharpoons PtO_{2(ads)} \tag{1.25}$$
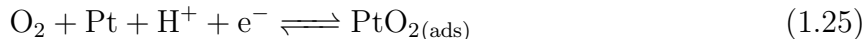
Followed either by the 4 electron pathway:

$$PtO_{2(ads)} + 4\,H^+ + 4\,e^- \rightleftharpoons 2\,H_2O + Pt \tag{1.26}$$

or the 2 electron pathway:

$$PtO_{2(ads)} + 2\,H^+ + 2\,e^- \rightleftharpoons PtH_2O_{2(ads)} \tag{1.27}$$

$$PtH_2O_{2(ads)} \rightleftharpoons H_2O_2 + Pt \tag{1.28}$$
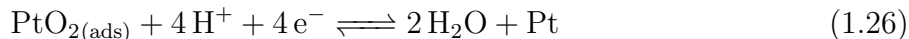
More recent studies suggest that the Wroblowa mechanism should be replaced by either the associative or dissociative pathways. Jinnouchi et al. [42] and Norskov at al. [43] considered that the ORR proceeds through the associative mechanism, as shown in eq. (1.29)-(1.32) while Wang et al. [44] suggested that it proceeds through a dissociative pathway, as shown in eq. (1.33)-(1.35).

- Associative mechanism:

$$O_2 + Pt + H^+ + e^- \rightleftharpoons PtO_2H_{(ads)} \tag{1.29}$$

$$PtO_2H_{(ads)} \rightleftharpoons PtO_{(ads)} + PtOH_{(ads)} \tag{1.30}$$

$$PtO_{(ads)} + H^+ + e^- \rightleftharpoons PtOH_{(ads)} \tag{1.31}$$

$$PtOH_{(ads)} + H^+ + e^- \rightleftharpoons H_2O + Pt \tag{1.32}$$

- Dissociative mechanism:

$$\frac{1}{2}\,O_2 + Pt \rightleftharpoons PtO_{(ads)} \tag{1.33}$$

$$PtO_{(ads)} + H^+ + e^- \rightleftharpoons PtOH_{(ads)} \tag{1.34}$$

$$PtOH_{(ads)} + H^+ + e^- \rightleftharpoons H_2O + Pt \tag{1.35}$$
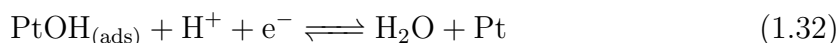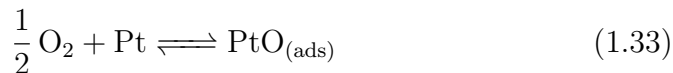
Another identified reaction mechanism related to the ORR is the oxide growth on a platinum surface [45, 46]. This phenomenon has been investigated via cyclic voltammetry and potentiostatic experiments in the absence of oxygen by several researchers [47–52]. This

mechanism can be characterized by the further oxidation of the adsorbed species by a place exchange on the platinum surface as shown in eq. (1.36)-(1.38).

$$PtO_{ads} \rightleftharpoons O-Pt \tag{1.36}$$

$$O-Pt + H_2O + H^+ + e^- \rightleftharpoons O-Pt-OH \tag{1.37}$$

$$O-Pt-OH + H^+ + e^- \rightleftharpoons O-Pt-O \tag{1.38}$$
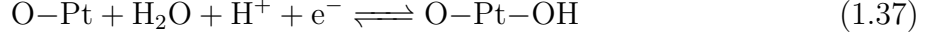
Other authors such as Chung et al. [53] suggest that, based on their experimental results, the platinum oxidation mechanism can lead to the degradation of the catalyst following these reactions:

$$Pt^0 + \frac{1}{2}O_2 \rightleftharpoons PtO_{(ads)} \tag{1.39}$$

$$PtO_{(ads)} + 2H^+ \rightleftharpoons Pt^{2+} + H_2O \tag{1.40}$$

$$Pt^{2+} + 2e^- \rightleftharpoons Pt^0 \tag{1.41}$$

$$\tag{1.42}$$
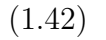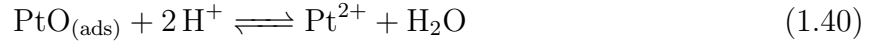
As it can be observed, these Pt degradation mechanism accounts for the formation of platinum ions Pt^{2+} and their re-precipitation to form platinum. The Pt oxidation mechanisms that lead to Pt degradation are not part of the scope of these thesis due to their complexity and uncertainty.

This work is limited to account the 4 electron transfer mechanism for ORR, the 2 electron transfer mechanism for the peroxide formation and 3 additional reactions that account for oxide growth through the formation of subsurface and place exchange species.

1.3.2   Numerical Models of the ORR

The numerical modeling of the ORR kinetics is an important area of research for the development of PEMFC. The oxygen reduction reaction that occurs in the cathode catalyst layer of the cell, is a complex, yet not well understood, multi-step reaction, that involves the formation of different intermediate species. Even though, this process is often modeled using the Butler-Volmer equation, or even a simpler version of it called the Tafel equation (see eq. (1.43)), that only accounts for simple and single step reactions,i.e.,

$$i = i_0 \left(\frac{P_{O_2}}{P_{O_2,ref}} \right)^\gamma \exp \left(\frac{-\alpha \eta F}{RT} \right) \tag{1.43}$$

where i_0 is the exchange current density at reference oxygen concentration $P_{O_2,ref}$, P_{O_2} is the actual oxygen concentration, γ is the kinetic reaction order with respect to partial

pressure of oxygen, η is the applied over-potential,i.e., $\eta = \phi_s - \phi_e - E^{eq}$, and α is the charge transfer coefficient.

Several assumptions are needed to simplify the complex reaction to a Tafel model and experimental data suggest the model cannot correctly capture the ORR behaviour, for example, the Tafel equation is not capable of capturing the doubling in the Tafel slope observed experimentally, from 60 mV/dec at low current densities to 120 mV/dec at high current densities [31]. This change in the slope is generally observed at 0.8 V, and has been explained in terms of the changing coverage surface due to the formation of different adsorbed species [37, 38].

In order to capture the effects of the changing surface coverage without losing the simplicity of the Tafel equation, a modified expression (see eq.(1.44)) has been used by several research groups [31, 54, 55]:

$$i = i_0(1 - \theta)\left(\frac{P_{O_2}}{P_{O_2,ref}}\right)^\gamma \exp\left(\frac{-\alpha\eta F}{RT}\right) \exp\left(\frac{-\omega\theta}{RT}\right) \tag{1.44}$$

This modified expression includes two extra terms: 1) the site blocking effect of surface oxides $(1 - \theta)$; and 2) an energetic effect $\exp\left(\frac{-\omega\theta}{RT}\right)$ akin to Temkin adsorption. This model requires the surface coverage at different potentials before computing the current, therefore the predictions of this coverage dependent ORR kinetic model depends on the accuracy of the coverage expression, which may be oxygen concentration dependent and is definitely potential dependent. That is why more recently, the scientific community in this area of study has started to develop multi-step models to capture these dependencies of the ORR kinetics [1, 42, 44, 56, 57].

The main objective of the multi-step models is to predict the surface coverage and the current generation simultaneously without needing to define explicitly the coverage. These models have the ability to predict the rate determining step (RDS) and analyze the cause of the doubling in the Tafel slope in terms of adsorbed species. The most representative models are the double trap kinetic model proposed by Wang et al. [44], the improved version of it proposed by Moore et al. [57] and the models developed by Jinnouchi et al. [42] and Markiewicz et al. [56] and older models such as the one proposed by Eikerling et al. [19].

In the past 5 years even, more complex models have been developed to account for the oxide growth mechanism in addition to the coverage dependent ORR kinetics. Baroody et al. [58] presented the first consistent mathematical model of oxide formation and growth on platinum. Then, Jayasankar and Karan [1] developed a multi-step ORR mechanism capable

of capturing the oxide growth phenomenon. The purpose of having this type of models is to understand platinum dissolution in the cathode catalyst layer of polymer electrolyte fuel cells.

1.3.3 Experimental Trends

In the process of developing a numerical model, experimental data is needed to validate the results obtained from the formulated model. In this work, the major experimental trends that the proposed model aims to reproduce are: steady state polarization curve, and coverage fractions, transient cyclic voltammograms, and logarithmic oxide growth. These are the same experimental trends that were used to validate the numerical models that have been developed for ORR kinetics presented in the previous section.

Early experimenters monitored the ORR half-cell reaction by using a three-electrode cell with an ideal reference electrode, a working electrode and a counter electrode. The reference electrode was intended to be unaffected by the production of current at the working electrode, by keeping its potential constant. These electrodes were placed in an acidic or alkaline media to allow the transport of ions and reactants. These experiments were conducted by authors such as Bockris et al. [59] and Damjanovic [37]. The results from these experiments showed that the effects of the concentration of the reactants were affecting the kinetics of the ORR, therefore rotating disk electrodes started to be used by experimenters in order to remove the mass transport effects. For example, Parthasarathy et al. [4, 60] used a solid-state electrolytic cell with a micro-electrode to study the steady state response of the ORR kinetics without mas transport effects at different operating conditions, obtaining polarization curves at different temperatures and pressures. The experimental data presented by them is one of the very few available in the literature as a good reference of how does the kinetic performance of the ORR in a PEMFC is. That is why it is commonly used to validate models [26, 29, 44, 57].

Another important characteristic of the ORR kinetics at steady state is the evolution of the coverage fractions of the intermediate species over the cell potential. The reason why this coverage behaviour is important is because the production of each intermediate specie is a key aspect for determining the performance of the cell. It has been observed experimentally that there is a correlation between the increase in the production of $PtO_{(ads)}$ and the decrease of $PtOH_{(ads)}$ at 0.8 V. These changes are also directly correlated to the change of the Tafel slope observed in the polarization curves. One of the methods used for obtaining experimentally the coverage of the intermediates is the X-ray absorption spectroscopy

(XPS) technique [61]. The most accepted experimental trend on the evolution of the adsorbed species over cell potentials is that the formation of $PtOH_{(ads)}$ commences at 0.6 V, followed by the transformation into $PtO_{(ads)}$ above 0.8 V. This is in agreement with what has been observed from the behaviour of the adsorbed species from DFT calculations and Monte Carlo simulations [62]. These have been used for validation of the simulated coverage fractions from several authors [1, 46, 58, 63].

1.4 Contributions and Objectives

Knowledge gap and contributions

Regardless of the exhaustive work that has been done towards the research on oxygen electrochemistry on platinum and the development of numerical models for capturing the phenomena that occurs in the complex oxygen reduction reaction, no attempts have been made to develop a consistent steady state and transient framework that accounts for ORR, oxide growth and peroxide formation. The aim of this work is first to contribute to the understanding of the ORR kinetics and the most recent models in this field. Then, propose a novel kinetic model that accounts for oxide species of three important phenomena (ORR, peroxide formation and surface and sub-surface oxide growth). The reason why these phenomenons are considered is because it is known that these affect the ORR and platinum degradation of fuel cells and that are strongly linked to Pt dissolution processes.

Thesis Objectives

This thesis project is on the development of a transient unified kinetic model of Oxygen Reduction Reaction (ORR) in Proton Exchange Membrane Fuel Cells (PEMFCs), that accounts for oxide growth and peroxide formation, and is capable of capturing experimental polarization curves and CVs. The main objectives are:

- Derive and formulate numerical expressions for a novel steady state and transient ORR kinetic model based on the previous model by Jayasankar and Karan [1].

- Estimate and fit kinetic parameters that characterize the kinetic model, based on experimental data obtained from the literature.

- Analyze and study the novel multi-step micro-kinetic model under steady-state and transient operation.

- Develop and implement a new transient unified multi-step ORR kinetic model.

1.5 Thesis Outline

The first chapter presents an introduction and background on the structure and operation of a PEMFC, the kinetics and formulation of numerical models of ORR and experimental data useful for validating simulations. Chapter 2 describes the previous model developed by Jayasankar and Karan [1] [2], it corrects the reported governing equations, the results of the implementation, a modification of that model and parametric analysis. In Chapter 3 is presented the reaction mechanism assumed for the new proposed model, the formulation and numerical derivation, an explanation of the solution strategy and the methodology for the parameter estimation (optimization). Chapter 4 covers the suitability of the proposed model by presenting the preliminary results of the new kinetic model, then the results of the optimization and an analysis of how good is the model to reproduce different sets of experimental data. Finally Chapter 5 presents the final conclusions and discussion as well as possibilities for future research on Pt dissolution.

Chapter 2

Analysis of a previously reported unified multi-step model for oxygen reduction and oxide growth

2.1 Introduction

In the previous chapter, a background on PEM fuel cells and electrochemical reaction kinetics was presented covering the most recent numerical models in the literature capable of capturing some of the features of the complex ORR mechanism. From that literature review, it was concluded that the most recent and complete developed model on ORR kinetics is the one presented by Jayasankar and Karan [1]. They presented a micro kinetic model partially based on the double trap model from Wang et al. [44] and Moore et al. [57], but also including transient effects and oxide growth. The purpose of the development of the unified multi-step model from Jayasankar and Karan was to capture the water oxidation and the oxide growth, which were not considered either by Wang et al. or Moore et al. when developing the double trap model and the modified version, respectively.

The two mechanisms assumed for the formulation of this numerical model are the oxygen reduction reaction and the platinum oxide formation, which are represented on Figure 2.1.

The main differences between the double trap model and the unified multi step model are the following:

- The ORR mechanism assumed for the double trap model consists of two possible pathways, as shown in eq. (1.33)-(1.35), the oxygen reacts with active platinum sites through either an electrochemical reductive adsorption (RA) reaction forming $PtOH_{(ads)}$ or a chemical dissociative adsorption (DA) reaction forming $PtO_{(ads)}$ and
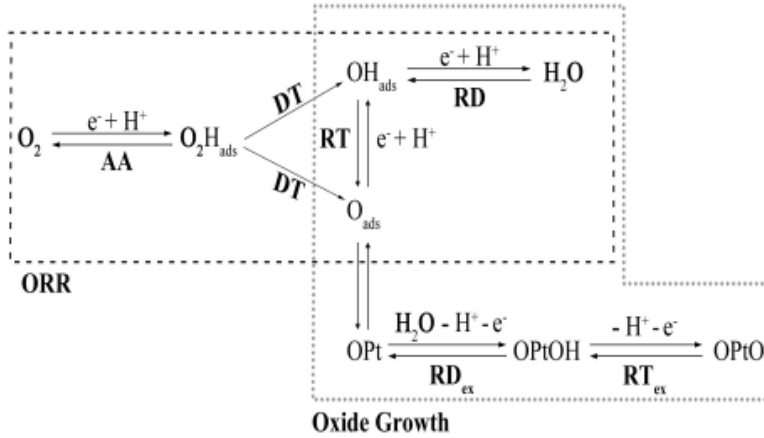
Figure 2.1 – Proposed reaction mechanism. Reproduced with permission from ref [1].

then converting it into $PtOH_{(ads)}$ through an electrochemical reductive (RT) reaction. And finally, through a reductive desorption (RD) step the adsorbed $PtO_2H_{(ads)}$ is reduced to water. The ORR mechanism in ref. [1] however assumed only one possible pathway where the oxygen and platinum react to form $PtO_2H_{(ads)}$ through an associative adsorption (AA) step as shown in figure 2.1. Then, the $PtO_2H_{(ads)}$ is chemically dissociated into $PtO_{(ads)}$ and $PtOH_{(ads)}$ in a dissociative transition (DT) reaction and then RT and RD reactions proceed as in the double trap. The unified multi step model also includes the oxide growth formation assuming that the oxides formed further change their composition and structure at high potentials, forming place exchange oxides, which is not considered for the double trap model. Another addition of this last model are the Temkin terms for accounting for the energies of interaction between the adsorbed species in some of the steps.

- The accounted adsorbed species by the double trap model are only $PtO_{(ads)}$ and $PtOH_{(ads)}$, while the unified multi-step model accounts for those two adsorbed species plus $PtO_2H_{(ads)}$ and the place exchange $OPt_{(sub)}$, $OPtOH_{sub}$ and $OPtO_{sub}$.

- The formulation of the kinetic equations that govern the double trap model are free energies of activation dependent, while the model in ref [1] has a mixed formulation where some reactions are modelled using the free activation energies, while others are individual equilibrium potentials dependent. Furthermore, Temkin terms also need to be obtained for the model in ref [1], while not included in the formulation of the double trap model.

Given that the unified multi-step model for oxygen reduction and oxide growth developed by Jayasankar and Karan [1] is the most complete model available in the literature, in this

chapter, this model is redeveloped using Python (it was originally developed in MATLAB), analyzed and modified with the objective of studying the validity of its formulation. Further on, this study will be the starting point for the development of an improved model that depends only on energies of activation and Temkin terms.

2.2 Formulation

Given that the double trap kinetic model was limited by the thermodynamic reaction order of the oxygen concentration and Moore et al. [57] and Wang et al. [44] predicted reaction orders different that the ones reported experimentally [56], this model tried to improve this aspect by replacing the reductive adsorption (RA) step with an associative adsorption (AA) step where the oxygen reacts with the platinum surface forming the adsorbed specie $PtO_2H_{(ads)}$ as shown in equation (2.1). Then, the surface adsorbed specie is assumed to dissociate into $PtO_{(ads)}$ and $PtOH_{(ads)}$ surface adsorbed species through a dissociative transition (DT) step as shown in equation (2.2). Later on, during anodic scan, the surface adsorbed $PtO_{(ads)}$ and $PtOH_{(ads)}$ species are reduced to form water as shown in equations (2.3) and (2.4). This ORR mechanism was assumed as a successive one electron transfer steps.

At high cell potentials, when the surface $O_{(ads)}$ specie increase, energetically speaking, the formation of place exchanged oxide O-Pt is suspected to be very favorable. The place exchange step is the first step assumed in this work for the oxide growth mechanism as in equation (2.5). Afterwards, as the potential is further increased, the place exchanged platinum can further oxidize to form O-Pt-OH and O-Pt-O as shown in reactions (2.7) and (2.6), respectively.

$$\text{AA:} \underset{\theta_{Pt}}{\text{Pt(site)}} + O_2 + H^+(aq) + e^- \underset{\text{k}_{-AA}}{\overset{\text{k}_{AA}}{\rightleftharpoons}} \underset{\theta_{O_2H}}{O_2H_{ads}} \tag{2.1}$$

$$\text{DT:} \underset{\theta_{O_2H}}{O_2H_{ads}} \underset{\text{k}_{-DT}}{\overset{\text{k}_{DT}}{\rightleftharpoons}} \underset{\theta_O}{O_{ads}} + \underset{\theta_{OH}}{OH_{ads}} \tag{2.2}$$

$$\text{RT:} \underset{\theta_O}{O_{ads}} + H^+(aq) + e^- \underset{\text{k}_{-RT}}{\overset{\text{k}_{RT}}{\rightleftharpoons}} \underset{\theta_{OH}}{OH_{ads}} \tag{2.3}$$

$$\text{RD:} \underset{\theta_{OH}}{OH_{ads}} + H^+(aq) + e^- \underset{\text{k}_{-RD}}{\overset{\text{k}_{RD}}{\rightleftharpoons}} \underset{\theta_{Pt}}{\text{Pt(site)}} + H_2O \tag{2.4}$$

$$\text{SUB:} \underset{\theta_{sub}}{O-Pt} \underset{\text{k}_{-sub}}{\overset{\text{k}_{sub}}{\rightleftharpoons}} \underset{\theta_O}{O_{ads}} \tag{2.5}$$

$$\text{RT}_{ex}\text{:} \underset{\theta_{O_{ex}}}{O-Pt-O} + H^+(aq) + e^- \underset{\text{k}_{-RT_{ex}}}{\overset{\text{k}_{RT_{ex}}}{\rightleftharpoons}} \underset{\theta_{OH_{ex}}}{O-PtOH} \tag{2.6}$$

$$\text{RD}_{ex}\text{:} \underset{\theta_{OH_{ex}}}{O-Pt-OH} + H^+(aq) + e^- \underset{\text{k}_{-RD_{ex}}}{\overset{\text{k}_{RD_{ex}}}{\rightleftharpoons}} \underset{\theta_{sub}}{O-Pt} + H_2O \tag{2.7}$$
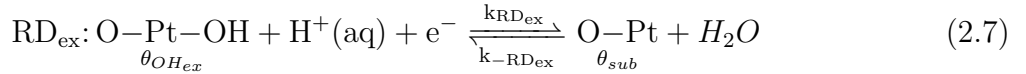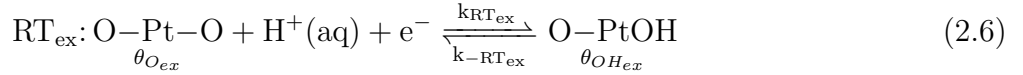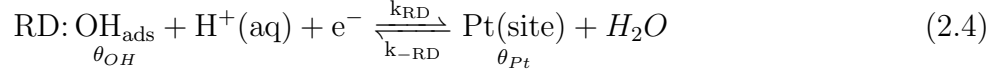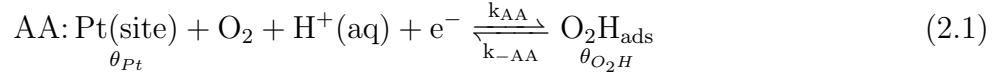
2.2.1 Original

According to ref. [1, 2] , the reaction rates for modelling the elementary reaction rates assumed for this model are the following:

$$v_{AA} = j^* \exp\left(\frac{-\Delta G_{AA}^{*0}}{kT}\right)\left[\theta_{Pt} a_{O_2} a_{H^+} \exp\left(\frac{-\beta\eta - \omega_{AA}(\theta_{OH} + \theta_O)}{kT}\right) - \theta_{O_2H}\exp\left(\frac{(1-\beta)\eta + \Delta G_{AA}^{ref}}{kT}\right)\right] \tag{2.8}$$

$$v_{DT} = k_{DT}\theta_{O_2H} \tag{2.9}$$

$$v_{RT} = k_{RT}\left[\theta_O a_{H^+}\exp\left(\frac{-\beta(E - E_{RT})}{kT}\right)\exp\left(\frac{\omega_{RT}\theta_O}{kT}\right) - \theta_{OH}\exp\left(\frac{(1-\beta)(E - E_{RT})}{kT}\right)\right] \tag{2.10}$$

$$v_{RD} = k_{RD}\left[\theta_{OH} a_{H^+}\exp\left(\frac{-\beta(E - E_{RD})}{kT}\right) - \theta_{Pt}\exp\left(\frac{(1-\beta)(E - E_{RD})}{kT}\right)\exp\left(-\frac{\omega_{RD}(\theta_{OH} + \theta_O)}{kT}\right)\right] \tag{2.11}$$

$$v_{sub} = k_{sub}\theta_O \exp\left(\frac{-\omega_{sub}\theta_{Oxide}}{kT}\right)(1 - \theta_{Oxide}) - k_{-sub}\theta_{SUB} \tag{2.12}$$

$$v_{RDex} = k_{RDex}\left[\theta_{OHex} a_{H^+}\exp\left(\frac{-\beta(E - E_{RDex})}{kT}\right) - \theta_{SUB}\exp\left(\frac{(1-\beta)(E - E_{RDex})}{kT}\right)\right] \tag{2.13}$$

$$v_{RTex} = k_{RTex}[\theta_{Oex}a_{H^+} \exp\left(\frac{-\beta(E - E_{RTex})}{kT}\right) \exp\left(\frac{-\omega_{RT_{ex}}\theta_{Oex}}{kT}\right) - \theta_{OHex} \exp\left(\frac{(1 - \beta)(E - E_{RTex})}{kT}\right)]$$

(2.14)

where $\eta = E - E^0$ is the over potential, E_i is the equilibrium potential of the ith elementary step, θ_i represent the coverage fractions of the ith adsorbed species, β is the reaction symmetry factor, and ω_i is the Temkin interaction term for the ith reaction. θ_{Pt} is the total of Pt surface available defined as $\theta_{Pt} = 1 - \theta_O - \theta_{OH} - \theta_{O_2H}$ and $\theta_{Oxide} = 1 - \theta_{O_{ex}} - \theta_{OH_{ex}} - \theta_{SUB}$.

And the parameter values obtained from their fitting are reported in ref. [1, 2] and summarised in Table 2.1.

Table 2.1 – Parameter groups and estimates [1, 2]

Parameter groups	Parameter	Parameter estimate
Rate constants $(mol(cm_{pt}^{-2}s^{-1}))$	k_{RD}	4.3 x 10^{-9}
	k_{RT}	4.3 x 10^{-8}
	k_{DT}	5 x 10^{-5}
	k_{sub}	4.3 x 10^{-11}
	k_{-sub}	4.3 x 3 x 10^{-11}
	k_{RDex}	4.3 x 10^{-11}
	k_{RTex}	4.3 x 10^{-11}
Equilibrium potential V	E_{RD}	0.79
	E_{RT}	0.79
	E_{sub}	1.2
	E_{RDex}	0.98
	E_{RTex}	0.98
Interaction energies eV	w_{AA}	0.1
	w_{RD}	0.46
	w_{RT}	0.07
	w_{sub}	1.4
	w_{RTex}	0.3
Energies eV	ΔG_{AA}^{*0}	0.5863
	ΔG_{AA}^{ref}	0.2754

2.3 Implementation

The equations reported in ref. [1, 2] were implemented with the aim of reproducing the results reported in those same references. This implementation was done in Python programming language and a Newton solver was used to solve the system of equations. This Newton solver from scipy optimize library returns the roots of the non-linear equations defined by a system of functions y(x) = 0 after giving a starting estimate. In this case, the solver tolerance was set at 1.49012e-08

The obtained results from this implementation ended up not matching the results reported in ref. [1]. Therefore, the authors of that article and PhD thesis were contacted, after analysing and discussing their MATLAB implementation, several typos and wrong reported equations were identified and corrected.

2.3.1 Correction of the reported governing equations and parameters

A steady state version of the model above was first developed by Jayasankar and Karan [1] and re-implemented in Python. The steady state accounted for AA, DT, RT and RD reactions using eq. (2.8)-(2.14), according to what they reported in ref. [1, 2], however, when looking at the code the authors provided, the actual implemented equations are slightly different for v_{DT}, v_{RT} and v_{RD}. Instead of having implemented the reaction rate constants (k_i), the reactions rates implemented have a reference pre-factor j^* and an exponential term of free energies. Below are the modifications to the equations reported in the article (marked in red).

$$v_{DT} = j^* 10^{-3} [\theta_{O_2H} - \exp\left(\frac{-\Delta G_{DT}}{kT}\right) \theta_O \theta_{OH}] \tag{2.15}$$

$$v_{RT} = j^* \exp\left(\frac{-\Delta G_{RT}}{kT}\right) [\theta_O a_{H^+} \exp\left(\frac{-\beta(E - E_{RT})}{kT}\right) \exp\left(\frac{\omega_{RT}\theta_O}{kT}\right) - \theta_{OH} \exp\left(\frac{(1-\beta)(E - E_{RT})}{kT}\right)] \tag{2.16}$$

$$v_{RD} = j^* exp\left(\frac{-\Delta G_{RD}}{kT}\right) 10^{-1} [\theta_{OH} a_{H^+} \exp\left(\frac{-\beta(E - E_{RD})}{kT}\right)$$
$$- \theta_{Pt} \exp\left(\frac{(1-\beta)(E - E_{RD})}{kT}\right) \exp\left(-\frac{\omega_{RD}(\theta_{OH} + \theta_O)}{kT}\right)] \tag{2.17}$$

For the transient implementation, used to simulate CVs, the oxide growth reaction mechanism was simulated using the following elementary reactions: RT, RD, SUB, RTex and

Table 2.2 – Comparison of steady state parameter values reported and actually implemented

Parameter groups	Parameter	Value reported	Value implemented
Rate constants $(mol(cm_{pt}^{-2}s^{-1}))$	k_{RD}	4.3 x 10^{-9}	3.089 x 10^{-7}
	k_{RT}	4.3 x 10^{-8}	1.473 x 10^{-5}
	k_{DT}	5 x 10^{-5}	5.182 x 10^{-5}
Reaction energy eV	ΔG_{RD}	-	0.2498
	ΔG_{RT}	-	0.2727
	ΔG_{DT}	-	0.6
Reference pre factor	j*	1e3	1e4/(2*F)
Equilibrium potential V	E_{RD}	0.79	1.05
	E_{RT}	0.79	0.85
Interaction energies eV	w_{AA}	0.1	0.1036
	w_{RD}	0.46	0.2498
	w_{RT}	0.07	0.0777
Energies eV	ΔG_{AA}^{*0}	0.5863	0.5863
	ΔG_{AA}^{ref}	0.2754	0.3109

RDex; however, the reactions rates are different to those reported in ref. [1, 2]. The reaction rate for SUB reaction, v_{sub}, was implemented as follows,

$$v_{sub} = j^* exp\left(\frac{-\Delta G_{sub}}{kT}\right) 10^{-3}[\theta_O exp\left(\frac{-\omega_{sub}\theta_{Oxide}}{kT}\right)(1 - \theta_{Oxide})exp\left(\frac{-\beta_{sub}(E - E_{sub})}{kT}\right) - b_{sub}\theta_{SUB}]$$

(2.18)

If we compare this equation with eq. 2.12 it can be observed that v_{sub} has several extra terms. In the case of v_{RT}, v_{RD}, v_{RDex} and v_{RTex} the only difference is the reaction rate constants that have the format of the reference pre-factor multiplied by an exponential term with the reaction free energy, e.g.,

$$v_{RT} = j^* exp\left(\frac{-\Delta G_{RT}}{kT}\right)[\theta_O a_{H^+} exp\left(\frac{-\beta(E - E_{RT})}{kT}\right) exp\left(\frac{\omega_{RT}\theta_O}{kT}\right) - \theta_{OH} exp\left(\frac{(1 - \beta)(E - E_{RT})}{kT}\right)]$$

(2.19)

$$v_{RD} = j^* exp\left(\frac{-\Delta G_{RD}}{kT}\right) 10^{-1}[\theta_{OH} a_{H^+} exp\left(\frac{-\beta(E - E_{RD})}{kT}\right)$$
$$- \theta_{Pt} exp\left(\frac{(1 - \beta)(E - E_{RD})}{kT}\right) exp\left(-\frac{\omega_{RD}(\theta_{OH} + \theta_O)}{kT}\right)]$$

(2.20)

$$v_{RDex} = j^* exp\left(\frac{-\Delta G_{RDex}}{kT}\right) 10^{-3} [\theta_{OHex} a_{H^+} exp\left(\frac{-\beta(E - E_{RDex})}{kT}\right) - \theta_{SUB} exp\left(\frac{(1-\beta)(E - E_{RDex})}{kT}\right)]$$

$$(2.21)$$

$$v_{RTex} = j^* exp\left(\frac{-\Delta G_{RTex}}{kT}\right) 10^{-3} [\theta_{Oex} a_{H^+} exp\left(\frac{-\beta(E - E_{RTex})}{kT}\right) exp\left(\frac{-\omega_{RT_{ex}} \theta_{Oex}}{kT}\right)$$
$$- \theta_{OHex} exp\left(\frac{(1-\beta)(E - E_{RTex})}{kT}\right)]$$

$$(2.22)$$

The comparison of the transient parameters can be found on Table 2.3. This comparison shows that there is no significant difference among the parameters reported on their article and the ones implemented. Therefore, it can be concluded that the parameters reported in their article are mainly the parameters that correspond to the transient model, however these ones do not correspond to the one in the steady state results such as the polarization curves.

It was concluded that there were two different frameworks in the implementation in ref [1], with a different set of parameters. Therefore, it was assumed that the model was fitted separately to steady-state and transient data. Summarizing, the main differences found between the reported governing equations and the ones actually implemented for obtaining the reported results are the following:

- The implemented reaction rate for DT step contains an extra term: $exp\left(\frac{-\Delta G_{DT}}{kT}\right) \theta_O \theta_{OH}$ which accounts for the backwards contribution of this reaction, therefore the statement made on ref [1] about assuming that the reverse of DT is energetically unfavourable is contradictory, because even though it was assumed in ref [1] that it is not energetically favourable, it is accounted.

- The implemented reaction rate for SUB step also contains an extra term: $exp\left(\frac{-\beta_{sub}(E - E_{sub})}{kT}\right)$ which doesn't make much sense given that this SUB reaction is not an electrochemical step, and given that there is not exchange of electrons, the reaction rate should not depend on the cell potential (E).

Later on, parametric studies were conducted to observe the contribution to the current generation of these terms with the objective of determining the physical meaning of accounting these extra terms.

Table 2.3 – Comparison of transient parameter values reported and actually implemented

Parameter groups	Parameter	Value reported	Value implemented
Rate constants $(mol(cm_{pt}^{-2}s^{-1}))$	k_{RD}	4.3 x 10^{-9}	4.3742 x 10^{-9}
	k_{RT}	4.3 x 10^{-8}	4.3742 x 10^{-8}
	k_{sub}	4.3 x 10^{-11}	4.3742 x 10^{-11}
	k_{-sub}	12.9 x 10^{-11}	13.846 x 10^{-11}
	k_{RDex}	4.3 x 10^{-11}	4.3742 x 10^{-11}
	k_{RTex}	4.3 x 10^{-11}	4.3742 x 10^{-11}
Reaction energy eV	ΔG_{RD}	-	0.3
	ΔG_{RT}	-	0.3
	ΔG_{DT}	-	0.6
	ΔG_{RDex}	-	0.3
	ΔG_{RTex}	-	0.3
	ΔG_{sub}	-	0.3
Reference pre factor	j*	10^3	10^3/(2*F)
SUB Constant	b_{sub}	-	3.22
Equilibrium potential V	E_{RD}	0.79	0.79
	E_{RT}	0.79	0.79
	E_{sub}	1.2	1.2
	E_{RDex}	0.98	0.98
	E_{RTex}	0.98	0.98
Interaction energies eV	w_{AA}	0.1	0.1036
	w_{RD}	0.46	0.41457
	w_{RT}	0.07	0.0777
	w_{sub}	1.4	1.39917
	w_{RTex}	0.3	0.3109

2.3.2 Python implementation of the model

After clearly identifying the real governing equations and parameters used for obtaining the results from ref. [1, 2], these were implemented in Python for reproducing the steady and transient results from the unified multi step model. In this section we will show the results that were reproduced by our own implementation in Python using the same equations developed by Dr. Barathram Jayasankar and Dr. Kunal Karan, and compared them to the results reported in their article.

First, the steady state polarization curve for the ORR mechanism was reproduced exactly as it can be observed in Fig. 2.2.
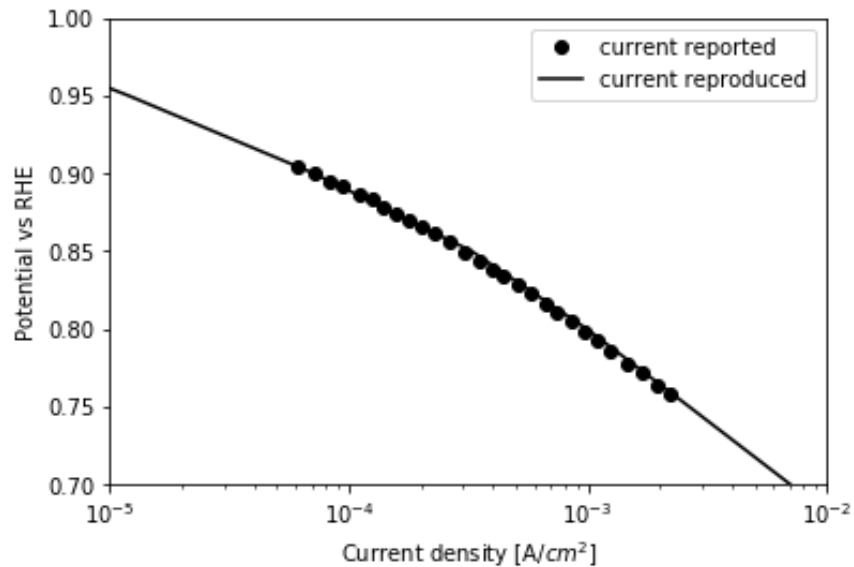
Figure 2.2 – Predicted polarization from Python implementation of their model compared to the data extracted from their reported polarization curve at 0.1 M $HClO_4$ and 298 K

As part of the steady state ORR implementation, the coverage fractions of the adsorbed species were also successfully reproduced as shown in Fig. 2.3.
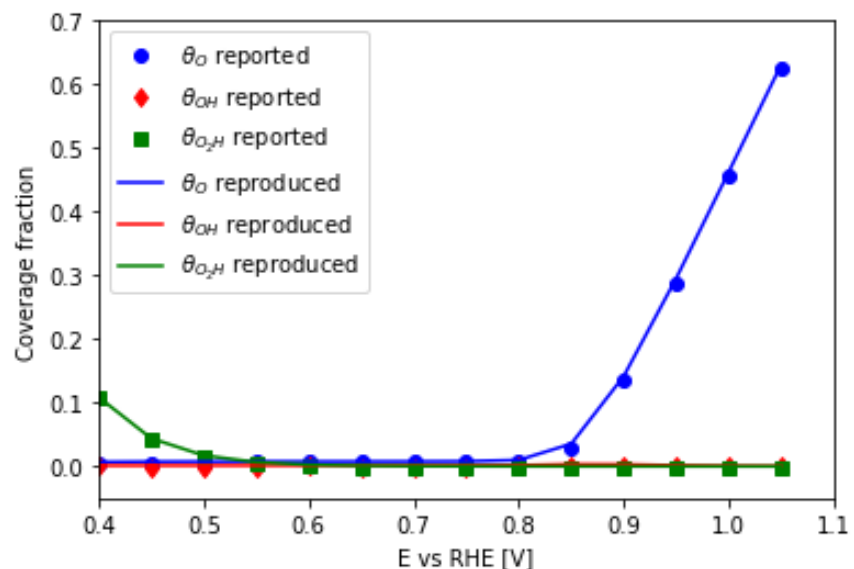
Figure 2.3 – Predicted coverage fraction from Python implementation of their model compared to their reported results

To compare the transient implementation, CVs were simulated and compared to the CV

reported in ref. [1]. This transient result was also successfully reproduced as shown in Fig. 2.4.
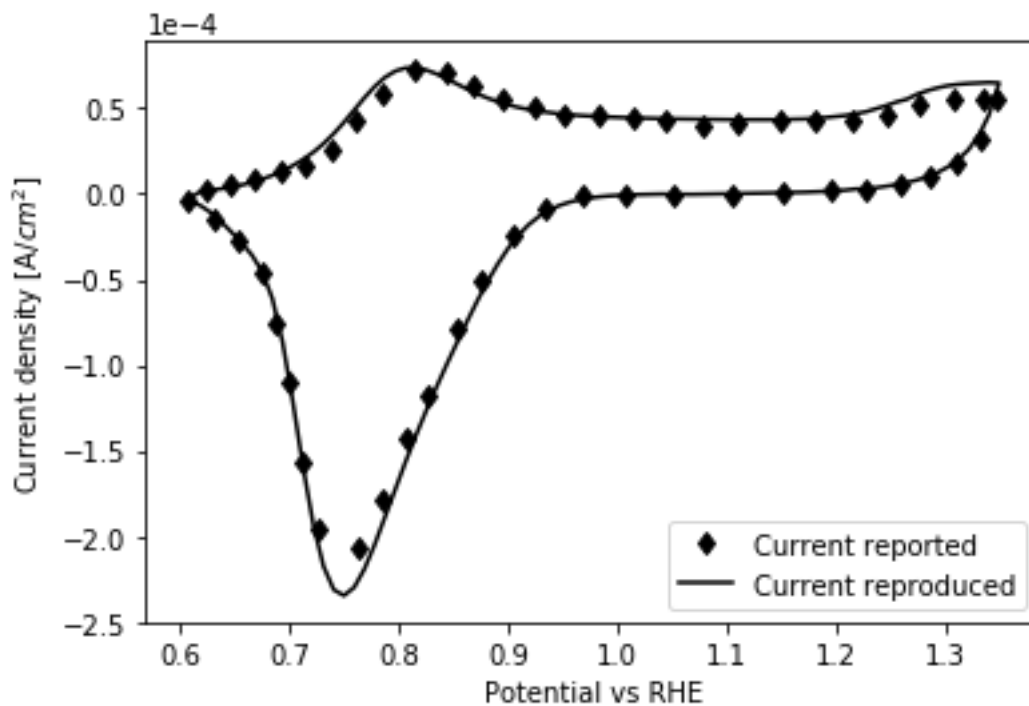
Figure 2.4 – Simulated CV from python implementation of their model compared to the reported data at 298 K and 0.1 M H^+ concentration.

In conclusion, the steady-state and transient results in ref [1] could be reproduced correctly by implementing the correct equations and parameters in Python, validating the equations and parameters presented in this work.

2.3.3 Energy based formulation

The model above, even though it was originally based on the method proposed by Wang et al. [44], which uses free energies of individual reactions, i.e., ΔG_i^0, and defines a single overpotential, $\eta = E - E^0$, it did not use the same approach to define the reaction rate of oxide species, therefore it resulted in a model with unnecessary fitting parameters and a mixed formulation. A clear and consistent procedure to derive the model was not followed.

2.3.4 Wang's form of model

The formulation of the model in ref [1] is not clearly defined. There is not a consistent derivation of the kinetic expressions because some reactions, such as RD and RT, are modelled through Butler-Volmer kinetics. Then, some reactions account for the Temkin interaction terms while others do not. For example, AA step is modelled using the Butler-Volmer approach, like Wang's approach for deriving the expressions for the Double Trap model, but adding a coverage dependent term. However, when looking at the expressions we can observe a mixed formulation where the reactions rates depend on individual equilibrium potentials and energy barriers and adsorption energies. So it has not been used the same approach to derive the expressions for all the steps of this reaction mechanism, therefore we can conclude that there is no consistency at least on the formulation of this model.

In order to try to develop a consistent formulation, the equations for each reaction were recalculated using the approach proposed by Wang et al. [44]. This means having the reaction rates dependent on a common overpotential, i.e., $\eta = E - E^0$, and energy barriers instead of individual reaction rate constants and equilibrium potentials. Even though the equation are rewritten, all terms in [1] are maintained such that the model is simply re-written not derived, this re-derivation will be done in Chapter 3. The governing equations of their model in an energy based form have the following form for the steady state implementation,

$$\Delta G_{AA}^* = \Delta G_{AA}^{*o} + \beta \eta + \omega_{AA}(\theta_O + \theta_{OH}) \tag{2.23}$$

$$\Delta G_{-AA}^* = \Delta G_{AA}^{*o} - (1 - \beta)\eta - \Delta G_{AA}^{ref} \tag{2.24}$$

$$j_{AA} = j^* \left[a_{H^+} a_{O_2} \theta_{Pt} exp\left(-\frac{\Delta G_{AA}^*}{kT}\right) - \theta_{O_2H} exp\left(-\frac{\Delta G_{-AA}^*}{kT}\right) \right] \tag{2.25}$$

$$\Delta G^*_{DT} = \Delta G^{*o}_{DT} \tag{2.26}$$

$$\Delta G^*_{-DT} = \Delta G^{*o}_{DT} + \Delta G^{ref}_{DT} \tag{2.27}$$

$$j_{DT} = j^* \left[\theta_{O_2H} exp\left(-\frac{\Delta G^*_{DT}}{kT} \right) - \theta_O \theta_{OH} exp\left(-\frac{\Delta G^*_{-DT}}{kT} \right) \right] \tag{2.28}$$

$$\Delta G^*_{RT} = \Delta G^{*o}_{RT} + \beta\eta - \omega_{RT}\theta_O \tag{2.29}$$

$$\Delta G^*_{-RT} = \Delta G^{*o}_{RT} - (1-\beta)\eta - \Delta G^{ref}_{RT} \tag{2.30}$$

$$j_{RT} = j^* \left[a_{H^+}\theta_O exp\left(-\frac{\Delta G^*_{RT}}{kT} \right) - \theta_{OH} exp\left(-\frac{\Delta G^*_{-RT}}{kT} \right) \right] \tag{2.31}$$

$$\Delta G^*_{RD} = \Delta G^{*o}_{RD} + \beta\eta + \Delta G^{ref}_{RD} \tag{2.32}$$

$$\Delta G^*_{-RD} = \Delta G^{*o}_{RD} - (1-\beta)\eta - \Delta G^{ref}_{RD} + \omega_{RD}(\theta_O + \theta_{OH}) \tag{2.33}$$

$$j_{RD} = j^* \left[a_{H^+}\theta_{OH} exp\left(-\frac{\Delta G^*_{RD}}{kT} \right) - \theta_{Pt} exp\left(-\frac{\Delta G^*_{-RD}}{kT} \right) \right] \tag{2.34}$$

The recalculated parameters that reproduce the results from ref. [1, 2] are indicated on Table 2.4.

Table 2.4 – Recalculated steady state kinetic parameters

Parameter	Value
ΔG^{0*}_{AA} [eV]	0.5863
ΔG^{ref}_{AA} [eV]	0.3109
ΔG^{0*}_{DT} [eV]	0.1773887594
ΔG^{ref}_{DT} [eV]	0.6
ΔG^{0*}_{RT} [eV]	0.4627
ΔG^{ref}_{RT} [eV]	0.38
ΔG^{0*}_{RD} [eV]	0.3089295865
ΔG^{ref}_{RD} [eV]	0.09
ω_{AA} [eV]	0.10364268818756729
ω_{RT} [eV]	0.07773201614067547
ω_{RD} [eV]	0.41457075275026917

For the transient formulation of the energy based form, RD and RT reactions are the same as in the steady state formulation, however the parameter values are different. And the kinetic expressions of the oxide growth reactions end up having the following form:

$$\Delta G^*_{RTex} = \Delta G^{*o}_{RTex} + \beta\eta + \omega_{RTex}\theta_{Oex} + \Delta G^{ref}_{RTex} \tag{2.35}$$

$$\Delta G^*_{-RTex} = \Delta G^{*o}_{RTex} - (1 - \beta)\eta - \Delta G^{ref}_{RTex} \tag{2.36}$$

$$j_{RTex} = j^* \left[a_{H^+}\theta_{Oex} exp\left(-\frac{\Delta G^*_{RTex}}{kT}\right) - \theta_{OHex} exp\left(-\frac{\Delta G^*_{-RTex}}{kT}\right) \right] \tag{2.37}$$

$$\Delta G^*_{RDex} = \Delta G^{*o}_{RDex} + \beta\eta + \Delta G^{ref}_{RDex} \tag{2.38}$$

$$\Delta G^*_{-RDex} = \Delta G^{*o}_{RDex} - (1 - \beta)\eta - \Delta G^{ref}_{RDex} \tag{2.39}$$

$$j_{RTex} = j^* \left[a_{H^+}\theta_{OHex} exp\left(-\frac{\Delta G^*_{RDex}}{kT}\right) - \theta_{sub} exp\left(-\frac{\Delta G^*_{-RDex}}{kT}\right) \right] \tag{2.40}$$

$$\Delta G^*_{sub} = \Delta G^{*o}_{sub} + \omega_{sub}\theta_{oxide} - \beta\eta - \Delta G^{ref}_{sub} \tag{2.41}$$

$$\Delta G^*_{-sub} = \Delta G^{*o}_{sub} - 2\Delta G^{ref}_{sub} \tag{2.42}$$

$$j_{sub} = j^* \left[\theta_O(1 - \theta_{oxide}) exp\left(-\frac{\Delta G^*_{sub}}{kT}\right) - \theta_{sub} exp\left(-\frac{\Delta G^*_{-sub}}{kT}\right) \right] \tag{2.43}$$

The recalculated parameters that reproduce the transient results from Karan et al. are indicated on Table 2.5.

Table 2.5 – Recalculated transient kinetic parameters

Parameter	Value
ΔG^{0*}_{RT} [eV]	0.52
ΔG^{ref}_{RT} [eV]	0.44
ΔG^{0*}_{RD} [eV]	0.3591295865
ΔG^{ref}_{RD} [eV]	0.22
ΔG^{0*}_{RTex} [eV]	0.4773887594
ΔG^{ref}_{RTex} [eV]	0.125
ΔG^{0*}_{RDex} [eV]	0.4773887594
ΔG^{ref}_{RDex} [eV]	0.125
ω_{RT} [eV]	0.07773201614067547
ω_{RD} [eV]	0.41457075275026917
ω_{sub} [eV]	1.3991762905321583
ω_{RTex} [eV]	0.31092916

Later on, these expressions are going to be compared to the ones derived for the new proposed model. The new proposed model used Wang's formulation and Barath's reaction mechanism.

2.4 Analysis

Several inconsistencies have been identified in the "unified" multi step model for oxygen reduction and oxide growth. The first problem was the divergence between the equations reported and the equations that were actually implemented as indicated on the previous section. To address this issue, parametric studies were conducted by removing the extra terms from DT and SUB reactions and analysing the physical meaning of these terms. Then, additional parametric studies were conducted by removing the Temkin terms, one by one from each step in order to identify which are the most important energy interactions to consider. Free energy diagrams were obtained at different overpotentials for analyzing the consistency of the model.

2.4.1 Assumptions made without physical meaning

Effect of DT backward term

DT is a chemical step where a $PtO_2H_{(ads)}$ intermediate species, attached to two Pt sites, is transformed into two new intermediate species $PtO_{(ads)}$ and $PtOH_{(ads)}$ which are separately attached to one Pt site each. This reaction is assumed to proceed only in the forward direction, because the reverse of DT is energetically unfavourable. Thus, a parametric study was conducted to see which are the effects on the results if this term, $exp\left(\frac{-\Delta G_{DT}}{kT}\right)\theta_O\theta_{OH}$, is zero.

It can be observed on Figure 2.7 that there is no difference on the results of the coverages or the current generation when removing the backwards term from DT reaction, on that account, numerically speaking the contribution of that term is zero and it can correctly be assumed that DT reaction proceeds only forwards.

Potential dependence of sub-surface oxide growth reaction

The subsurface oxide growth reaction is also a chemical step, i.e., there is no exchange of electrons. Therefore, in theory, it should not depend on the cell potential (E). Ref [1] model implementation had a term $exp\left(\frac{-\beta_{sub}(E-E_{sub})}{kT}\right)$ to account for the energy interaction of the motion of the molecules. When removing this term the predicted CV slightly changes at low cell potentials (0.6-0.7 V) and at high cell potentials (1.2-1.35 V), see Figure 2.8.

In order to identify the formation of which species is the one that affects the CV, the coverage fraction plots vs cell potential and time were obtained and compared to the original ones. Figure 2.9 shows that at low cell potentials the species that affect the results is $OPt_{(sub)}$ and at high cell potentials the intermediate species are $O_{(ads)}$ and $OPtO_{(sub)}$. This behaviour can also be observed in Figure 2.10. According to Karan et al. what this extra term captures
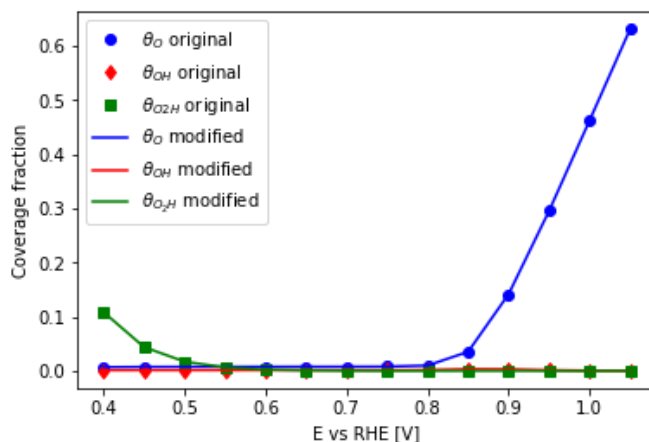
Figure 2.5 – Simulated coverage fraction vs cell potential
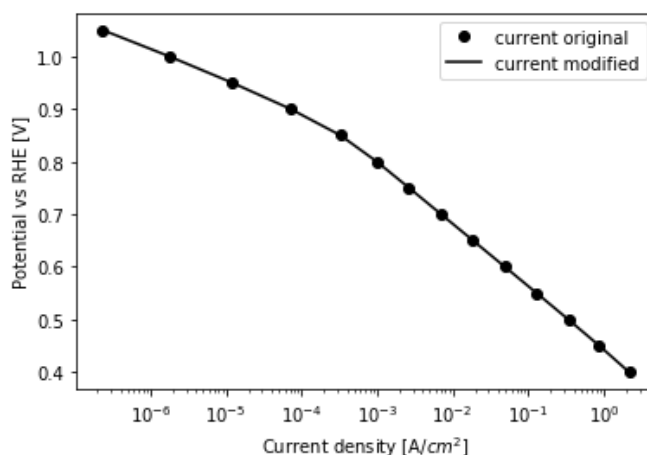
Figure 2.6 – Simulated polarization curve

Figure 2.7 – Analysis of the physical meaning of the backward term of DT reaction

is the energetic interaction of the movement of the molecules when having the place exchange species, and that is why it is necessary to capture that with an extra potential dependent term, however further in this thesis we will explore better ways of accounting for this physical phenomena.

2.4.2   Temkin terms

This model was formulated following Temkin kinetics. The reason why the Temkin interaction terms were added was to account for the fact that as oxide coverage increases, further oxidation is impeded. The numerical formulation for the Temkin terms in the kinetic equations is not well explained either in the article or the thesis. And in Wang's article it is discussed that accounting for this Temkin terms has not a significant contribution to the
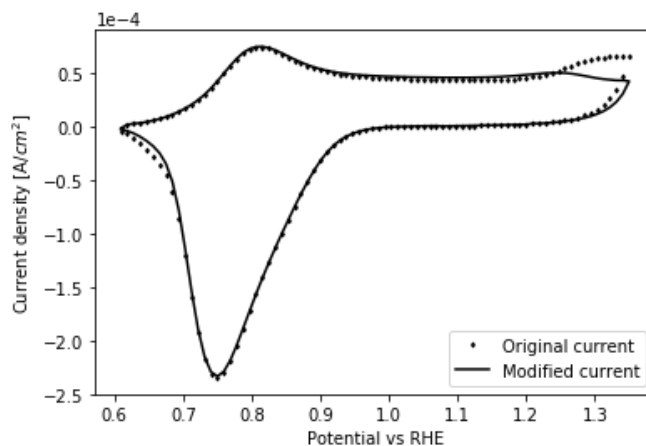
Figure 2.8 – Predicted cyclic voltammetry at $a_{O_2} = 0$, T=298 K and $a_{H^+} = 0.5$ without SUB term compared to the original. The upper potential limit at which these CVs were obtained is 1.35V.
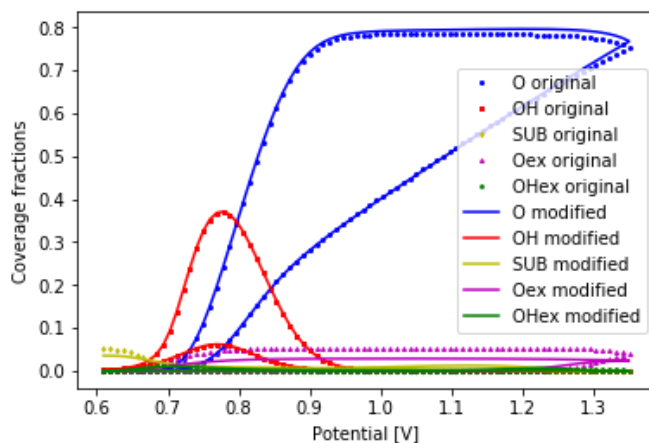
Figure 2.9 – Comparison of predicted transient coverage fractions over cell potential.

current generation, therefore they neglected them. In order to study the contribution of this terms in this model, the Temkin terms were deleted one by one and parametric studies were conducted to see the effects of neglecting these terms on the results.

By setting the value of ω_{AA} to zero, only the steady state results were affected because when running the transient model, it is in the absence of oxygen, therefore when the oxygen concentration is zero, the contribution from AA reaction is zero. It can be observed from Figure 2.11 that the coverage fraction of θ_O is the only one affected by deleting ω_{AA}. It slightly increases at high cell potentials and that also affects the current generation by increasing it as observed in Fig. 2.12. However this increase modifies the Tafel slope and the model stops capturing the doubling in the slope.

35
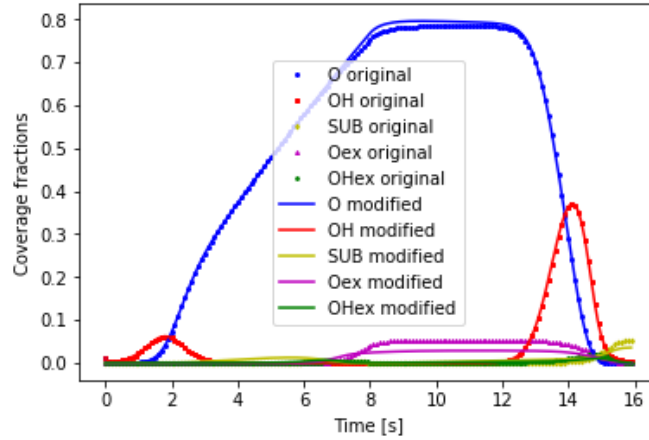
Figure 2.10 – Comparison of predicted transient coverage fractions over time.
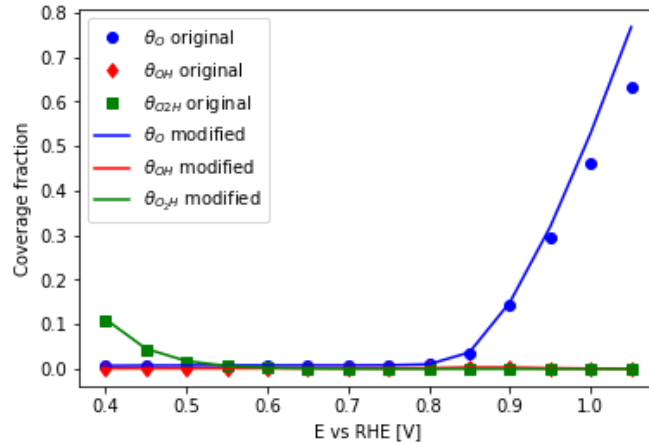
Figure 2.11 – Simulated coverage fraction vs cell potential from parametric study when deleting ω_{AA}.

Setting the value of ω_{RT} to zero, also affected the steady state and transient results. As it can be observed in Figures 2.13 and 2.14, the steady state results were slightly modified with the production of O species increasing a little bit at high cell potentials. The polarization curve however still captured the doubling of the Tafel slope.

The transient results show significant changes when deleting ω_{RT}. Figures 2.15 and 2.16 show that mainly $PtO_{(ads)}$ and $PtOH_{(ads)}$ are affected and the cathodic reduction peak is reduced in the CV at 0.75 V.
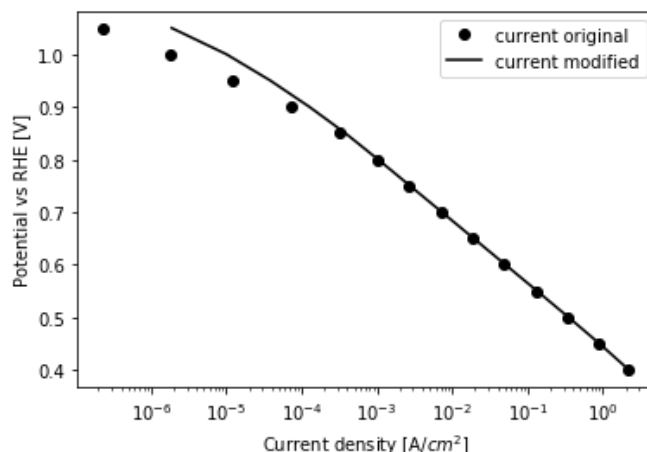
Figure 2.12 – Simulated polarization curve from parametric study when deleting ω_{AA}.
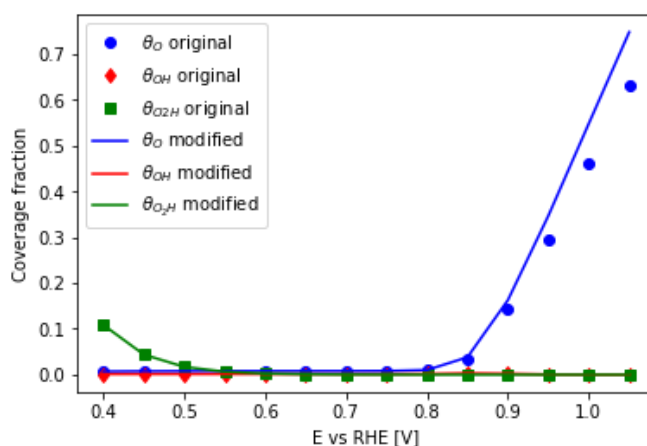
Figure 2.13 – Simulated coverage fraction vs cell potential from parametric study when deleting ω_{RT}.

The value of ω_{RD} was also set to zero. The steady-state and transient results were much more affected than previously when deleting other Temkin terms. As it can be observed in Figures 2.17 and 2.18, the steady state results were drastically modified, the production of O specie increased at high cell potentials until it reaches the maximun Pt surface coverage at 1V and the polarization curve generates much less current at high cell potentials. The upper potential slope also significantly decreases.

The transient results also show significant changes when deleting ω_{RD}. Figures 2.19 and 2.20 show that, same as with RT, mainly $PtO_{(ads)}$ and $PtOH_{(ads)}$ are affected but this time not only the cathodic reduction peak, but the anodic plateau are affected at 0.75V and 0.8V, respectively.
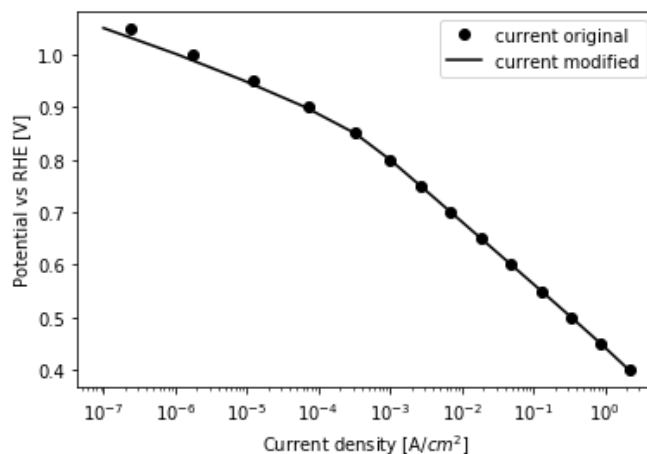
Figure 2.14 – Simulated polarization curve from parametric study when deleting ω_{RT}.
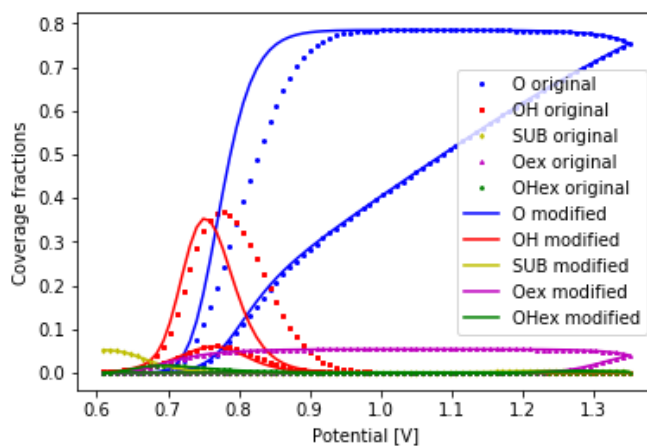
Figure 2.15 – Simulated coverage fraction vs cell potential from parametric study when deleting ω_{RT}.

Also, the constant oxidation current observed at high potentials during the forward sweep disappears indicating O is forming much faster (see Fig. 2.19)
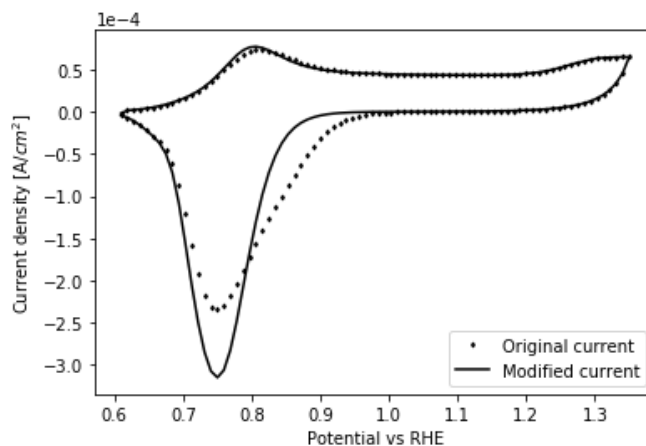
Figure 2.16 – Simulated CV for UPL of 1.35 V from parametric study when deleting ω_{RT}.
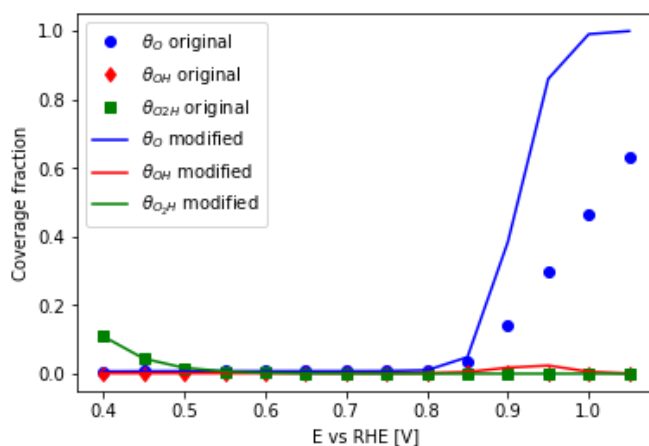
Figure 2.17 – Simulated coverage fraction vs cell potential from parametric study when deleting ω_{RD}.

ω_{SUB} had the most significant contribution on the transient results, generating the results from Figures 2.21 and 2.22. The results show that the model loses physical meaning because the coverages are significantly altered and the CV at very low and very high potentials deviates significantly from what should be.

Finally, the last Temkin term that was deleted from the model was ω_{RTex}, however the results from the model when setting this parameter to zero did not change at all. As it is shown in Figure 2.23, deleting ω_{RTex} from the model has zero effect on the simulated transient results, therefore it can be concluded that this term could be neglected.

Based on the results from the parametric studies conducted in this section, we can conclude that the most relevant Temkin terms belong to reactions RT, RD and SUB. It was
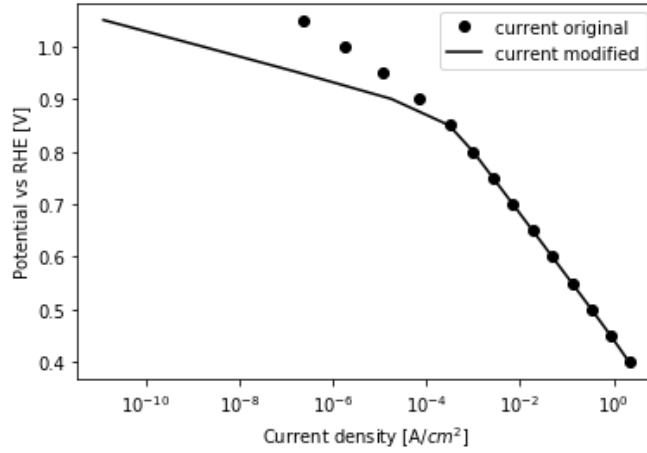
Figure 2.18 – Simulated polarization curve from parametric study when deleting ω_{RD}.
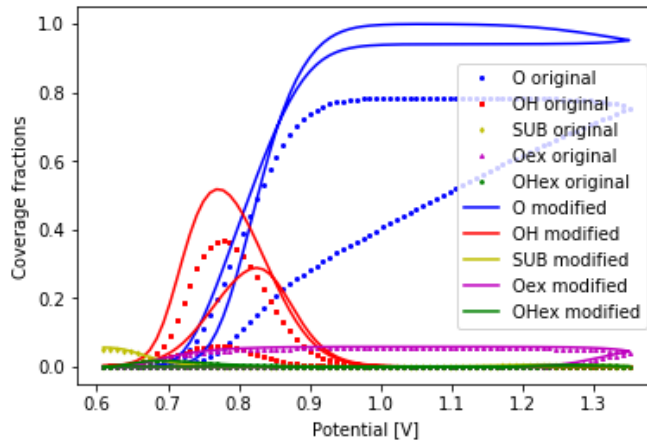
Figure 2.19 – Simulated coverage fraction vs cell potential from parametric study when deleting ω_{RD}.

observed that by accounting these energy interaction terms, the model is capable of capturing relevant features of the steady state and transient results that are observed in experimental data. Due to this, in the formulation of the new proposed model, the Temkin terms for reactions RT, RD and SUB will be added.
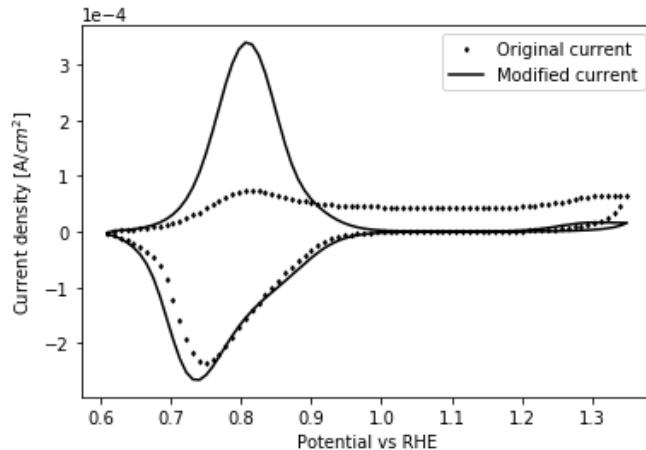
Figure 2.20 – Simulated CV for UPL of 1.35V from parametric study when deleting ω_{RD}.
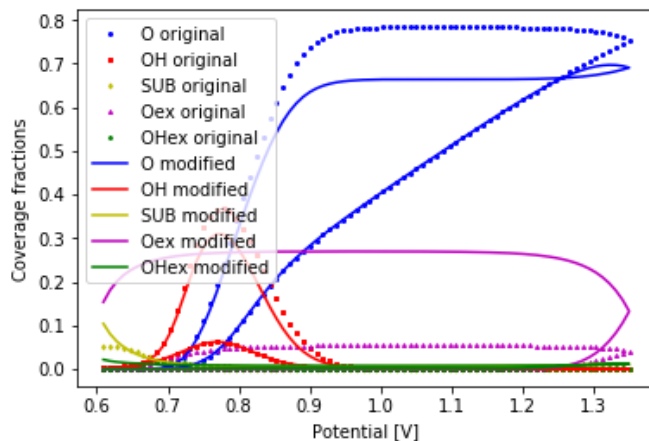
Figure 2.21 – Simulated coverage fraction vs cell potential from parametric study when deleting ω_{SUB}.

2.4.3 Free energy diagrams

The concept of the free energy diagrams was used by Wang et al. in ref. [44] to explain the reaction pathway. These diagrams can be constructed using the activation free energies and energies of adsorption, following the energy based numerical formulation that calculate the activity and energy barriers for each step and formation of species. Using the energy based form of the unified multi-step model, we are able to plot the free energy diagrams identify the rate determining step based on their assumed reaction mechanism.

From Figure 2.24 it can be observed that the rate determining step from this model mechanism is AA at zero overpotential. It can be also observed from this diagram that the numerical formulation of the ORR kinetics presented is inconsistent because the energy of the reactants should be equal to the energy of the products at zero overpotential since the
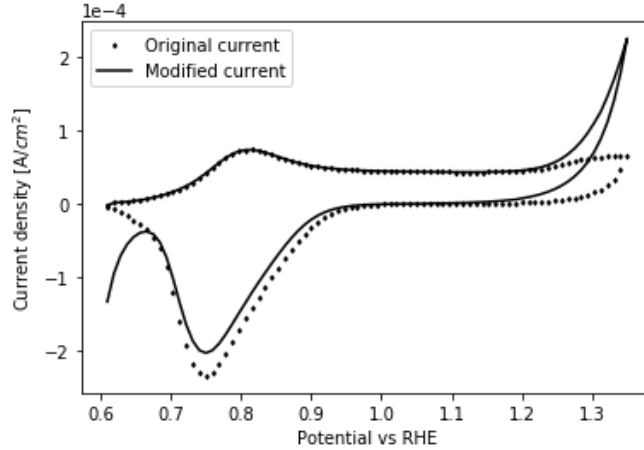
Figure 2.22 – Simulated CV for UPL of 1.35 V from parametric study when deleting ω_{SUB}.
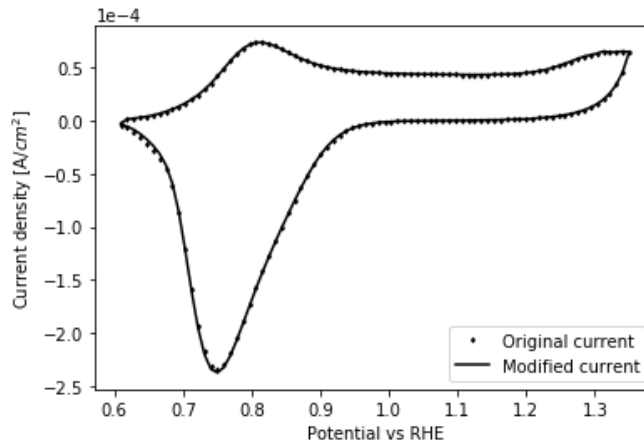
Figure 2.23 – Simulated CV for UPL of 1.35 V from parametric study when deleting ω_{RTex}.

whole system is in equilibrium. This is not the case, indicating the model is not consistent and would generate current at equilibrium. We even plot the free energy diagram without accounting for the Temkin terms, and we can observe there is a decrease on the energy levels as expected but still it does not meet the equilibrium principle of the same energy level of reactants and products.

2.5 Conclusions

The unified multi-step model for oxygen reduction and oxide growth in ref [1] has been studied, implemented and analyzed in this section. Throughout the analysis that was conducted for this model, corrections on the reported governing equations and parametric studies were conducted in order to understand the importance of kinetic parameters, such as the Temkin terms, on the formulation of numerical models for the ORR kinetics. The main conclusions
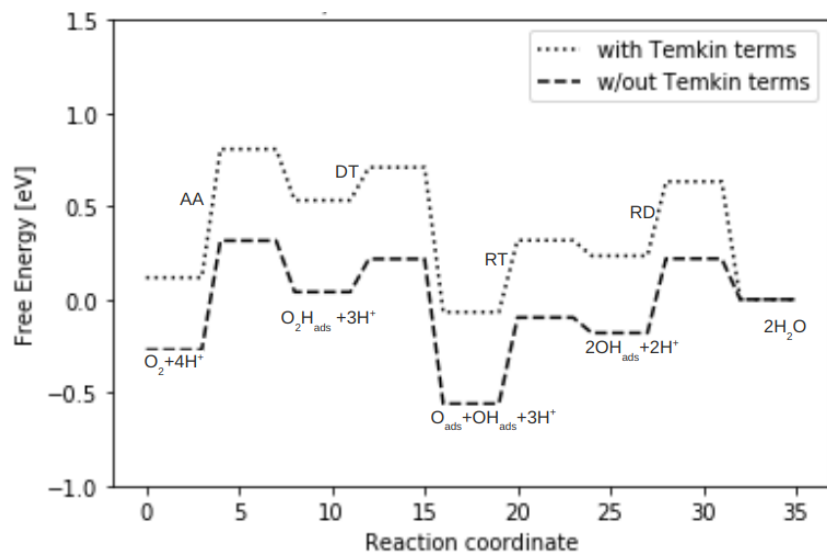
Figure 2.24 – Free energy diagram for the AA, DT, RT and RD reactions at zero overpotential with the equilibrium coverage for each reaction stage.

are:

- The model is not unified, as it is claimed to be in ref [1]. It was implemented in two different frameworks and the steady-state and transient results can only be re-porduceded with different sets of parameters. Therefore, there is still not an available unified model in the literature capable of capturing ORR and oxide growth in a single working numerical framework.

- The backwards term from DT reaction can be neglected given that it has insignificant contribution to the current generation.

- The potential dependent term in SUB reaction is necessary to be included given that it accounts for the energy interaction of the motion of the molecules in this step, however we could reformulate it and find a better way of numerically capture this phenomena without using an exponential term.

- The most representative Temkin terms correspond to reactions RT, RD and SUB. Based on this, in our new proposed model, we will include the formulation of the Temkin terms for these 3 reactions.

- Finally, the free energy diagrams showed that this model is not consistent due to the different energy levels between reactants and products at equilibrium. Consequently, this shows the need of developing a new model formulation for ORR kinetics that is coherent and capable of capturing ORR, oxide growth and peroxide formation. This

last feature was not part of Jayasankar and Karan's work but the peroxide pathway is a possible ORR mechanism that needs to be considered too.

Chapter 3

Development of an energy based model for oxygen reduction, oxide growth and peroxide formation

3.1 Introduction

Chapter 1 presented an exhaustive literature review on state of the art models to predict the kinetics of the ORR in PEM fuel cells. From that literature review, it was concluded that one of the most recent models developed is the unified multistep model proposed by Jayasankar and Karan [1]. It was capable of capturing the doubling in the Tafel slope observed experimentally in polarization curves at steady state and also reproduce transient results such as experimental CVs at varying scan rates. However after analyzing the model in Chapter 2, it was concluded that the formulation of this microkinetic model is not consistent, i.e., several added terms lack physical meaning and, more importantly, the claimed unified model was not really implemented in a unified framework, with different sets of parameters and equations used for reproducing their steady state and transient results.

There is no universal consensus in the literature on which is the mechanism of the oxygen reduction reaction (ORR) on platinum because it is a complex reaction where many intermediate species are formed and consumed at different potentials and operating conditions and it is very difficult to identify that experimentally. However, it is known that the ORR can proceed either through a 4 electron or a 2 electron pathway, being the 4 step associative mechanism the most generally accepted for modeling the ORR kinetics [17]. Jayasankar and Karan [1] assumed for the ORR pathway a sequence of 4 elementary steps: AA, DT, RT and RD, which is going to be the same ORR mechanism assumed for the developed of the model presented in this work.

45

The problem with this four-electron reaction is that it does not account for peroxide species and the further oxidation of the platinum surface by place exchange species at high operating potentials [18]. The unified multi step model developed by Jayasankar and Karan [1] already includes the oxide growth mechanism due to place exchange. The model proposed in this chapter also accounts for the peroxide formation mechanism, which is necessary to estimate peroxide formation and eventually, predict degradation rates. It is important to understand all these three physical phenomenons (ORR, oxide growth and peroxide formation) for analysing and improving the performance and durability of PEM fuel cells.

Another relevant feature analysed in Chapter 2 from the unified multi step model is the utilization of Temkin terms for capturing the energy of interaction between the active species in each intermediate step. From the parametric studies performed, it was concluded that it was important to account for these terms in order to predict a more accurate behaviour of the model, especially when running transient simulations and trying to observe similar trends to the broad anodic plateau and the cathodic reduction peak observed experimentally. This is the reason why those Temkin terms will be also considered for the formulation of the new developed model.

Even though the reaction mechanism in ref. [1] forms the basis for the reaction mechanisms in this chapter, the methodology for deriving the kinetic expressions for this model is not similar to the mixed formulation presented in ref. [1]. In order to develop a consistent and coherent model with physical meaning, the methodology proposed by Wang et al. [44], which is the same formulation used by Moore et al. [57], is used. It uses the free energy of activation for each intermediate step and the free energy of adsorption of the intermediate species. This is why the developed model was called an energy based model.

In this chapter, an energy based model for oxygen reduction, oxide growth and hydrogen peroxide formation is presented. The first section will introduce the electrochemical reaction pathway and the intermediate species. The second section will derive the mathematical multi-step model formulation and present the final governing equations that describe the production rates of each elementary step and the production of each intermediate species and total current in the cell. The third section will present a solution strategy for the implementation of the model in a unified kinetic framework in Python. The fourth section will describe the parameter estimation process that will be used to predict the new kinetic parameters for the model and the results from this process.

3.1.1 Electrochemical reaction pathway

The proposed model is intended to capture three different reaction mechanisms: the oxygen reduction reaction (ORR), oxide growth and hydrogen peroxide formation.

ORR Pathway

The associative reaction pathway for the ORR described in Jayasankar and Karan [1] and Huang et al. [64] is used to capture four elementary steps, AA, DT, RT and RD and its adsorbed intermediates, $PtO_{(ads)}$, $PtOH_{(ads)}$ and $PtO_2H_{(ads)}$, i.e.,

$$\text{AA:} \underset{\theta_{Pt}}{\text{Pt(site)}} + \text{O}_2 + \text{H}^+(\text{aq}) + \text{e}^- \underset{\text{k}_{-\text{AA}}}{\overset{\text{k}_{\text{AA}}}{\rightleftharpoons}} \underset{\theta_{O_2H}}{\text{O}_2\text{H}_{\text{ads}}} \tag{3.1}$$

$$\text{DT:} \underset{\theta_{Pt}}{\text{Pt(site)}} + \underset{\theta_{O_2H}}{\text{O}_2\text{H}_{\text{ads}}} \underset{\text{k}_{-\text{DT}}}{\overset{\text{k}_{\text{DT}}}{\rightleftharpoons}} \underset{\theta_{O}}{\text{O}_{\text{ads}}} + \underset{\theta_{OH}}{\text{OH}_{\text{ads}}} \tag{3.2}$$

$$\text{RT:} \underset{\theta_{O}}{\text{O}_{\text{ads}}} + \text{H}^+(\text{aq}) + \text{e}^- \underset{\text{k}_{-\text{RT}}}{\overset{\text{k}_{\text{RT}}}{\rightleftharpoons}} \underset{\theta_{OH}}{\text{OH}_{\text{ads}}} \tag{3.3}$$

$$\text{RD:} \underset{\theta_{OH}}{\text{OH}_{\text{ads}}} + \text{H}^+(\text{aq}) + \text{e}^- \underset{\text{k}_{-\text{RD}}}{\overset{\text{k}_{\text{RD}}}{\rightleftharpoons}} \underset{\theta_{Pt}}{\text{Pt(site)}} + H_2O \tag{3.4}$$
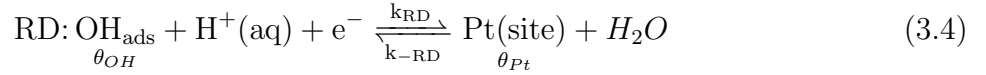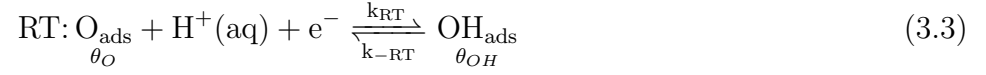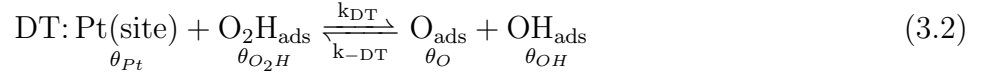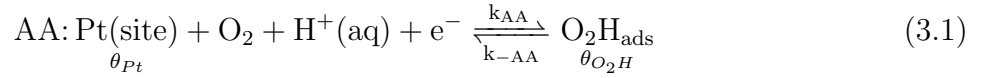
The first reactions is the associative adsorption (AA) of oxygen onto the platinum surface where one active platinum site reacts with oxygen in an aqueous media to adsorb the oxygen and form an intermediate species $PtO_2H_{(ads)}$ as shown in eq. (3.1). This surface adsorbed species, in the presence of another platinum site available, is then assumed to dissociate into $PtO_{(ads)}$ and $PtOH_{(ads)}$ surface species through a dissociative transition (DT) step. Eq. (3.2) is a chemical reaction that does not involve externally provided electrons and protons so it is assumed that its reaction rate is unaffected by the presence of the potential difference across the electrode/electrolyte interface. Then, the adsorbed oxygen, $PtO_{(ads)}$ with a hydrogen proton and an electron is reduced into an adsorbed hydroxyl $PtOH_{(ads)}$ in a reductive transition (RT) step from eq. (3.3), later, the adsorbed hydroxyl $PtOH_{(ads)}$ is reduced to produce water, also with a hydrogen proton and an electron, through a reductive desorption (RD) step as shown in eq. (3.4). In an ORR mechanism, these would be the most representative steps, where this last RD step occurs twice because there are two $PtOH_{(ads)}$ available to form two water molecules and free the two platinum site available that were initially taken in AA and DT steps.

Oxide growth mechanism

For the oxide growth reaction mechanism it was assumed that there are three additional place exchange reactions that account for the oxide formation. The accounted for adsorbed

intermediate species are $OPt_{(sub)}$, $OPtO_{(sub)}$ and $OPtOH_{(sub)}$ as described in Jayasankar and Karan [1]. They are formed following:

$$\text{RT}_{\text{ex}}\colon \underset{\theta_{Oex}}{O-Pt-O} + H^+(aq) + e^- \underset{\text{k}_{-\text{RTex}}}{\overset{\text{k}_{\text{RTex}}}{\rightleftharpoons}} \underset{\theta_{OHex}}{O-Pt-OH} \tag{3.5}$$

$$\text{RD}_{\text{ex}}\colon \underset{\theta_{OHex}}{O-Pt-OH} + H^+(aq) + e^- \underset{\text{k}_{-\text{RDex}}}{\overset{\text{k}_{\text{RDex}}}{\rightleftharpoons}} \underset{\theta_{sub}}{O-Pt} + H_2O \tag{3.6}$$

$$\text{SUB}\colon \underset{\theta_{sub}}{O-Pt} \underset{\text{k}_{-\text{sub}}}{\overset{\text{k}_{\text{sub}}}{\rightleftharpoons}} \underset{\theta_{O}}{O_{\text{ads}}} \tag{3.7}$$
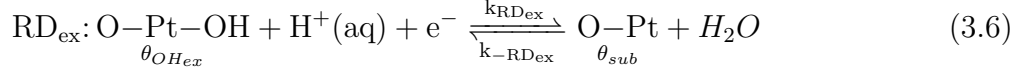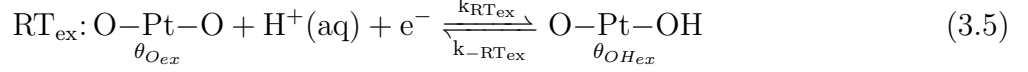
At high cell potentials, i.e., above 0.7 V, the adsorbed oxygen $PtO_{(ads)}$ can place exchange a platinum site that forms a sub surface oxide $OPt_{(sub)}$ through an oxide place exchange (SUB) step as shown in eq. (3.7). This reaction does not involve protons or electrons, because it is a chemical reaction, therefore this reaction is not affected by the potential. Then a sub surface oxide $OPt_{(sub)}$, in the presence of water can form a $OPtOH_{(sub)}$ through a reductive desorption place exchanged platinum (RDex) step, see eq. (3.6). Afterwards, that $OPtOH_{(sub)}$ can form a $OPtO_{(sub)}$ through a reductive transition place exchanged platinum (RTex) step like in eq. (3.5).

Hydrogen peroxide formation

For the hydrogen peroxide formation reaction mechanism, the two-electron transfer reaction of oxygen reduction to hydrogen peroxide presented in ref. [5, 36] was assumed. This mechanism consist of two steps, where the first one is the oxygen associative adsorption onto the platinum surface to form an intermediate specie $PtO_2H_{(ads)}$ as shown in eq. (3.1), and then the adsorbed specie is taken to form hydrogen peroxide as shown in eq. (3.8).

$$\text{PEROX}\colon \underset{\theta_{O_2H}}{O_2H_{\text{ads}}} + H^+(aq) + e^- \underset{\text{k}_{-\text{PEROX}}}{\overset{\text{k}_{\text{PEROX}}}{\rightleftharpoons}} \underset{\theta_{Pt}}{Pt(\text{site})} + H_2O_2 \tag{3.8}$$
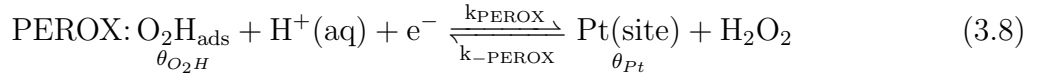
Accounting for this mechanism is crucial for a future membrane electrode assembly model because there is strong evidence that shows that the peroxide radicals attack the ionomer and degrade the electrodes [21].

3.1.2 Illustration of reaction mechanisms

Based on the intermediate reactions there are three possible reaction pathways. The first one is the four electron ORR path. The second one is the two electron ORR pathway leading

to the formation of peroxide. The third one is the oxide formation path.

$$Path1 = AA_f + DT_f + RT_f + 2 * RD_f \tag{3.9}$$

$$Path2 = AA_f + PEROX_f \tag{3.10}$$

$$Path3 = AA_f + DT_f + RT_b + 2 * SUB_b \tag{3.11}$$

$$\tag{3.12}$$

In order to illustrate the reaction mechanism assumed for this work, Figure 3.1 shows a 2D idealization of the molecules of reactants and products for each elementary step previously explained in this section.
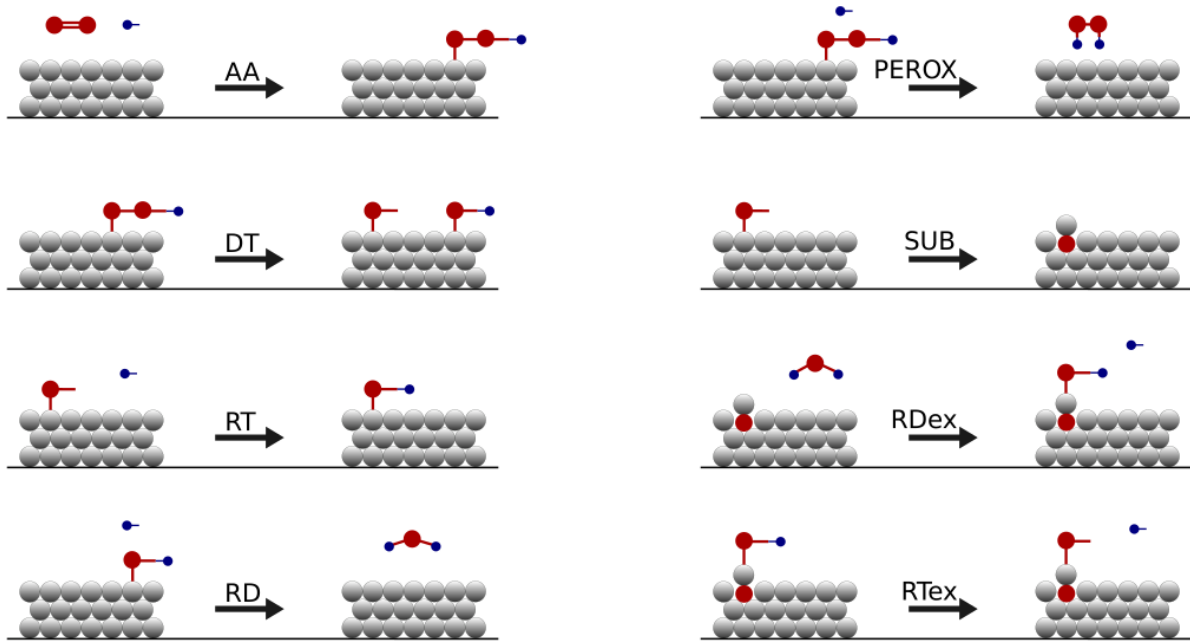
Figure 3.1 – Schematic diagram of the reaction mechanism assumed for the proposed model

It is important to note that these reactions can proceed in either the forward or backward direction, depending on the applied cell potential, the free energies of activation of the steps and the free energies of adsorption of the intermediate species. The free energy kinetic parameters will be fitted and fixed for this model, while the cell potential can vary during fuel cell operation, leading to some steps becoming more dominant than others at different potentials. Also note that the three identified reaction pathways can occur concurrently and no assumptions are made regarding a rate determining step. The rates of each elementary reaction are determined using the approach followed by Wang et al. [44] in the following section 3.2.

3.2 Numerical formulation

3.2.1 Derivation

Following the methodology outlined in Wang et al. [44], the governing equations for the new proposed model were derived. For each elementary step, the net reaction rate can be expressed as the difference between the rates of forward and backward reactions:

$$v_{AA} = k_{AA}C_{O_2}C_{H^+}\theta_{Pt}exp\left(\frac{-\beta E}{kT}\right) - k_{-AA}\theta_{O_2H}exp\left(\frac{(1-\beta)E}{kT}\right) \tag{3.13}$$

$$v_{DT} = k_{DT}\theta_{O_2H}\theta_{Pt} - k_{-DT}\theta_O\theta_{OH} \tag{3.14}$$

$$v_{RT} = k_{RT}C_{H^+}\theta_O exp\left(\frac{-\beta E}{kT}\right) - k_{-RT}\theta_{OH}exp\left(\frac{(1-\beta)E}{kT}\right) \tag{3.15}$$

$$v_{RD} = k_{RD}C_{H^+}\theta_{OH}exp\left(\frac{-\beta E}{kT}\right) - k_{-RD}\theta_{Pt}exp\left(\frac{(1-\beta)E}{kT}\right) \tag{3.16}$$

$$v_{RTex} = k_{RTex}C_{H^+}\theta_{O_{ex}}exp\left(\frac{-\beta E}{kT}\right) - k_{-RTex}\theta_{OHex}exp\left(\frac{(1-\beta)E}{kT}\right) \tag{3.17}$$

$$v_{RDex} = k_{RDex}C_{H^+}\theta_{OHex}exp\left(\frac{-\beta E}{kT}\right) - k_{-RDex}\theta_{SUB}exp\left(\frac{(1-\beta)E}{kT}\right) \tag{3.18}$$

$$v_{sub} = k_{sub}\theta_{sub} - k_{-sub}\theta_O \tag{3.19}$$

$$v_{perox} = k_{perox}\theta_{O_2H}C_{H^+}exp\left(\frac{-\beta E}{kT}\right) - k_{-perox}C_{H_2O_2}\theta_{Pt}exp\left(\frac{(1-\beta)E}{kT}\right) \tag{3.20}$$

where k_i is the reaction rate constant for the i-th elementary reaction step, θ_i is the coverage fraction of the i-th intermediate species, and C_{H^+}, C_{O_2} and $C_{H_2O_2}$ are the hydrogen proton, oxygen and peroxide concentrations, respectively.

It is important to note that the reaction rates for all the intermediate steps that are being derived for this model are written as a function of a common equilibrium potential E^o = 1.23 V, while many other authors of numerical models for ORR kinetics such as in ref. [1, 64], used an specific equilibrium potential for each intermediate step.

At the reversible potential, E^0, the net current is zero and the magnitude of the forward and backward reaction rates are equal. Therefore, the exchange rate constants for the elementary reactions can be expressed as:

$$v_{AA}^o = k_{AA}C_{H^+}^o C_{O_2}^o \theta_{Pt}^o exp\left(\frac{-\beta E^o}{kT}\right) = k_{-AA}\theta_{O_2H}^o exp\left(\frac{(1-\beta)E^o}{kT}\right) \tag{3.21}$$

$$v_{DT}^o = k_{DT}\theta_{O_2H}^o\theta_{Pt}^o = k_{-DT}\theta_O^o\theta_{OH}^o \tag{3.22}$$

$$v^o_{RT} = k_{RT}C^o_{H^+}\theta^o_O exp\left(\frac{-\beta E^o}{kT}\right) = k_{-RT}\theta^o_{OH}exp\left(\frac{(1-\beta)E^o}{kT}\right) \tag{3.23}$$

$$v^o_{RD} = k_{RD}C^o_{H^+}\theta^o_{OH} exp\left(\frac{-\beta E^o}{kT}\right) = k_{-RD}\theta^o_{Pt}exp\left(\frac{(1-\beta)E^o}{kT}\right) \tag{3.24}$$

$$v^o_{RTex} = k_{RTex}C^o_{H^+}\theta^o_{O_{ex}} exp\left(\frac{-\beta E^o}{kT}\right) = k_{-RTex}\theta^o_{OHex}exp\left(\frac{(1-\beta)E^o}{kT}\right) \tag{3.25}$$

$$v^o_{RDex} = k_{RDex}C^o_{H^+}\theta^o_{OH_{ex}} exp\left(\frac{-\beta E^o}{kT}\right) = k_{-RDex}\theta^o_{sub}exp\left(\frac{(1-\beta)E^o}{kT}\right) \tag{3.26}$$

$$v^o_{sub} = k_{sub}\theta^o_{sub} = k_{-sub}\theta^o_O \tag{3.27}$$

$$v^o_{perox} = k_{perox}\theta^o_{O_2H}C^o_{H^+} exp\left(\frac{-\beta E^o}{kT}\right) = k_{-perox}C^o_{H_2O_2}\theta^o_{Pt}exp\left(\frac{(1-\beta)E^o}{kT}\right) \tag{3.28}$$

where θ^0_i and C^0_i denote the coverages and concentrations at $E = E^0$. Dividing the net reaction rates by their respective exchange rates and defining the overpotential as $\eta = E - E^0$, leads to:

$$v_{AA} = v^o_{AA}\left[\left(\frac{C_{O_2}}{C^o_{O_2}}\right)\left(\frac{C_{H^+}}{C^o_{H^+}}\right)\left(\frac{\theta_{Pt}}{\theta^o_{Pt}}\right) exp\left(\frac{-\beta\eta}{kT}\right) - \left(\frac{\theta_{O_2H}}{\theta^o_{O_2H}}\right) exp\left(\frac{(1-\beta)\eta}{kT}\right)\right] \tag{3.29}$$

$$v_{DT} = v^o_{DT}\left[\left(\frac{\theta_{O_2H}}{\theta^o_{O_2H}}\right)\left(\frac{\theta_{Pt}}{\theta^o_{Pt}}\right) - \left(\frac{\theta_O}{\theta^o_O}\right)\left(\frac{\theta_{OH}}{\theta^o_{OH}}\right)\right] \tag{3.30}$$

$$v_{RT} = v^o_{RT}\left[\left(\frac{C_{H^+}}{C^o_{H^+}}\right)\left(\frac{\theta_O}{\theta^o_O}\right) exp\left(\frac{-\beta\eta}{kT}\right) - \left(\frac{\theta_{OH}}{\theta^o_{OH}}\right) exp\left(\frac{(1-\beta)\eta}{kT}\right)\right] \tag{3.31}$$

$$v_{RD} = v^o_{RD}\left[\left(\frac{C_{H^+}}{C^o_{H^+}}\right)\left(\frac{\theta_{OH}}{\theta^o_{OH}}\right) exp\left(\frac{-\beta\eta}{kT}\right) - \left(\frac{\theta_{Pt}}{\theta^o_{Pt}}\right) exp\left(\frac{(1-\beta)\eta}{kT}\right)\right] \tag{3.32}$$

$$v_{RTex} = v^o_{RTex}\left[\left(\frac{C_{H^+}}{C^o_{H^+}}\right)\left(\frac{\theta_{Oex}}{\theta^o_{Oex}}\right) exp\left(\frac{-\beta\eta}{kT}\right) - \left(\frac{\theta_{OHex}}{\theta^o_{OHex}}\right) exp\left(\frac{(1-\beta)\eta}{kT}\right)\right] \tag{3.33}$$

$$v_{RDex} = v^o_{RDex}\left[\left(\frac{C_{H^+}}{C^o_{H^+}}\right)\left(\frac{\theta_{OHex}}{\theta^o_{OHex}}\right) exp\left(\frac{-\beta\eta}{kT}\right) - \left(\frac{\theta_{sub}}{\theta^o_{sub}}\right) exp\left(\frac{(1-\beta)\eta}{kT}\right)\right] \tag{3.34}$$

$$v_{sub} = v^o_{sub}\left[\left(\frac{\theta_{sub}}{\theta^o_{sub}}\right) - \left(\frac{\theta_O}{\theta^o_O}\right)\right] \tag{3.35}$$

$$v_{perox} = v^o_{perox}\left[\left(\frac{\theta_{O_2H}}{\theta^o_{O_2H}}\right)\left(\frac{C_{H^+}}{C^o_{H^+}}\right) exp\left(\frac{-\beta\eta}{kT}\right) - \left(\frac{C_{H_2O_2}}{C^o_{H_2O_2}}\right)\left(\frac{\theta_{Pt}}{\theta^o_{Pt}}\right) exp\left(\frac{(1-\beta)\eta}{kT}\right)\right] \tag{3.36}$$

Then, the intrinsic exchange currents are defined considering that $j = nFv$, where n is the number of electrons transferred on each intermediate reaction:

$$j^o_{AA} = nFv^o_{AA} = nFk_{AA}C^o_{H^+}C^o_{O_2}\theta^o_{Pt} \tag{3.37}$$

51

$$j^o_{DT} = nFv^o_{DT} = nFk_{DT}\theta^o_{O_2H}\theta^o_{Pt} \tag{3.38}$$

$$j^o_{RT} = nFv^o_{RT} = nFk_{RT}C^o_{H^+}\theta^o_O \tag{3.39}$$

$$j^o_{RD} = nFv^o_{RD} = nFk_{RD}C^o_{H^+}\theta^o_{OH} \tag{3.40}$$

$$j^o_{RTex} = nFv^o_{RTex} = nFk_{RTex}C^o_{H^+}\theta^o_{O_{ex}} \tag{3.41}$$

$$j^o_{RDex} = nFv^o_{RDex} = nFk_{RDex}C^o_{H^+}\theta^o_{OHex} \tag{3.42}$$

$$j^o_{sub} = nFv^o_{sub} = nFk_{sub}\theta^o_{sub} \tag{3.43}$$

$$j^o_{perox} = nFv^o_{perox} = nFk_{perox}C^o_{H^+}\theta^o_{O_2H} \tag{3.44}$$

By relating the reaction rate constants, k_i, to Gibbs free energies, ΔG^{*0}_i, and rearranging, the following equations are obtained:

$$j^o_{AA} = \frac{nFv^o_{AA}}{\theta^o_{Pt}} = nFk_{AA}C^o_{H^+}C^o_{O_2} = j^*exp\left(-\frac{\Delta G^{*0}_{AA}}{kT}\right) \tag{3.45}$$

$$j^o_{DT} = \frac{nFv^o_{DT}}{\theta^o_{Pt}\theta^o_{O_2H}} = nFk_{DT} = j^*exp\left(-\frac{\Delta G^{*0}_{DT}}{kT}\right) \tag{3.46}$$

$$j^o_{RT} = \frac{nFv^o_{RT}}{\theta^o_O} = nFk_{RT}C^o_{H^+} = j^*exp\left(-\frac{\Delta G^{*0}_{RT}}{kT}\right) \tag{3.47}$$

$$j^o_{RD} = \frac{nFv^o_{RD}}{\theta^o_{OH}} = nFk_{RD}C^o_{H^+} = j^*exp\left(-\frac{\Delta G^{*0}_{RD}}{kT}\right) \tag{3.48}$$

$$j^o_{RTex} = \frac{nFv^o_{RTex}}{\theta^o_{O_{ex}}} = nFk_{RTex}C^o_{H^+} = j^*exp\left(-\frac{\Delta G^{*0}_{RTex}}{kT}\right) \tag{3.49}$$

$$j^o_{RDex} = \frac{nFv^o_{RDex}}{\theta^o_{OHex}} = nFk_{RDex}C^o_{H^+} = j^*exp\left(-\frac{\Delta G^{*0}_{RDex}}{kT}\right) \tag{3.50}$$

$$j^o_{sub} = \frac{nFv^o_{sub}}{\theta^o_{sub}} = nFk_{sub} = j^*exp\left(-\frac{\Delta G^{*0}_{sub}}{kT}\right) \tag{3.51}$$

$$j^o_{perox} = \frac{nFv^o_{perox}}{\theta^o_{O_2H}} = nFk_{perox}C^o_{H^+} = j^*exp\left(-\frac{\Delta G^{*0}_{perox}}{kT}\right) \tag{3.52}$$

where $j^*[A/cm^2]$ is a reference prefactor setting the scale for activation free energy. This parameter is assumed to be constant and is fitted to experimental data.

Knowing that $j = nFv$, and rearranging, the individual current generation of each step can be expressed in terms of the individual reaction rates:

$$j_{AA} = nFv_{AA} = \frac{nFv^o_{AA}}{\theta^o_{Pt}}\left[a_{H^+}a_{O_2}\theta_{Pt}exp\left(\frac{-\beta\eta}{kT}\right) - \theta_{O_2H}\left(\frac{\theta^o_{Pt}}{\theta^o_{O_2H}}\right)exp\left(\frac{(1-\beta)\eta}{kT}\right)\right] \tag{3.53}$$

$$j_{DT} = nFv_{DT} = \frac{nFv_{DT}^o}{\theta_{Pt}^o \theta_{O_2H}^o} \left[\theta_{O_2H}\theta_{Pt} - \theta_O\theta_{OH} \left(\frac{\theta_{Pt}^o}{\theta_O^o} \right) \left(\frac{\theta_{Pt}^o}{\theta_{OH}^o} \right) \left(\frac{\theta_{O_2H}^o}{\theta_{Pt}^o} \right) \right] \tag{3.54}$$

$$j_{RT} = nFv_{RT} = \frac{nFv_{RT}^o}{\theta_O^o} \left[a_{H^+}\theta_O exp\left(\frac{-\beta\eta}{kT} \right) - \theta_{OH} \left(\frac{\theta_{Pt}^o}{\theta_{OH}^o} \right) \left(\frac{\theta_O^o}{\theta_{Pt}^o} \right) exp\left(\frac{(1-\beta)\eta}{kT} \right) \right]$$
$$\tag{3.55}$$

$$j_{RD} = nFv_{RD} = \frac{nFv_{RD}^o}{\theta_{OH}^o} \left[a_{H^+}\theta_{OH} exp\left(\frac{-\beta\eta}{kT} \right) - \theta_{Pt} \left(\frac{\theta_{OH}^o}{\theta_{Pt}^o} \right) exp\left(\frac{(1-\beta)\eta}{kT} \right) \right] \tag{3.56}$$

$$j_{RTex} = nFv_{RTex} = \frac{nFv_{RT_{ex}}^o}{\theta_{Oex}^o} \left[a_{H^+}\theta_{Oex} exp\left(\frac{-\beta\eta}{kT} \right) - \theta_{OHex} \left(\frac{\theta_{Oex}^o}{\theta_{Pt}^o} \right) \left(\frac{\theta_{Pt}^o}{\theta_{OHex}^o} \right) exp\left(\frac{(1-\beta)\eta}{kT} \right) \right]$$
$$\tag{3.57}$$

$$j_{RDex} = nFv_{RDex} = \frac{nFv_{RD_{ex}}^o}{\theta_{OHex}^o} \left[a_{H^+}\theta_{OHex} exp\left(\frac{-\beta\eta}{kT} \right) - \theta_{sub} \left(\frac{\theta_{OHex}^o}{\theta_{Pt}^o} \right) \left(\frac{\theta_{Pt}^o}{\theta_{sub}^o} \right) exp\left(\frac{(1-\beta)\eta}{kT} \right) \right]$$
$$\tag{3.58}$$

$$j_{sub} = nFv_{sub} = \frac{nFv_{sub}^o}{\theta_{sub}^o} \left[\theta_{sub} - \theta_O \left(\frac{\theta_{sub}^o}{\theta_{Pt}^o} \right) \left(\frac{\theta_{Pt}^o}{\theta_O^o} \right) \right] \tag{3.59}$$

$$j_{perox} = nFv_{perox} = \frac{nFv_{perox}^o}{\theta_{O_2H}^o} \left[\theta_{O_2H}a_{H^+} exp\left(\frac{-\beta\eta}{kT} \right) - a_{H_2O_2}\theta_{Pt} \left(\frac{\theta_{O_2H}^o}{\theta_{Pt}^o} \right) exp\left(\frac{(1-\beta)\eta}{kT} \right) \right]$$
$$\tag{3.60}$$

where a_i is the activity of the oxygen, hydrogen proton or peroxide that is equal to the concentration over the reference concentration of these species, $\frac{C_i}{C_i^o}$.

Then, by substituting the rate constants by the Gibbs free energies at zero overpotentials, the expressions for the kinetic current for each elementary reaction can be written as:

$$j_{AA} = j^* exp\left(-\frac{\Delta G_{AA}^{*0}}{kT} \right) \left[a_{H^+}a_{O_2}\theta_{Pt} exp\left(\frac{-\beta\eta}{kT} \right) - \theta_{O_2H} \left(\frac{\theta_{Pt}^o}{\theta_{O_2H}^o} \right) exp\left(\frac{(1-\beta)\eta}{kT} \right) \right]$$
$$\tag{3.61}$$

$$j_{DT} = j^* exp\left(-\frac{\Delta G_{DT}^{*0}}{kT} \right) \left[\theta_{O_2H}\theta_{Pt} - \theta_O\theta_{OH} \left(\frac{\theta_{Pt}^o}{\theta_O^o} \right) \left(\frac{\theta_{Pt}^o}{\theta_{OH}^o} \right) \left(\frac{\theta_{O_2H}^o}{\theta_{Pt}^o} \right) \right] \tag{3.62}$$

$$j_{RT} = j^* exp\left(-\frac{\Delta G_{RT}^{*0}}{kT} \right) \left[a_{H^+}\theta_O exp\left(\frac{-\beta\eta}{kT} \right) - \theta_{OH} \left(\frac{\theta_{Pt}^o}{\theta_{OH}^o} \right) \left(\frac{\theta_O^o}{\theta_{Pt}^o} \right) exp\left(\frac{(1-\beta)\eta}{kT} \right) \right]$$
$$\tag{3.63}$$

$$j_{RD} = j^* exp\left(-\frac{\Delta G_{RD}^{*0}}{kT} \right) \left[a_{H^+}\theta_{OH} exp\left(\frac{-\beta\eta}{kT} \right) - \theta_{Pt} \left(\frac{\theta_{OH}^o}{\theta_{Pt}^o} \right) exp\left(\frac{(1-\beta)\eta}{kT} \right) \right] \tag{3.64}$$

$$j_{RTex} = j^* exp\left(-\frac{\Delta G_{RTex}^{*0}}{kT} \right) \left[a_{H^+}\theta_{Oex} exp\left(\frac{-\beta\eta}{kT} \right) - \theta_{OHex} \left(\frac{\theta_{Oex}^o}{\theta_{Pt}^o} \right) \left(\frac{\theta_{Pt}^o}{\theta_{OHex}^o} \right) exp\left(\frac{(1-\beta)\eta}{kT} \right) \right]$$
$$\tag{3.65}$$

$$j_{RDex} = j^* exp\left(-\frac{\Delta G_{RDex}^{*0}}{kT}\right)\left[a_{H^+}\theta_{OHex}exp\left(\frac{-\beta\eta}{kT}\right) - \theta_{sub}\left(\frac{\theta_{OHex}^o}{\theta_{Pt}^o}\right)\left(\frac{\theta_{Pt}^o}{\theta_{sub}^o}\right)exp\left(\frac{(1-\beta)\eta}{kT}\right)\right]$$

(3.66)

$$j_{sub} = j^* exp\left(-\frac{\Delta G_{sub}^{*0}}{kT}\right)\left[\theta_{sub} - \theta_O\left(\frac{\theta_{sub}^o}{\theta_{Pt}^o}\right)\left(\frac{\theta_{Pt}^o}{\theta_O^o}\right)\right]$$

(3.67)

$$j_{perox} = j^* exp\left(-\frac{\Delta G_{perox}^{*0}}{kT}\right)\left[\theta_{O_2H}a_{H^+}exp\left(\frac{-\beta\eta}{kT}\right) - a_{H_2O_2}\theta_{Pt}\left(\frac{\theta_{O_2H}^o}{\theta_{Pt}^o}\right)exp\left(\frac{(1-\beta)\eta}{kT}\right)\right]$$

(3.68)

The adsorption free energies were defined for the reaction intermediates at $\eta = 0$ with the equilibrium coverages as in equations (20) and (21) in ref. [44]:

$$exp\left(-\frac{\Delta G_O^o}{kT}\right) = \frac{\theta_O^o}{\theta_{Pt}^o}$$

(3.69)

$$exp\left(-\frac{\Delta G_{OH}^o}{kT}\right) = \frac{\theta_{OH}^o}{\theta_{Pt}^o}$$

(3.70)

$$exp\left(-\frac{\Delta G_{O_2H}^o}{kT}\right) = \frac{\theta_{O_2H}^o}{\theta_{Pt}^o}$$

(3.71)

$$exp\left(-\frac{\Delta G_{Oex}^o}{kT}\right) = \frac{\theta_{Oex}^o}{\theta_{Pt}^o}$$

(3.72)

$$exp\left(-\frac{\Delta G_{OHex}^o}{kT}\right) = \frac{\theta_{OHex}^o}{\theta_{Pt}^o}$$

(3.73)

$$exp\left(-\frac{\Delta G_{sub}^o}{kT}\right) = \frac{\theta_{sub}^o}{\theta_{Pt}^o}$$

(3.74)

Finally, by substituting the adsorption free energies on the expressions for the kinetic current for each elementary reaction, the final expressions for the individual kinetic current and the potential-dependent activation free energies can be expressed as:

$$\Delta G_{AA}^* = \Delta G_{AA}^{*o} + \beta\eta$$

(3.75)

$$\Delta G_{-AA}^* = \Delta G_{AA}^{*o} - (1-\beta)\eta - \Delta G_{O_2H}^o$$

(3.76)

$$j_{AA} = nFv_{AA} = j^*\left[a_{H^+}a_{O_2}\theta_{Pt}exp\left(-\frac{\Delta G_{AA}^*}{kT}\right) - \theta_{O_2H}exp\left(-\frac{\Delta G_{-AA}^*}{kT}\right)\right]$$

(3.77)

$$\Delta G^*_{DT} = \Delta G^{*o}_{DT} \tag{3.78}$$

$$\Delta G^*_{-DT} = \Delta G^{*o}_{DT} - \Delta G^o_O - \Delta G^o_{OH} + \Delta G^o_{O_2H} \tag{3.79}$$

$$j_{DT} = nFv_{DT} = j^* \left[\theta_{O_2H}\theta_{Pt}exp\left(-\frac{\Delta G^*_{DT}}{kT}\right) - \theta_O\theta_{OH}exp\left(-\frac{\Delta G^*_{-DT}}{kT}\right) \right] \tag{3.80}$$

$$\Delta G^*_{RT} = \Delta G^{*o}_{RT} + \beta\eta \tag{3.81}$$

$$\Delta G^*_{-RT} = \Delta G^{*o}_{RT} - (1-\beta)\eta - \Delta G^o_{OH} + \Delta G^o_O \tag{3.82}$$

$$j_{RT} = nFv_{RT} = j^* \left[a_{H^+}\theta_O exp\left(-\frac{\Delta G^*_{RT}}{kT}\right) - \theta_{OH}exp\left(-\frac{\Delta G^*_{-RT}}{kT}\right) \right] \tag{3.83}$$

$$\Delta G^*_{RD} = \Delta G^{*o}_{RD} + \beta\eta \tag{3.84}$$

$$\Delta G^*_{-RD} = \Delta G^{*o}_{RD} - (1-\beta)\eta + \Delta G^o_{OH} \tag{3.85}$$

$$j_{RD} = nFv_{RD} = j^* \left[a_{H^+}\theta_{OH} exp\left(-\frac{\Delta G^*_{RD}}{kT}\right) - \theta_{Pt}exp\left(-\frac{\Delta G^*_{-RD}}{kT}\right) \right] \tag{3.86}$$

$$\Delta G^*_{RTex} = \Delta G^{*o}_{RTex} + \beta\eta \tag{3.87}$$

$$\Delta G^*_{-RTex} = \Delta G^{*o}_{RTex} - (1-\beta)\eta + \Delta G^o_{Oex} - \Delta G^o_{OHex} \tag{3.88}$$

$$j_{RTex} = nFv_{RTex} = j^* \left[a_{H^+}\theta_{Oex} exp\left(-\frac{\Delta G^*_{RTex}}{kT}\right) - \theta_{OHex}exp\left(-\frac{\Delta G^*_{-RTex}}{kT}\right) \right] \tag{3.89}$$

$$\Delta G^*_{RDex} = \Delta G^{*o}_{RDex} + \beta\eta \tag{3.90}$$

$$\Delta G^*_{-RDex} = \Delta G^{*o}_{RDex} - (1-\beta)\eta - \Delta G^o_{sub} + \Delta G^o_{OHex} \tag{3.91}$$

$$j_{RDex} = nFv_{RDex} = j^* \left[a_{H^+}\theta_{OHex} exp\left(-\frac{\Delta G^*_{RDex}}{kT}\right) - \theta_{sub}exp\left(-\frac{\Delta G^*_{-RDex}}{kT}\right) \right] \tag{3.92}$$

$$\Delta G^*_{sub} = \Delta G^{*o}_{sub} \tag{3.93}$$

$$\Delta G^*_{-sub} = \Delta G^{*o}_{sub} + \Delta G^o_{sub} - \Delta G^o_O \tag{3.94}$$

$$j_{sub} = nFv_{sub} = j^* \left[\theta_{sub}exp\left(-\frac{\Delta G^*_{sub}}{kT}\right) - \theta_O exp\left(-\frac{\Delta G^*_{-sub}}{kT}\right) \right] \tag{3.95}$$

$$\Delta G^*_{perox} = \Delta G^{*o}_{perox} + \beta\eta \tag{3.96}$$

$$\Delta G^*_{-perox} = \Delta G^{*o}_{perox} + \Delta G^o_{O_2H} - (1-\beta)\eta \tag{3.97}$$

$$j_{perox} = nFv_{perox} = j^* \left[a_{H^+}\theta_{O_2H}exp\left(-\frac{\Delta G^*_{perox}}{kT}\right) - a_{H_2O_2}\theta_{Pt}exp\left(-\frac{\Delta G^*_{-perox}}{kT}\right) \right] \tag{3.98}$$

In order to account for the energy from the lateral repulsion of the species, a potential dependent term can be added to the activation free energies of the reactions AA, RT, RD and SUB as proposed in ref [1]. The reason why these terms are added only to these specific steps is because, based on the results from the parametric studies from Jayasankar and Karan multistep model showed in Chapter 2, the Temkin terms only have a relevant influence on the current generated when included in these steps. Therefore, the modified free energies accounting for the Temkin energy interactions are:

$$\Delta G^*_{AA} = \Delta G^{*o}_{AA} + \beta\eta + \omega_{AA}(\theta_O + \theta_{OH} + \theta_{O_2H}) \tag{3.99}$$

$$\Delta G^*_{RT} = \Delta G^{*o}_{RT} + \beta\eta - \omega_{RT}(\theta_O + \theta_{OH} + \theta_{O_2H}) \tag{3.100}$$

$$\Delta G^*_{-RD} = \Delta G^{*o}_{RD} - (1-\beta)\eta + \Delta G^o_{OH} + \omega_{RD}(\theta_O + \theta_{OH} + \theta_{O_2H}) \tag{3.101}$$

$$\Delta G^*_{sub} = \Delta G^{*o}_{sub} + \omega_{sub}(\theta_{sub} + \theta_{Oex} + \theta_{OHex}) \tag{3.102}$$

For steady state simulations, the production rates of species and the current generation were defined using only the ORR and peroxide mechanisms because it was observed by Jayasankar and Karan that the contribution of the place exchange reactions to the current generation at steady state is negligible. Therefore the system of equations for simulating steady state results can be expressed as indicated here:

- ORR:

$$\tau\frac{\partial\theta_O}{\partial t} = v_{DT} - v_{RT} = 0 \tag{3.103}$$

$$\tau\frac{\partial\theta_{OH}}{\partial t} = v_{DT} + v_{RT} - v_{RD} = 0 \tag{3.104}$$

$$\tau\frac{\partial\theta_{O_2H}}{\partial t} = v_{AA} - v_{DT} = 0 \tag{3.105}$$

$$v_{DT} = v_{RT} \tag{3.106}$$

$$v_{DT} + v_{RT} = v_{RD} = 2v_{RT} \tag{3.107}$$

$$v_{AA} = v_{DT} = v_{RT} \tag{3.108}$$

$$i_{ORR} = F(v_{AA} + v_{RT} + v_{RD}) \tag{3.109}$$

$$i_{ORR} = 4F(v_{RT}) \tag{3.110}$$

$$i_{ORR} = 2F(v_{RD}) \tag{3.111}$$

- Peroxide:

$$\tau \frac{\partial \theta_{O_2H}}{\partial t} = v_{AA} - v_{perox} = 0 \tag{3.112}$$

$$v_{AA} = v_{perox} \tag{3.113}$$

$$i_{Peroxide} = F(v_{AA} + v_{perox}) \tag{3.114}$$

$$i_{Peroxide} = 2F(v_{AA}) \tag{3.115}$$

$$i_{Peroxide} = 2F(v_{perox}) \tag{3.116}$$

- Total:

$$\tau \frac{\partial \theta_O}{\partial t} = v_{DT} - v_{RT} = 0 \tag{3.117}$$

$$\tau \frac{\partial \theta_{OH}}{\partial t} = v_{DT} + v_{RT} - v_{RD} = 0 \tag{3.118}$$

$$\tau \frac{\partial \theta_{O_2H}}{\partial t} = v_{AA} - v_{DT} - v_{perox} = 0 \tag{3.119}$$

$$v_{DT} = v_{RT} \tag{3.120}$$

$$v_{DT} + v_{RT} = v_{RD} = 2v_{RT} \tag{3.121}$$

$$v_{AA} - v_{DT} = v_{perox} \tag{3.122}$$

$$v_{AA} - v_{RT} = v_{perox} \tag{3.123}$$

$$v_{AA} - 1/2v_{RD} = v_{perox} \tag{3.124}$$

$$i_{total} = F(v_{AA} + v_{RT} + v_{RD} + v_{perox}) \tag{3.125}$$

$$i_{total} = F(v_{perox} + 1/2v_{RD} + 1/2v_{RD} + v_{RD} + v_{perox}) \tag{3.126}$$

$$i_{total} = F(2v_{perox} + 2v_{RD}) \tag{3.127}$$

$$i_{total} = i_{Peroxide} + i_{ORR} \tag{3.128}$$

The final system of equations for solving steady state simulations are equations ((3.117))-((3.119)), and the total current generation is the sum of the contribution of both mechanisms, equation (3.128).

For the transient simulations, where the contribution of the oxide growth mechanism is much more significant, the place exchange reaction rates are part of the system of equations

as indicated below:

$$\tau \frac{\partial \theta_O}{\partial t} = v_{DT} - v_{RT} + v_{sub} \tag{3.129}$$

$$\tau \frac{\partial \theta_{OH}}{\partial t} = v_{DT} + v_{RT} - v_{RD} \tag{3.130}$$

$$\tau \frac{\partial \theta_{O_2H}}{\partial t} = v_{AA} - v_{DT} - v_{perox} \tag{3.131}$$

$$\tau \frac{\partial \theta_{Oex}}{\partial t} = -v_{RTex} \tag{3.132}$$

$$\tau \frac{\partial \theta_{OHex}}{\partial t} = v_{RTex} - v_{RDex} \tag{3.133}$$

$$\tau \frac{\partial \theta_{sub}}{\partial t} = v_{RDex} - v_{sub} \tag{3.134}$$

$$i_{total} = F(v_{AA} + v_{RT} + v_{RD} + v_{RTex} + v_{RDex} + v_{perox}) \tag{3.135}$$

Where τ refers to the moles of sites per unit surface area of platinum. This constant is calculated by dividing the hydrogen adsorption charge of 220 $\mu C cm_{Pt}^{-2}$ by Faraday's constant.

3.3 Model Implementation

The equations presented in the previous section were implemented in Python. The methodology for the implementation of those equations is explained in this section.

3.3.1 Initial kinetic parameters

To be able to obtain preliminary results from this model, the values for the unknown kinetic parameters, i.e. the free energies of adsorption and the free energies of activation of all the intermediate species, were obtained. Given that the reaction mechanism assumed for this model was based on the reaction mechanism assumed for the model developed by Jayasankar and Karan [1], there are several kinetic parameters in common between these two models. Other models with similar steps and intermediate species are Wang et al. [44] and Moore et al. [57], specially the free energy of steps RT and RD and the energies of adsorption for $PtO_{(ads)}$ and $PtOH_{(ads)}$, for which there are also available values for the free energy parameters obtained from DFT calculations. Based on the literature values, the initial parameters used are found in Tables 3.1 and 3.2.

3.3.2 Steady State

The steady state model implementation was divided in two segments. Given that the governing equations of this model are coverage dependent, first the system of non-linear equations

((3.117))-((3.119)) needs to be solved in order to get the coverages of the different intermediate species.

To this end, the Python routine fsolve was used to solve the system of equations. This solver, part of the library scipy.optimize, finds the roots of a function using the Levenberg–Marquardt algorithm, also known as the damped least-squares (DLS) method, with a tolerance of $2x10^{-8}$. Then, the reaction rates and the current generation at different cell potentials are calculated using the obtained values of the coverages. The algorithm on how the steady state solver was implemented is shown in Fig. 3.2. First, an initial guess and an initial voltage are required for starting the loop. Inside the loop, the reactions rates of all the intermediate reactions are computed, as well as the production rates of all the intermediate species. Given that, in steady state, all the production rates should be in equilibrium (this means $d\theta/dt = 0$), the solver minimizes those functions and gives a solution for the unknown variables, which in this case are the surface coverages (θ). With that solution the remaining reactions rates are computed for the specific potential, and with that, the current generation is obtained. This loop goes until the current generation is computed at all potentials E.

Table 3.1 – Initial steady state kinetic parameters obtained from ref. [1]

Parameter	Value
ΔG_{AA}^{0*} [eV]	0.5863 eV
ΔG_{DT}^{0*} [eV]	0.4883 eV
ΔG_{RT}^{0*} [eV]	0.4627 eV
ΔG_{RD}^{0*} [eV]	0.3989 eV
ΔG_{O}^{o} [eV]	0.0453 eV
ΔG_{OH}^{o} [eV]	-0.3347 eV
$\Delta G_{O_2H}^{o}$ [eV]	0.3109 eV

3.3.3 Transient

In order to solve the transient problem given by eq. ((3.129))-((3.134)), an initial value for all coverages and an expression for the potential as a function of time are needed. To specify the electrode potential, a triangular function with respect to time was used. It was defined with 4 arguments: minimum and maximum voltage, time step and the maximum time. For the backward scan,

$$E = E_{max} + (E_{min} - E_{max}) * t/(t_{max}/2) \tag{3.136}$$
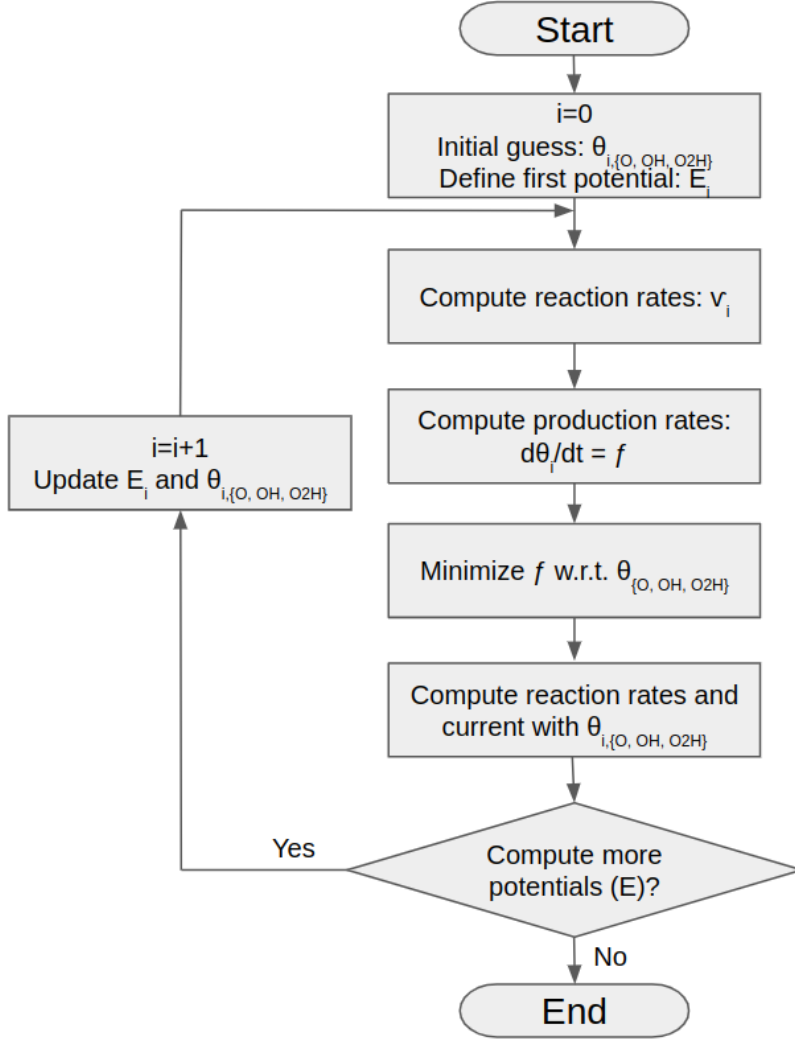
Figure 3.2 – Flow chart of the steady state algorithm.

And for the forward scan,

$$E = E_{min} + (E_{max} - E_{min}) * (t - t_{max}/2)/(t_{max}/2) \tag{3.137}$$

Equations ((3.129))-((3.134)) result in a system of ordinary differential equations (ODEs). The python solver *solve_ivp* was used for solving this problem. *solve_ivp* is designed for solving initial value problems with a stiff system of ODEs, like the system of equations in this work. This function numerically integrates the provided system of ODEs using different methods: Explicit Runge-Kutta method of order 8, 5, 4, 3 or 2, Implicit Runge-Kutta method of the Radau IIA family of order 5, Implicit multi-step variable-order (1 to 5) method based on a backward differentiation formula for the derivative approximation or BDF method with automatic stiffness detection and switching. The method chosen for this problem is the implicit multi-step variable-order 5 method based on a BDF for the derivative approximation.

This method uses a "quasi-constant" step scheme, this means that the solver chooses the best time step for solving the problem and that way the accuracy of the solution is enhanced. The solver keeps the local error estimates to less than 1e-7.

The algorithm of the transient implementation is shown in Fig. 3.3. First, the initial guess of the coverages is provided and the potential is defined with respect to time. The initial guesses for the unknown variables provided are : $\theta_O = 0.01$, $\theta_{OH} = 0.01$, $\theta_{SUB} = 0.0$, $\theta_{O_{ex}} = 0.0$ and $\theta_{OH_{ex}} = 0.0$. This information is given to the solver at each time step so that it can compute the reactions rates. Then, the production rates of all the species, which would be the system of ODEs, will solve the system of ODEs integrating it using the backward differentiation formula (BDF method). With the solution of the coverages, the current generation is computed. At the next time step, the coverages at the previous solution are used as the initial guess and the porcess above is repeated. This loop goes on until the maximum time (t_{max}) has been reached.

Table 3.2 – Initial transient kinetic parameters obtained from ref. [1]

Parameter	Value
ΔG_{RT}^{0*} [eV]	0.52
ΔG_{RD}^{0*} [eV]	0.5791
ΔG_{RTex}^{0*} [eV]	0.6023
ΔG_{RDex}^{0*} [eV]	0.6023
ΔG_{sub}^{0*} [eV]	0.4623
ΔG_O^o [eV]	-0.7191
ΔG_{OH}^o [eV]	-0.2791
ΔG_{Oex}^o [eV]	-1.23412
ΔG_{OHex}^o [eV]	-0.9841
ΔG_{sub}^o [eV]	-0.3412

Cyclic Voltammetry is experimentally obtained in the absence of oxygen, therefore, in the transient solution the only active reactions are RT, RD, RTex, RDex and SUB.
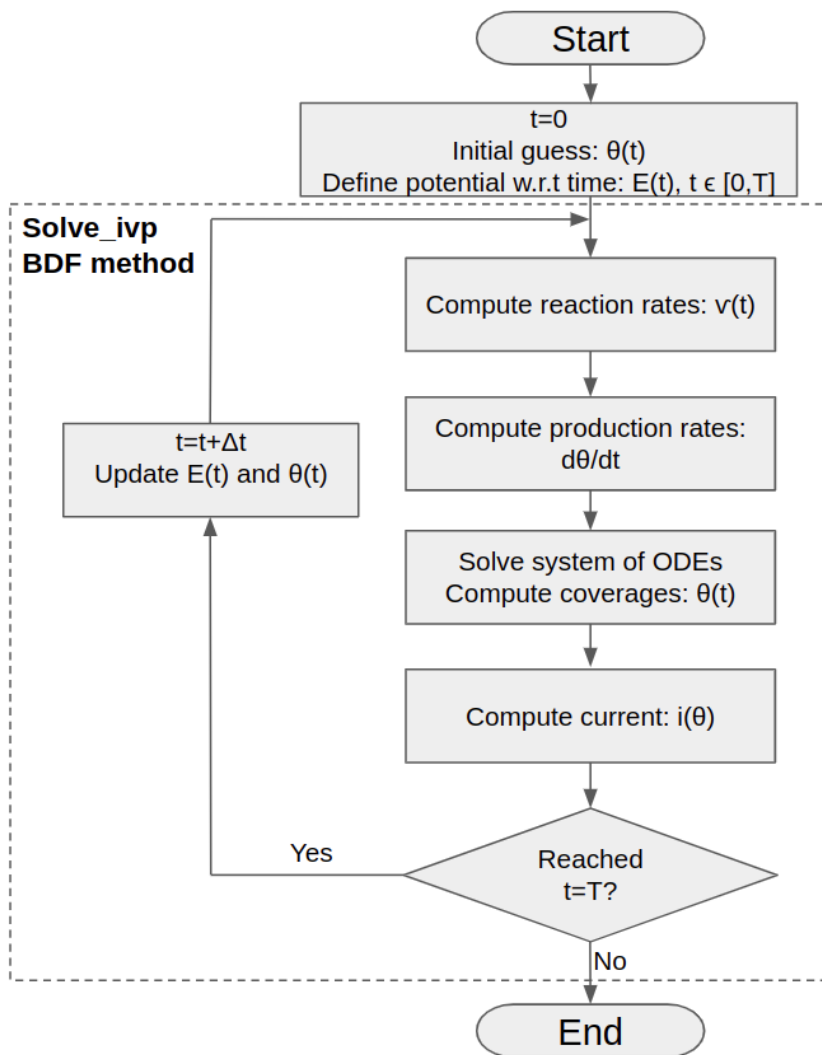
Figure 3.3 – Flow chart of the transient algorithm.

3.4 Parameter Estimation

The initial values of the kinetic parameters used for obtaining the preliminary results of the model are just an approximation based on ref [1]. These values do not provide good results for the model and do not capture accurately experimental trends. Therefore, it is required to fit the model to experimental data in order to get better values for the kinetic parameters.

The performance of the model is dictated by the free energies of adsorption of the intermediate species and the free energies of activation of the intermediate steps. The values of these parameters could be estimated through DFT calculations, however it is very difficult to obtain them due to the complexity of the molecular interactions at a platinum surface.

Therefore, in this work, these parameters were obtained through solving a parameter estimation problem. This was achieved by minimizing the error between model results and experimental data by adjusting the free energies of the reaction. Given that the experimental data available in the literature is different for steady state and transient results, this model was fitted separately first to steady state polarization curves and then to transient CVs.

3.4.1 Optimization problem

A non linear optimization method was needed for fitting the model to experimental data. The optimization method used was provided by an open source library developed Sandia National Laboratory called DAKOTA (Design Analysis Kit for Optimization and Terascale Applications). The optimization problem to be solved is the least-square parameter estimation problem, (3.138)-(3.139).

$$Minimize : f(x) = \sum_{i=1}^{N} \left[\frac{j_i^{exp} - j_i^{num}}{j_i^{exp}} \right]^2 \tag{3.138}$$

$$w.r.t. : x = \Delta G_{step}^{0*}, \Delta G_{specie}^{o}, j^* \tag{3.139}$$

A derivative free optimization method, called coliny pattern search, was used for solving this optimization problem. This non gradient-based optimization method uses a set of offsets from the current iteration to locate improved points in the design space. Given that this is a local method, a total of 500 random initial guesses were used for finding the best solution. The parameters for this optimization problem are defined in Table 3.3.

Table 3.3 – Optimization parameters

Parameter	Value
Seed	1,000
Max iterations	500,000
Convergence tolerance	1e-4
Max function evaluations	8,000,000
Solution target	0.1
Constraint penalty	100,000,000

In this optimization problem, the parameters that need to be optimized in order to minimize the difference between the numerical and experimental data are the free energies of adsorption of the intermediate species: ΔG_O^o, ΔG_{OH}^o and ΔG_{O2H}^o, the free energies of activation of the intermediate steps: $\Delta G_{AA,DT}^{0*}$, ΔG_{RT}^{0*}, ΔG_{RD}^{0*}, G_{PEROX}^{0*}, the Temkin term

for the AA reaction, w_{AA}, and the pre-exponential factor j^*, which is basically scaling factor that linearly affects the order of magnitude of the current generation. This parameters, were bounded as follows,

$$Bounds: 0.1 < \Delta G^{0*}_{AA,DT} < 0.8 \tag{3.140}$$
$$0.5 < \Delta G^{0*}_{RT} < 0.8 \tag{3.141}$$
$$0.5 < \Delta G^{0*}_{RD} < 0.7 \tag{3.142}$$
$$0.1 < \Delta G^{0*}_{PEROX} < 0.9 \tag{3.143}$$
$$-0.5 < \Delta G^{o}_{O} < 0.5 \tag{3.144}$$
$$-0.2 < \Delta G^{o}_{OH} < 0.2 \tag{3.145}$$
$$-0.8 < \Delta G^{o}_{O2H} < 0.8 \tag{3.146}$$
$$0.01 < j^* < 100 \tag{3.147}$$
$$0.01 < w_{AA} < 0.8 \tag{3.148}$$

Given that some of these parameters have been part of the formulation of previous ORR kinetic models available in the literature, the constraints applied were set based on those previous values. RT and RD reactions as well as O and OH species are common reactions and species with the double trap model, therefore the fitted values obtained in references [44, 57] were used for defining the bounds. And in the case of the parameters related to AA and DT reactions and $PtO_2H_{(ads)}$ adsorbed species, the bounds were obtained based on the reported fitted values from references [1, 2].

In addition to the optimization problem, certain constraints were applied to the coverage fractions at specific potentials because the model not only needs to be able to match experimental currents, but also experimental data of coverage fractions. The imposed constraints were defined based on the literature review conducted on Chapter 1 and are shown in eq. (3.149) - (3.160).

$$Constraints : 0.9V : 0.1 < \theta_O < 0.35 \qquad (3.149)$$
$$0.15 < \theta_{OH} < 0.3 \qquad (3.150)$$
$$0.0 < \theta_{O2H} < 0.05 \qquad (3.151)$$
$$0.8V : 0.0 < \theta_O < 0.1 \qquad (3.152)$$
$$0.2 < \theta_{OH} < 0.4 \qquad (3.153)$$
$$0.0 < \theta_{O2H} < 0.2 \qquad (3.154)$$
$$0.6V : 0.0 < \theta_O < 0.05 \qquad (3.155)$$
$$0.05 < \theta_{OH} < 0.1 \qquad (3.156)$$
$$0.2 < \theta_{O2H} < 0.8 \qquad (3.157)$$
$$0.4V : 0.0 < \theta_O < 0.05 \qquad (3.158)$$
$$0.0 < \theta_{OH} < 0.1 \qquad (3.159)$$
$$0.4 < \theta_{O2H} < 0.9 \qquad (3.160)$$

Most of the data available in the literature on surface coverages is from numerical models, DFT or Montecarlo simulations, however Jinnouchi et al. [42] and Huang et al. [64] reported experimental values for the surface coverage of $PtO_{(ads)}$ and $PtOH_{(ads)}$ adsorbed species, which showed that at low potentials these species are very small (< 0.1), between 0.6 and 0.8 V, $PtOH_{(ads)}$ starts to grow up to 0.4 V and then significantly drops at higher potentials, and $PtO_{(ads)}$ only starts to grow rapidly at 0.4 V. There is no experimental data on the surface coverage of $PtO_2H_{(ads)}$ but the following references [1, 56, 65] simulate high values for the coverage of $PtO_2H_{(ads)}$ at low potentials that drastically drop at 0.6 V because it is when the other two species start to be formed.

Chapter 4

Results and discussion

In this chapter, the suitability of the proposed kinetic model in Chapter 3 is evaluated by trying to reproduce experimental data available in literature. In order to reproduce the data, the free energies and Temkin terms in the proposed model are used as fitting parameters. The deviation between experimental and numerically predicted results are then analyzed. The aim is to ascertain if the model can reproduce the experimentally observed steady-state and transient behaviour and, if so, to obtain the set of free energy and Temkin parameters that reproduce the results.

The features to capture in steady-state simulations are: current density vs voltage curves relations at different operating conditions, coverage fractions, and, energy barriers for the elementary steps and overall mechanism. In transient simulations, the experimental features to capture are: the broad anodic plateau; a cathodic reduction peaks in cyclic voltammograms (CVs); and, the logarithmic growth of oxide mass over time.

As explained in the previous chapter, the proposed model accounts for three reaction mechanisms that affect the kinetics of PEMFC: i) the oxygen reduction reaction; ii) subsurface oxide growth; and, iii) hydrogen peroxide formation. The numerical kinetic expressions derived in Chapter 3 for modeling these mechanisms were implemented in a steady-state and a transient framework for obtaining different types of simulations.

4.1   Results with previous free-energies data set

After implementing the model described in Chapter 3, the initial parameters obtained from ref. [1] and presented in Tables 2.4 and 2.5 were used for simulating preliminary steady state and transient results. These results were compared to the numerical data reported by

Jayasankar and Karan [2] with the aim of comparing the simulated results from their model with the ones from the new developed model.

Figure 4.1 shows the polarization curve obtained using the new energy based model presented in Chapter 3. To obtain these steady-state results, in order to be able to directly compare it to the unified multi-step model studied in Chapter 2, the peroxide formation mechanism is deactivated. It can be observed that, without fitting the model to experimental data, a reasonable polarization curve is obtained; however, the change in slope is generated at around 1.0 V, when it has been observed experimentally to occur at around 0.8 V, this could be due to the formation of platinum oxides at a higher potential (1.0 V) instead of at 0.8 V. At low cell potentials (< 0.4 V), the current shuts downs and all the Pt surface is covered by $PtO_2H_{(ads)}$.
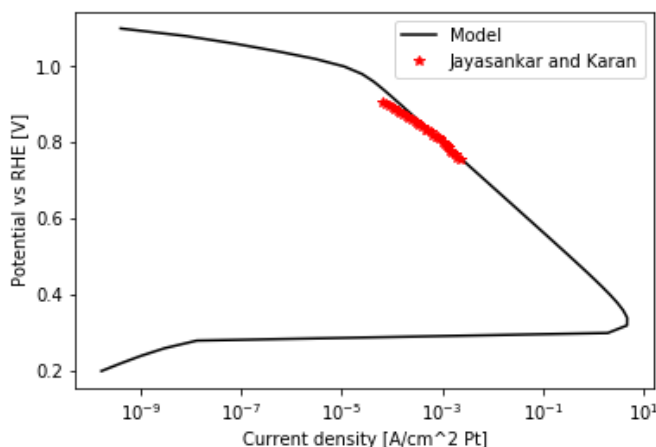
Figure 4.1 – Predicted polarization curve at $a_{O_2} = 1$, T = 298 K and $a_{H+} = 0.1$.

The predicted oxide coverage fraction in Fig. 4.2 shows that at 1.0 V, O_{ads} starts to grow rapidly, which is likely the reason for the change in slope at this potential and not earlier at 0.8 V. Given that the results from the model presented in this section does not account any extra Temkin term, these terms are one of the major differences between the model proposed by Jayansakar and Karan and the proposed model, and a possible explanation of why our model starts producing $PtO_{(ads)}$ at higher potentials.

Fig. 4.3 shows the CV reported by Jayansakar and Karan [1] from their model simulations and one obtained using the proposed model, both at a scan rate of 10 mV/dec and an upper potential and lower potential of 1.35 V and 0.6 V, respectively. The CV obtained with the model is able to capture two of the most representative peaks, but not at the right voltages.
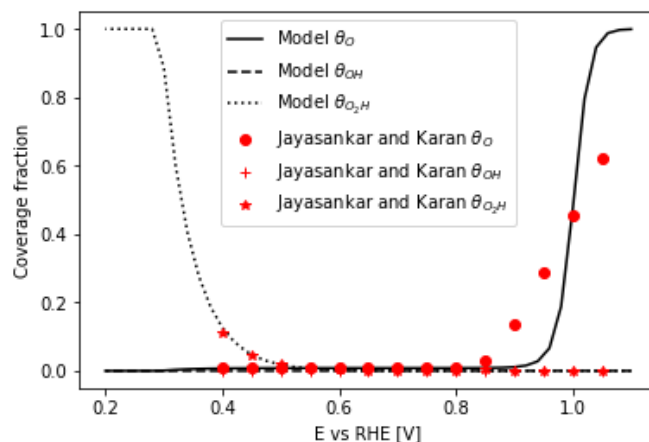
Figure 4.2 – Predicted oxide coverage fraction at $a_{O_2} = 1$, T = 298 K and $a_{H+} = 0.1$.

The model is not producing the positive current at high potentials due to oxide growth that gives the plateau effect, which is captured by the model from Jayasankar and Karan. The current generation is also underestimated. Even though these two cyclic voltammograms were obtained at the same scan rate and voltage limits, they may not be matching because the reaction mechanism assumed is slightly different, and the energy of interaction between the adsorbed species is not accounted in the preliminary results of the proposed model.
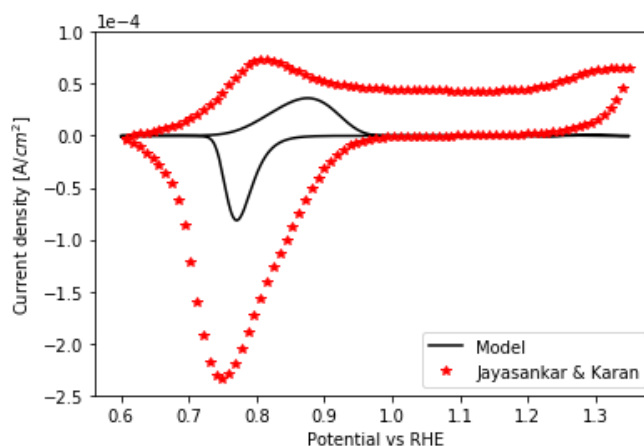
Figure 4.3 – Predicted numerical cyclic voltammetry at $a_{O_2} = 0$, T = 298 K and $a_{H+} = 0.1$ from two models (Jayansakar and Karan's unified model and the proposed model). The upper potential limit at which these CVs were obtained is 1.35 V with a scan rate of 10 mV/dec.

4.2 Steady-state kinetic model parameter estimation using Pt micro-electrode data

In order to estimate the free energies for the proposed model, the optimization strategy designed in Chapter 3 was utilized to estimate the free energies that minimize the difference between model predictions and the experimental data from ref. [4] at different pressures.

First, the optimization problem was solved without any constraints and with broad parameter bounds, just to observe the natural behaviour of the model, and if the optimizer was going to be able to fit the model to experimental data. The results of the initial optimization were obtained within 5 hours and showed a good fit to the polarization curves, however the surface coverage values did not match the experimental values reported in refs. [42, 64]. As a result, constraints on the coverages and narrow bounds on the free energies were imposed to the optimization problem.

A multi-start method was used involving a randomized set of 500 starting points, and the optimization problem was solved for each starting point to obtain a global solution. The colliny pattern search method, explained in Chapter 3, was used. Running these 500 optimization problems took around 3 days. The best solution had a residual of 1.84, reducing the residual from 10^5 to a significantly smaller number. Fig. 4.4 shows the residual evolution vs the number of iteration. An exponential decay of the residual with the increasing number of iterations can be observed.

Table 4.1 shows the optimal set of parameters used for running steady state simulations in this section and those used in section 4.1. Note that, in this section, the peroxide mechanism is included in the formulation even though ΔG^{*o}_{perox} is not fitted and is set at 0.5 eV.

Figures 4.5 and 4.6 show the current density and intermediate species coverage predicted by the model and experimental results obtained from Parthasarathy et al. [4] for the polarization curve and from references [42, 46, 63] for an average of the coverage fractions. From the polarization curves, it can be observed that the fitted model better reproduces the experimental data from Parthasarathy et al. [4] compared to the previous free energy data set from Section 4.1. At low cell potentials (< 0.8 V) the linear fit is very good, and the slope is the same (120 mV/dec). At high potentials (> 0.8 V), a clear slope cannot be observed. Figure 4.6 shows that the predicted surface coverage of $PtOH_{(ads)}$ adsorbed species matches the experimental data very well at high potentials. At intermediate potentials it does not match perfectly, but it does follow a similar trend. In the case of adsorbed $PtO_{(ads)}$,
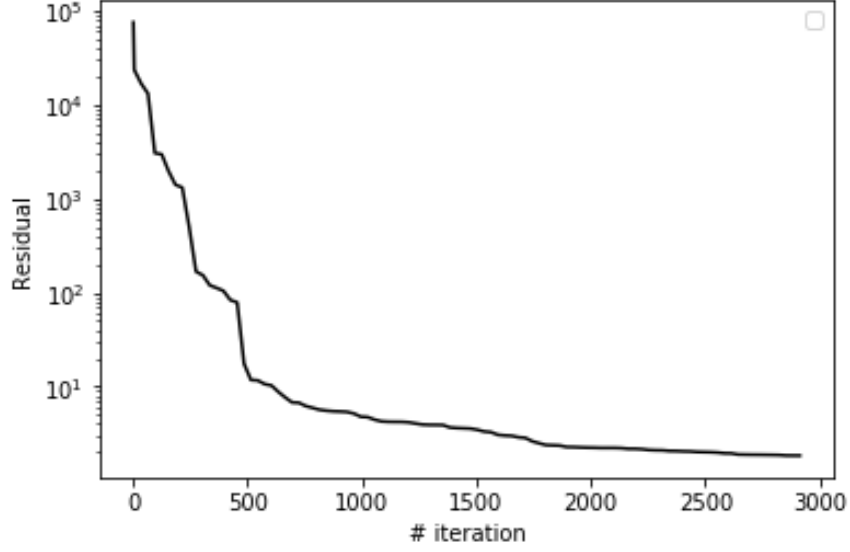
Figure 4.4 – Residual evolution vs number of iteration when fitting the model to Pt micro-electrode data.

Table 4.1 – Parameters for steady state simulations

Fitted parameters	Section 4.2	Section 4.1
ΔG_{AA}^{0*} [eV]	0.7135	0.5863
ΔG_{DT}^{0*} [eV]	0.2979	0.1773
ΔG_{RT}^{0*} [eV]	0.6772	0.4627
ΔG_{RD}^{0*} [eV]	0.6907	0.3089
ΔG_{O}^{o} [eV]	-0.1271	-0.33455
ΔG_{OH}^{o} [eV]	0.0845	0.04545
$\Delta G_{O_2H}^{o}$ [eV]	0.5838	0.3109
j^*	2.4393	0.05182
Other parameters		
Temperature [K]	323	298
a_{O_2}	1	1
a_{H^+}	0.1	0.1
β	0.5	0.5
E^0 [V]	1.23	1.23
ΔG_{perox}^{*o} [eV]	0.5	-
$a_{H_2O_2}$	0	-

the surface coverage is overestimated at intermediate potentials, but at higher potentials it matches the experimental data.
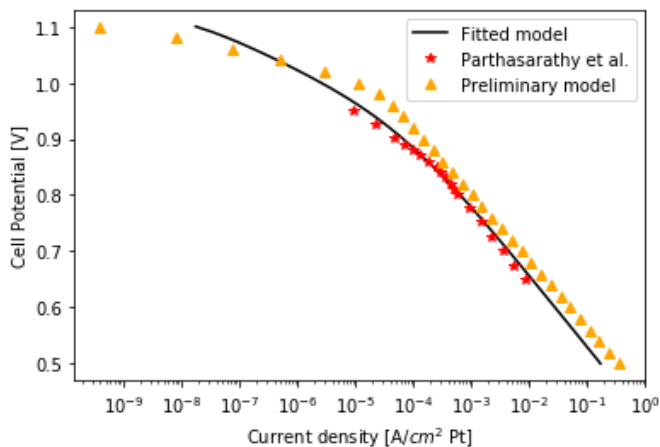
Figure 4.5 – Predicted polarization curve at $a_{O_2} = 1$, T = 323 K and $a_{H^+} = 0.1$ fitted to Parthasarathy et al. [4] and compared to the model results from section 4.1.
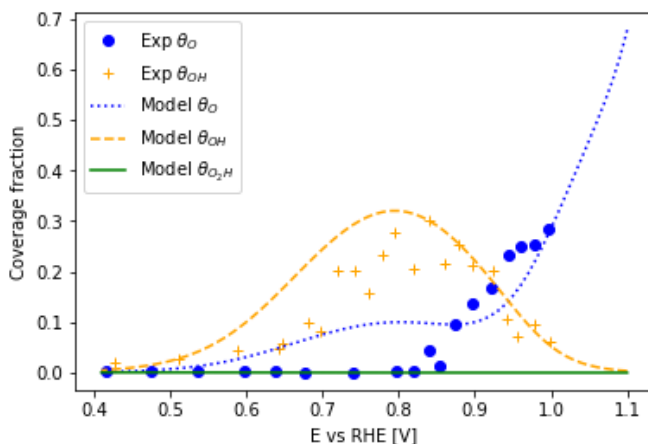
Figure 4.6 – Predicted oxide coverage fraction at $a_{O_2} = 1$, T = 323 K and $a_{H^+} = 0.1$.

Figure 4.7 shows three polarization curves at different oxygen partial pressures, i.e., 0.21, 1.05 and 1.88 atm, and the experimental data from Parthasarathy et al. [4]. The obtained parameters are capable of predicting the change in current generation with oxygen partial pressure.

In the formulation of this model, a rate determining step (RDS) was not assumed. Instead, the activation free energies were used to describe the reaction barriers of the ORR and Peroxide mechanisms. Figure 4.8 shows the free energy diagrams for ORR and peroxide reactions at zero over-potentials obtained using the fitted free energies to Pt micro-electrode data. An important feature from these energy diagrams, it the consistency of the model
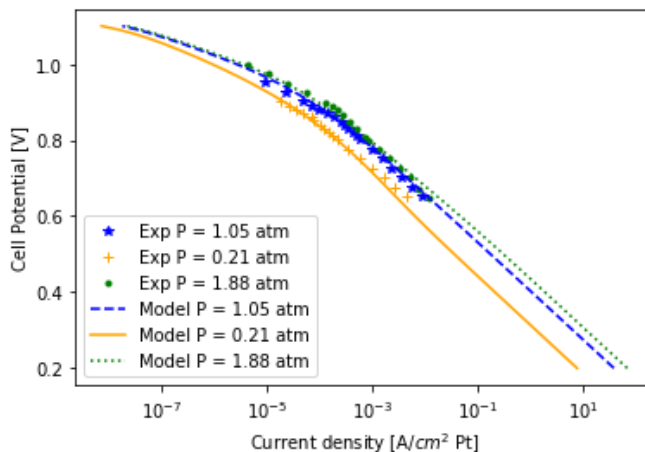
Figure 4.7 – Predicted polarization curve at $a_{O_2} = 0.2/1/1.79$, T = 323 K and $a_{H^+} = 0.1$ fitted to Parthasarathy et al. [4] at different pressures.

because the energy level of the reactants and products are equal at the start and end of the reaction mechanisms, at equilibrium.

The free energy diagram in Figure 4.8 illustrates that the $4e^-$ ORR mechanism on Pt electrode is desorption-limited because the energy barrier needed for the forward reductive desorption (RD) reaction to proceed is the highest, while the energy required for the reactions AA, DT and RT to proceed, is lower, which means that these reactions will take place easier. In the case of the $2e^-$ peroxide formation mechanism, overall, the energy required for the peroxide reaction is smaller than the total energy required for the ORR mechanism, therefore, it could be concluded that the most favourable pathway is the peroxide one.

Figure 4.9 shows the comparison of the energy diagrams obtained with the two different set of parameters from Table 4.1. It can be observed that the RDS is the same for both sets of parameters, RD reaction, however the energy barrier for RD step is significantly bigger for the set of parameters fitted to Pt electrode data, this can be because when fitting this set of parameters, the peroxide mechanism is active, while the preliminary results don't account for the peroxide mechanism.

The free energy diagrams presented so far have been obtained at zero over potential, this means at a cell potential equal to the equilibrium potential (1.23 V). Figure 4.10 shows the free energy diagrams obtained at 0.7 V. It can be observed that at this potential the RDS for all the mechanisms and sets of parameters is AA step, being the energy barrier from this step the one that needs to be overcome in order to proceed with the rest of the reactions.
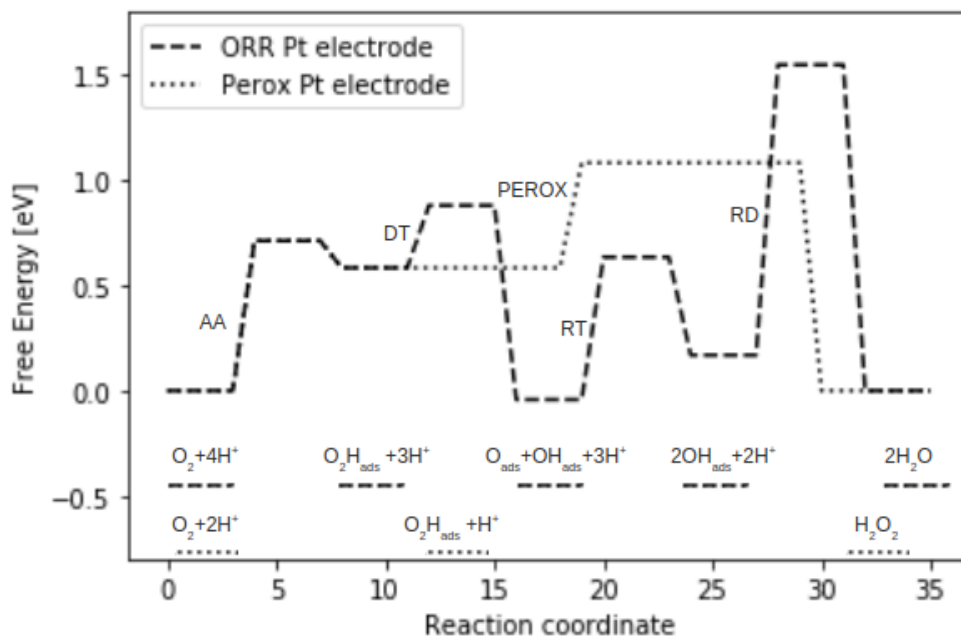
Figure 4.8 – Free energy diagram of the ORR and Peroxide mechanisms of the fitted model to Pt electrode data at zero overpotential.
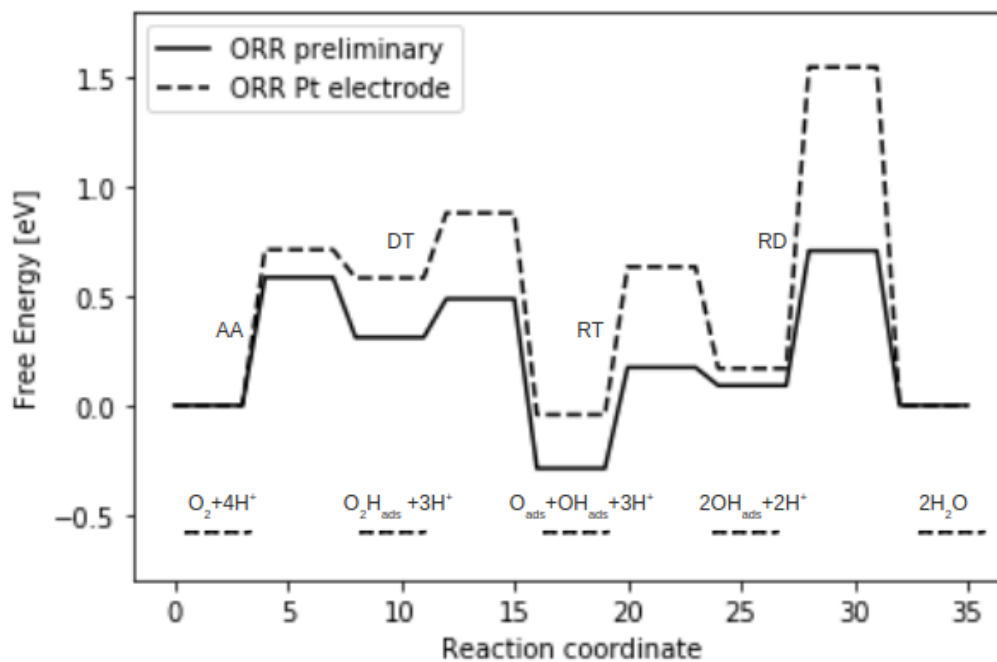
Figure 4.9 – Free energy diagram of the ORR mechanism with the preliminary set of parameters from section 4.1 and from the fitted model to Pt electrode data at zero overpotential.
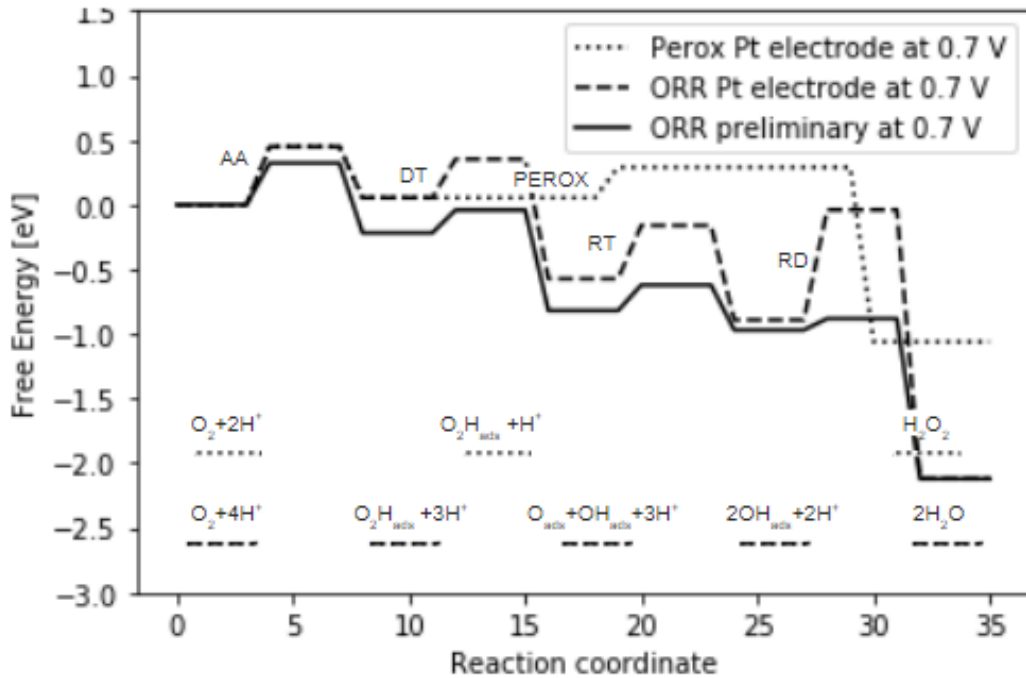
Figure 4.10 – Free energy diagrams at 0.7 V ($\eta = 0.53$) of the ORR mechanism with the preliminary set of parameters from section 4.1 and from the fitted model to Pt electrode data.

4.2.1 Effect of oxygen concentration on the formation of adsorbed species

Figures 4.11,4.12 and 4.13, show the effect of changing the oxygen concentration on the coverage fractions of the adsorbed species over the cell potential. It can be observed that by increasing the activity of the oxygen, the formation of all the oxides increases too. This could be due to a higher availability of reactant to form more platinum oxides.
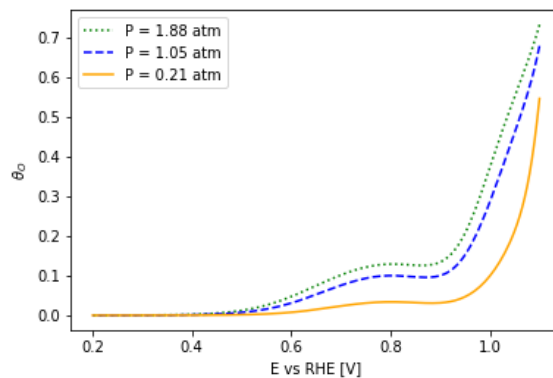
Figure 4.11 – Predicted $PtO_{(ads)}$ coverage fraction at $a_{O_2} = 0.2/1/1.79$, T = 323 K and $a_{H+} = 0.1$.
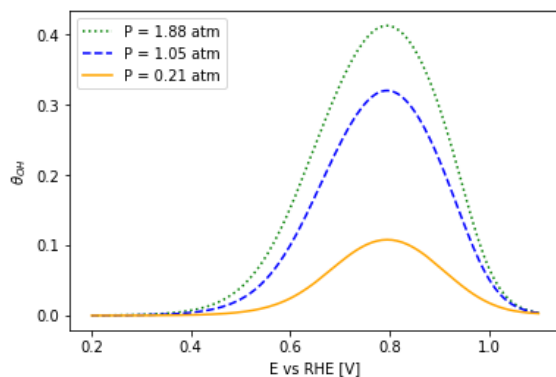
Figure 4.12 – Predicted $PtOH_{(ads)}$ coverage fraction at $a_{O_2} = 0.2/1/1.79$, T = 323 K and $a_{H^+} = 0.1$.
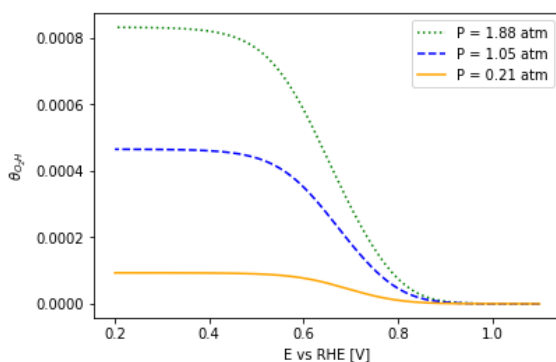
Figure 4.13 – Predicted $PtO_2H_{(ads)}$ coverage fraction at $a_{O_2} = 0.2/1/1.79$, T = 323 K and $a_{H^+} = 0.1$.

4.2.2   Effect of peroxide formation

To observe what is the effect of including the peroxide formation reaction in the model, this reaction was removed and the results are shown in Figures 4.14 and 4.15. The polarization curve shows that there is not change in the total current generation if the peroxide mechanism is ignored up to 0.4 V, however at lower potentials the current generation immediately is shutdown. This can be explained by looking at the surface coverage, the adsorbed species $PtO_{(ads)}$ and $PtOH_{(ads)}$ barely cover the Pt surface and the $PtO_2H_{(ads)}$ adsorbed species covers rapidly the whole Pt surface at potentials below 0.4 V. In addition, the simulated results without the peroxide mechanism are very distant from the experimental coverages, predicting a much higher presence of $PtOH_{(ads)}$ adsorbed specie at low potentials.

The peroxide current generation was also studied individually and compared to experimental data from Sethuraman et al. [5] which measured polarization curves for the peroxide formation rates from a rotating ring disk electrode (RRDE), using a Pt/Vulcan catalyst 20%
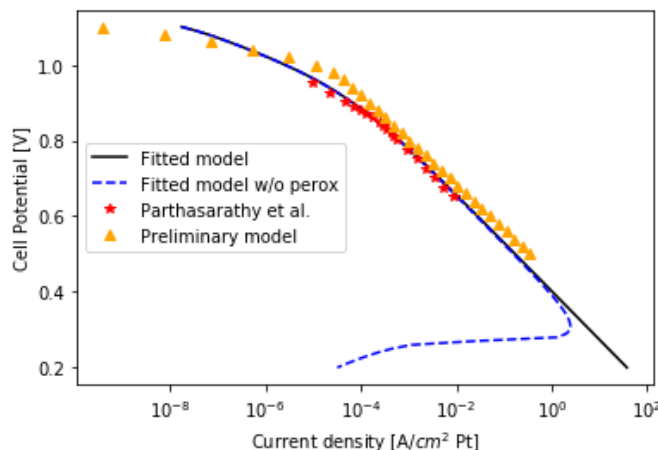
Figure 4.14 – Predicted polarization curve at $a_{O_2} = 1$, T $= 323$ K and $a_{H+} = 0.1$ fitted to Parthasarathy et al. [4] accounting for the peroxide reaction (black solid line) and neglecting the peroxide reaction (blue dashed line)
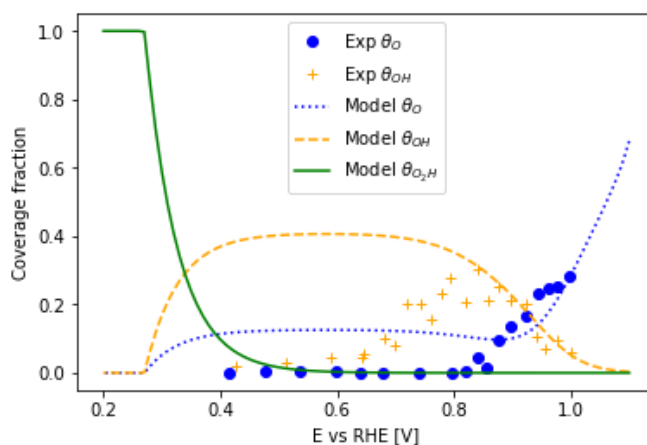
Figure 4.15 – Predicted oxide coverage fraction at $a_{O_2} = 1$, T $= 323$ K and $a_{H+} = 0.1$ without having active the peroxide mechanism.

Pt on Vulcan XC-72R carbon. These experiments were conducted at 298 K with an RRDE rotating at 2500 rpm in 2.0 M $HClO_4$ solution bubbled with 10% $O_2/.$, air and pure oxygen. Figure 4.16 shows the polarization curves of the reported experimental data from ref. [5] and the simulated peroxide formation current from the model at different oxygen concentrations. It can be observed that the simulated results do not fit well the experimental data, however it does follow the trend of the decreasing current at increasing potentials. One of the limitations of this model is that the backward term for the peroxide reaction is neglected because it is assumed that the reaction only proceeds forward. It is possible that the contribution of this term is leading to the difference. To asses if this is the case the model with hand without backward reaction should be fitted to the experimental data.

76
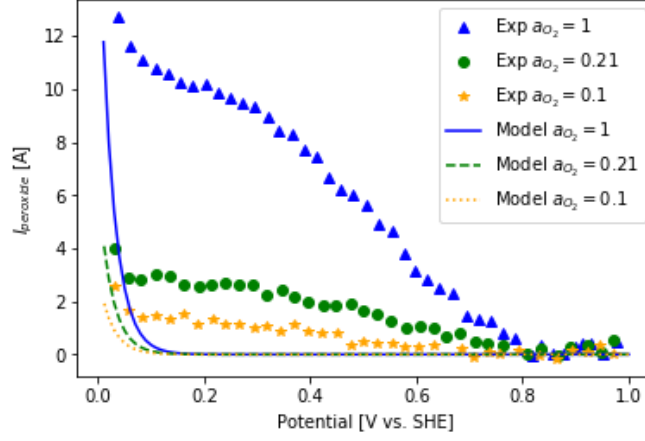
Figure 4.16 – Predicted polarization curve of the peroxide mechanism at three oxygen coc-nentrations (10%, 21% and pure oxygen), T = 298 K and $a_{H+} = 0.1$ compared to experimental data from ref. [5].

It is known that the equilibrium potential of the peroxide formation reaction is 0.695 V [36]. At this potential, the contribution of the peroxide mechanism to the overall current generation should be zero. Therefore, the value of the activation free energy of the peroxide formation reaction ΔG^{*o}_{perox} could be obtained by setting the rate of the peroxide formation equal to zero. This value, based on eq. (3.98), can be obtained by solving the following equation:

$$j_{perox} = j^* \left[a_{H+} \theta_{O_2H} exp \left(-\frac{(\Delta G^{*o}_{perox} + \beta(E^{OCV}_{PEROX} - E^0))}{kT} \right) \right] = 0 \qquad (4.1)$$

Given that ΔG^{*o}_{perox} was not fitted to this model and was assumed a constant value of 0.5 eV for fitting the other parameters, a parametric study was conducted with lower and higher values of this parameter to see the effects on the predicted current generation. The values used for this parametric study are : 0.3, 0.4, 0.5, 0.6 and 0.7 eV.

Fig. 4.17 shows that the total current generation is barely affected by increasing or decreasing this parameter in that range. However, the ORR and the peroxide currents (see Fig 4.18) are significantly affected individually by the changes. This can be explained by looking at Figures 4.19, 4.20 and 4.21, changing this parameter affects the coverages of the adsorbed species. The value for the peroxide formation free energy that best fits the experimental data of surface coverage is between 0.4 and 0.5 eV, however by looking at the individual current of ORR and peroxide, when $\Delta G^{*o}_{perox} = 0.4$ eV the peroxide current is much higher than the

ORR current at 0.9 V and below, which represents an issue, because it would be expected to have only at very low potentials (~0.2 V) a peroxide current higher than the ORR, the ORR should be the predominant because at mpst of the voltage range, and that is only achieved with high values of the peroxide formation free energy ($\Delta G^{*o}_{perox} = 0.7$ eV).
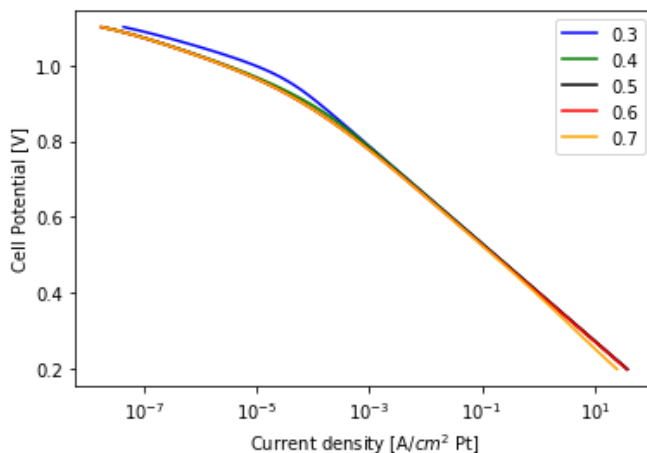
Figure 4.17 – Predicted total current generation at $a_{O_2} = 1$, T=323 K and $a_{H+} = 0.1$ at different G^{*o}_{perox} values.
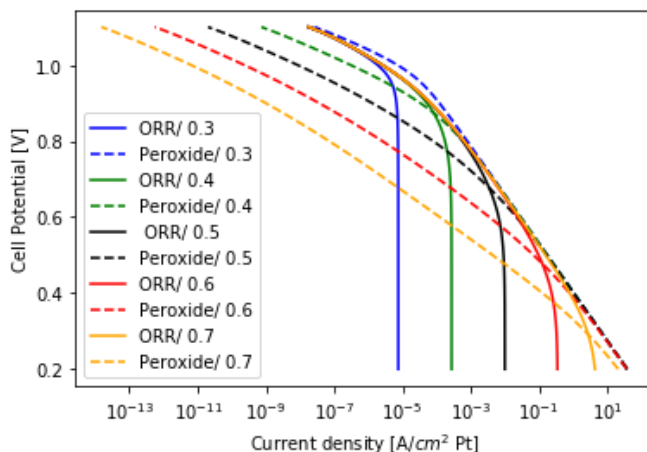
Figure 4.18 – Predicted individual ORR and peroxide currents at $a_{O_2} = 1$, T=323 K and $a_{H+} = 0.1$ at different G^{*o}_{perox} values.

It is important to note that given that the equilibrium potential of the peroxide formation reaction is 0.695 V [36], at that potential, the current generation from the peroxide formation pathway should be zero, and at higher potentials (> 0.695 V) should be negative. However, the model is predicting peroxide current at that potential and that is wrong. One of the assumptions made at the beginning of the formulation of this model was that the equilibrium
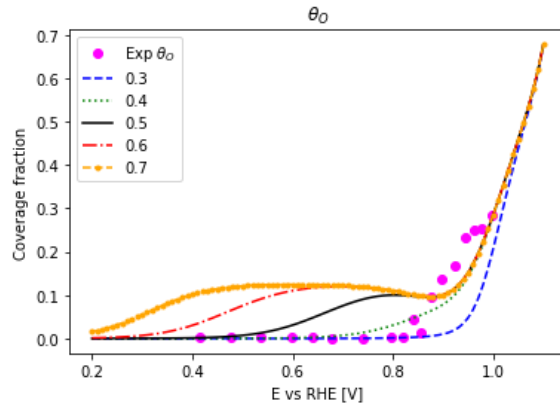
Figure 4.19 – Effect of peroxide formation free energy on the surface coverage of $PtO_{(ads)}$.
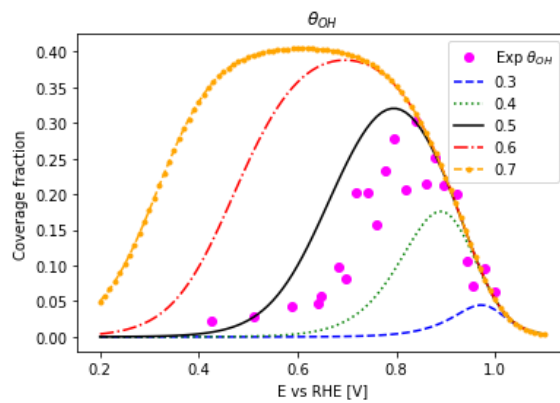
Figure 4.20 – Effect of peroxide formation free energy on the surface coverage of $PtOH_{(ads)}$.
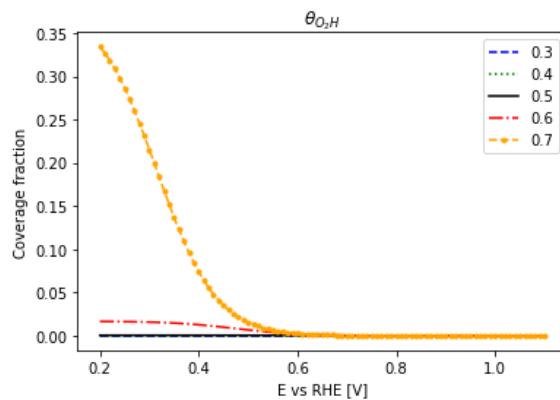
Figure 4.21 – Effect of peroxide formation free energy on the surface coverage of $PtO_2H_{(ads)}$.

potential, 1.23 V, is the same for all the steps, including the peroxide formation step. This assumption may be the reason why the behaviour of the peroxide mechanism is not been captured correctly, therefore, this should be considered for future work.

4.3 Transient analysis

In the previous sections, the proposed kinetic model was used to reproduce steady-state data. In this case, Temkin terms were not included when fitting to platinum electrode. In this section, the kinetic parameters from section 4.2 are first used, without adding any Temkin terms, to predict the cyclic voltammogram of Pt electrode and supported Pt nanoparticles. Then, parametric studies are conducted to study the effect of adding the Temkin terms on the transient results.

4.3.1 Transient results for platinum electrode

Fig. 4.22 shows the CV obtained with the fitted parameters from the previous section and experimental data from Savinova et al. [66]. The model is capable of capturing the two peaks due to oxide formation but the peaks occur at higher potentials, e.g., the cathodic reduction peak has been observed experimentally between 0.7 and 0.8 V, due to the formation of $PtO_{(ads)}$ and $PtOH_{(ads)}$ adsorbed species, and the model is predicting this at 1.1 V. Furthermore, the oxide growth plateau is not captured.
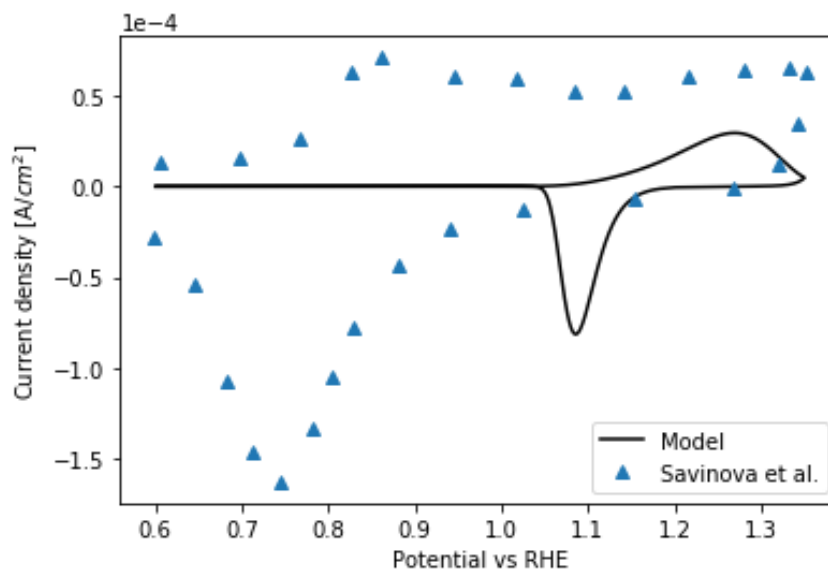
Figure 4.22 – Predicted cyclic voltammetry at $a_{O_2} = 0$, T=298 K and $a_{H^+} = 0.5$ with SS fitted parameters for platinum electrode. The upper potential limit at which these CVs were obtained is 1.35V, with a scan rate of 10 mV/sec.

Several studies have been done to understand the nature and rate of growth of oxide species on platinum. Given that this is an important feature that numerical models should capture when predicting the performance of the ORR kinetics of PEMFC, Jayasankar and

Karan [1] not only used polarization curves and CVs for fitting their model, but they also used oxide growth data for their parameter estimation. This data was obtained by conducting oxide growth measurements with a quartz crystal micro-balance technique [2]. The oxide mass as a function of potential is obtained through these experiments and then plotted against time, which gives a logarithmic oxide growth plot. These experiments monitor the change in the oxide mass during potential step. Fig. 4.23 shows the oxide growth predicted by the model compared to the experimental logarithmic oxide growth reported in ref. [1]. It can be observed that the model does not capture the shape of the logarithmic oxide growth over time observed experimentally. The model predicts a gradually increasing formation of oxide mass after running some time, while in the experiment, the oxides grow immediately the reaction starts.
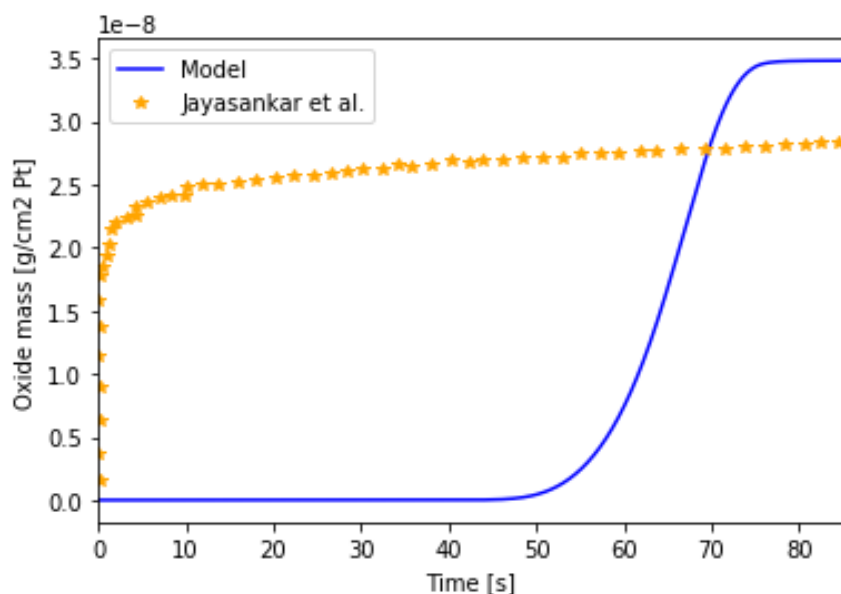
Figure 4.23 – Predicted oxide mass on Pt electrode in the absence of O_2, at T=298 K, in aqueous acidic electrolyte 0.5 M and at a fixed potential 1.1 V.

Parametric studies

Temkin terms for RT and RD were introduced and parametric studies were conducted in order to evaluate the effect of these parameters on the predicted current. Results from the parametric study with ω_{RT} and ω_{RD} are shown in Figures 4.24 and 4.25, respectively. Figure 4.24 shows that ω_{RT} only affects the cathodic reduction peak. Increasing this value reduces the height of the peak and slightly shifts it to higher potentials. It is important to note that the size of the peak (area under the curve) does not change, it only gets wider and the height of the peak reduced.

Fig. 4.25 shows that increasing ω_{RD} affects the amount of oxide produced thereby affecting both anodic and cathodic peaks.
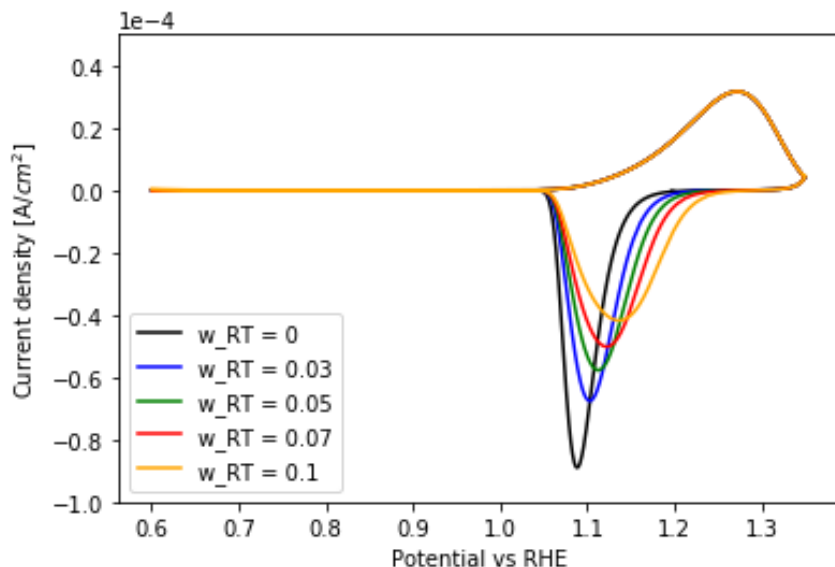
Figure 4.24 – Predicted cyclic voltammetry at $a_{O_2} = 0$, T=298 K and $a_{H+} = 0.5$ with SS fitted parameters for platinum electrode and different ω_{RT} values. The upper potential limit at which these CVs were obtained is 1.35 V, with a scan rate of 0.01 V/sec.
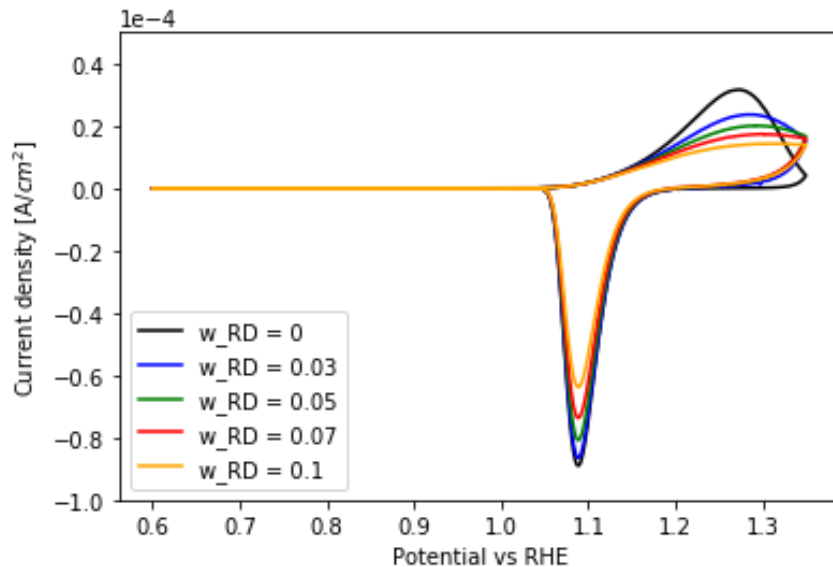
Figure 4.25 – Predicted cyclic voltammetry at $a_{O_2} = 0$, T=298 K and $a_{H^+} = 0.5$ with SS fitted parameters for platinum electrode and different ω_{RD} values. The upper potential limit at which these CVs were obtained is 1.35 V, with a scan rate of 0.01 V/sec.

4.4   Analysis of the model

In this section the suitability of this model for reproducing experimental trends was studied by fitting the kinetic parameters to Pt electrode data. In steady state the main features that the model should capture are the polarization curves and coverage fractions. In the transient simulations, the experimental features to capture are the broad anodic plateau and a cathodic reduction peaks in cyclic voltammograms (CVs), and the logarithmic growth of oxide mass over time.

From Section 4.2, it can be concluded that the model can successfully reproduce experimental steady state results because a very good fit to Partharathy et al. [4] at different operating conditions was obtained. The predicted coverage fractions for Pt electrode simulations are also fairly similar to the observed experimental coverages. The peroxide mechanism has no significant effect on the current generation until voltages below 0.4 V. However, it is essential for capturing the right surface coverage fractions of the adsorbed species and also for obtaining positive currents below 0.4 V. The parametric studies for studying the effect of peroxide formation free energy showed that this parameter has an negligible effect on the predicted polarization curves, however when looking at the individual current from the ORR and peroxide mechanisms, a value of 0.7 eV for this parameter gives results with a more accurate physical meaning, because over most of the voltage range, the ORR current is

83

predominant over the peroxide current and only at very low potentials (0.3 V), the peroxide current exceeds the ORR current. Nevertheless, this value does not predict surface coverage fractions that fit the experimental data.

Section 4.3 showed that the parameters obtained from fitting the model to steady state data, do not predict CVs that match experimental results. The model is capable of capturing cathodic reduction peak, and to some extend the anodic peak, but not the broad anodic plateau. However this peaks are not captured at the right potentials. Therefore, this model needs to be fitted separately to transient data, in order to be able to predict more accurate transient results. Temkin terms were added to observe their effect on the predicted CV. Results showed that these parameters only modify slightly the size of the peaks but not the potentials at which they occur.

Chapter 5

Conclusions and Future Work

The main focus of this work was to investigate one of the two electrochemical half-cell reactions that occurs in a PEM fuel cell. Specifically, the reaction kinetics of the oxygen reduction reaction on a platinum catalyst. An energy based kinetic model was developed using, as an starting point, the reaction mechanism proposed by Jayasankar and Karan [1] and the methodology for deriving kinetic expressions proposed by Wang et al. [44]. To the best of my knowledge, the model presented in this work is the first attempt to provide a single kinetic model framework that accounts for three common mechanisms observed to affect the cathodic kinetic performance of PEMFC: the oxygen reduction reaction, the oxide growth and the peroxide formation.

5.1 Conclusions

The literature study conducted on novel kinetic models for ORR revealed that fuel cell modelers rarely account for the complexity of the ORR when performing simulations. It is commonly assumed that the the ORR can be modeled using simple Tafel kinetics that cannot properly account for the change in Tafel slope or the surface coverage fractions. There is not a universal agreement on the reaction mechanisms that occur on the platinum surface during the cathodic reaction, therefore different researchers have assumed different reaction pathways. No attempts have been made to develop a consistent steady state and transient framework that accounts not only for the ORR and oxide growth, but also the peroxide formation.

Given that the most recent and complex model available in the literature was proposed by Jayasankar and Karan [1], the results of this model were successfully reproduced in Chapter 2. During this process, several inconsistencies were identified in this formulation. First, the framework was not unified, as it was claimed to be. There were two separate formulations,

with different sets of parameters for steady state and transient results. Second, the model had a mixed formulation, containing individual reaction equilibrium potentials, as well as free energies. Therefore, a clear methodology for deriving the kinetic expressions was not developed. As a result of the lack of consistency of the model, the free energy diagram at zero over-potential do not meet the equilibrium condition. A consistent unified energy based kinetic model for the reaction mechanisms was therefore developed in this thesis, and the peroxide mechanism was also added. The methodology and assumptions made were detailed in Chapter 3. The consistency of the model formulation was proved in all the energy diagrams obtained with this model with different sets of parameters.

The proposed energy-based kinetic model successfully predicts experimentally observed features of the polarization curve including the transition in the Tafel slope from 120 mV/dec high current densities to 60 mV/dec at 1.0 V for Pt electrode simulations. Unfortunately, species coverage predictions even though they reproduce general trends, are not well predicted by the model.

In terms of transient data, the model is capable of capturing the two most representative peaks from experimental CVs using the set of parameters obtained from fitting to polarization curves. However, they are in the wrong potential. Further, the anodic oxide plateu and the linear logarithmic oxide growth trends could not be reproduced. Future work is needed as the new model predictions are worse than those in ref [1].

5.2   Future Work

Some of the key issues pertaining to the energy based kinetic model for ORR, oxide growth and peroxide formation in platinum surface that can be addressed in the future are:

- The model parameters were estimated by fitting model predictions to steady-state ORR polarization curves data, but the model was not fitted to transient CV data for estimating the parameters. As a result, the model does not predict CVs and oxide growth correctly. Future modelling effort could address this issue and fit the transient predictions of the model to transient experimental data such as CVs and logarithmic oxide growth. In addition, more detailed parametric studies and sensitivity analysis could be performed to narrow more the bounds of the fitted parameters and potentially reduce the number of parameters in the model.

- Another future research area for improving the process of the parameter estimation

and model validation is to conduct DFT calculations or Monte Carlo simulations for obtaining kinetic parameters. Given that this model is energy based, the Gibbs free energies corresponding to the intermediate species formed could be obtained or predicted through these studies, and that would serve as further data for model validation.

- In the proposed kinetic framework, the reaction mechanism assumed is just one of the many possible reaction mechanisms that can occur in the Pt catalyst layer of a PEMFC. The ORR mechanism was assumed to proceed through the associative adsorption pathway and is comprised by 4 elementary steps, leading to the formation only of $PtO_{(ads)}$, $PtOH_{(ads)}$ and $PtO_2H_{(ads)}$ adsorbed species. Even though most people now agree on this ORR mechanism, other species could be formed such as PtO_2 during the reaction. The same with the oxide growth, three place exchange reaction are assumed and treated as sources of 3 new adsorbed species $OPtO_{(sub)}$, $OPtOH_{(sub)}$ and $OPt_{(sub)}$, however other intermediate species and steps could occur during these complex reaction and still be unknown and miscounted in the models.

- This model assumes that the oxides formed during the oxide growth mechanism are not moving, just formed and removed from the Pt surface through the cell operation. However, it is known that over time, the oxide film grows, that can lead to the migration of oxides and metal ions and that is the start of the platinum dissolution process. Therefore, the formulation of this model as it is can not predict any Pt dissolution, however can be treated as the basis for developing in the future a Pt dissolution model because it accounts for the most representative mechanisms that contribute to the fuel cell degradation.

References

[1] Jayasankara Barathram and Karan Kunal. O2 electrochemistry on pt: A unified multi-step model for oxygen reduction and oxide growth. *Electrochimica Acta*, 273(1):367–378, 2018.

[2] Barathram Jayasankar. *Multistep kinetic models for oxygen reduction reaction and platinum dissolution in polymer electrolyte membrane fuel cell.* PhD thesis, Queen's University, 2018.

[3] Ryan O'Hayre, Suk-Won Cha, Whitney Colella, and Fritz B. Prinz. *Fuel Cell Fundamentals.* John Wiley & Sons, 2016.

[4] Arvind Parthasarathy, Supramaniam Srinivasan, and A. John Appleby. Pressure dependence of the oxygen reduction reaction at the platinum microelectrode/nafion interface: Electrode kinetics and mass transport. *Journal of Electrochemical Society*, 139(9):2530–2537, 1992.

[5] Vijay A. Sethuraman, John W. Weidner, Andrew T. Haug, Sathya Motupally, and Lesia V. Protsailo. Hydrogen peroxide formation rates in a pemfc anode and cathode. *Journal of The Electrochemical Society*, 155(1):B50–B57, 2008.

[6] Secretariat. Nationally determined contributions under the paris agreement. Technical report, United Nations, 2021.

[7] Wolfgang Lubitz and Bill Tumas. Hydrogen: An overview. *Chem. Rev*, 107(10):3900–3903, 2007.

[8] IEA. Average price and driving range of bevs, 2010-2019. Technical report, IEA, 2020.

[9] G.J.Offer, D.Howey, M.Contestabile, R.Clague, and N.P.Brandon. Comparative analysis of battery electric, hydrogen fuel cell and hybrid vehicles in a future sustainable road transport system. *Energy Policy*, 38(1):24–29, 2010.

[10] C.E.Thomas. Fuel cell and battery electric vehicles compared. *International Journal of Hydrogen Energy*, 34(15):6005–6020, 2009.

[11] Roberto Álvarez Fernández, Fernando Beltrán Cilleruelo, and Iñaki Villar Martínez. A new approach to battery powered electric vehicles: A hydrogen fuel-cell-based range extender system. *International Journal of Hydrogen Energy*, 41(8):4808–4819, 2016.

[12] Simon T. Thompson, Brian D. James, Jennie M. Huya-Kouadio, Cassidy Houchins, Daniel A. DeSantis, Rajesh Ahluwalia, Adria R. Wilson, Gregory Kleen, and Dimitrios Papageorgopoulos. Direct hydrogen fuel cell electric vehicle cost analysis: System and high volume manufacturing description, validation, and outlook. *Journal of Power Sources*, 399:304–313, 2018.

[13] Laetitia Dubau, Luis Castanheira, Frédéric Maillard, Marian Chatenet, Olivier Lottin, Gaël Maranzana, Jérôme Dillet, Adrien Lamibrac, Jean-Christophe Perrin, Eddy Moukheiber, Assma ElKaddouri, Gilles De Moor, Corine Bas, Lionel Flandin, and Nicolas Caqué. A review of pem fuel celldurability: materials degradation,local heterogeneities of aging andpossible mitigation strategies. *WIREs Energy and Environment*, 3:540–560, 2014.

[14] Jinfeng Wu, Xiao Zi Yuan, Jonathan J. Martin, Haijiang Wang, Jiujun Zhang, Jun Shen, Shaohong Wu, and Walter Merida. A review of pem fuel cell durability: Degradation mechanisms and mitigation strategies. *Journal of Power Sources*, 184:104–119, 2008.

[15] James Larminie and Andrew Dicks. *Fuel Cell Systems Explained*. John Wiley & Sons, 2003.

[16] Inc EG&G Technical Services. Fuel cell handbook. Technical report, U.S. Department of Energy, National Energy Technology Laboratory, Morgantown, West Virginia, 2004.

[17] Sheng Sui, Xiaoying Wang, Xintong Zhou, Yuehong Su, Saffa Riffat, and Chang jun Liu. A comprehensive review of pt electrocatalysts for the oxygen reduction reaction: Nanostructure, activity, mechanism and carbon support in pem fuel cells. *J. Mater. Chem. A*, 5:1808–1825, 2017.

[18] R. M. Felix-Navarro, M. Beltran-Gastelum, E. A. Reynoso-Soto, F. Paraguay-Delgado, G. Alonso-Nunez, and J. R. Flores-Hernandez. Bimetallic pt-au nanoparticles supported on multi-wall carbon nanotubes as electrocatalysts for oxygen reduction. *Renewable Energy*, 87:31–41, 2016.

[19] M. Eikerling and A.A. Kornyshev. Modelling the performance of the cathode catalyst layer of polymer electrolyte fuel cells. *Journal of Electroanalytical Chemistry*, 453:89–106, 1998.

[20] Andrew A. Gewirth and Matthew S. Thorum. Electroreduction of dioxygen for fuel-cell applications: Materials and challenges. *Inorg. Chem.*, 49:3557–3566, 2010.

[21] Eiji Endoh, Shinji Terazono, Hardiyanto Widjaja, and Yasuyuki Takimoto. Degradation study of mea for pemfcs under low humidity conditions. *Electrochemical and Solid-State Letters*, 7(7):A209–A211, 2004.

[22] Minkmas V. Williams, H. Russell Kunz, and James M. Fenton. Analysis of polarization curves to evaluate polarization sources in hydrogen/air pem fuel cells. *J. Electrochem. Soc.*, 152(3):A635–A644, 2005.

[23] Lin Wang, Attila Husar, Tianhong Zhou, and Hongtan Liu. A parametric study of pem fuel cell performances. *International Journal of Hydrogen Energy*, 28(11):1263–1272, 2003.

[24] K. Broka and P. Ekdunge. Modelling the pem fuel cell cathode. *Journal of Applied Electrochemistry*, 27:281–289, 1997.

[25] Sudarshan L.Chavan and Dhananjay B.Talange. Modeling and performance evaluation of pem fuel cell by controlling its input parameters. *Energy*, 138(1):437–445, 2017.

[26] Lalit M. Pant, Zhiwei Yang, Michael L. Perry, and Adam Z. Weber. Development of a simple and rapid diagnostic method for polymer-electrolyte fuel cells. *Journal of The Electrochemical Society*, 165(6):F3007–F3014, 2018.

[27] MD Shenan Habib, Paroma Arefin, MD Abdus Salam, Kawsar Ahmed, MD Sahab Uddin, Tareq Hossain, Nasrin Papri, and Tauhidul Islam. Proton exchange membrane fuel cell (pemfc) durability factors,challenges, and future perspectives: A detailed review. *Material Science Research India*, 18(2):217–234, 2021.

[28] Xingwen Yu and Siyu Ye. Recent advances in activity and durability enhancement of pt/c catalytic cathode in pemfc part ii: Degradation mechanism and durability enhancement of carbon supported platinum catalyst. *Journal of Power Resources*, 172: 145–154, 2007.

[29] Robert M. Darling and Jeremy P. Meyers. Kinetic model of platinum dissolution in pemfcs. *Journal of The Electrochemical Society*, 150(11):A1523–A1527, 2003.

[30] Allen J. Bard and Larry R. Faulkner. *Electrochemical Methods: Fundamentals and Applications*. Wiley Global Education, 2000.

[31] N. P. Subramanian, T. A. Greszler, J. Zhang, W. Gu, and R. Makharia. Pt-oxide coverage-dependent oxygen reduction reaction (orr) kinetics. *Journal of The Electrochemical Society*, 159(5):B531–B540, 2012.

[32] I. E. L. Stephens, A. S. Bondarenko, U. Gronbjerg, J. Rossmeisl, and I. Chorkendorff. Understanding the electrocatalysis of oxygen reduction on platinum and its alloys. *Energy Environ.*, 5:6744–67620, 2012.

[33] Y. Liu, M. Mathias, and J. Zhang. Measurement of platinum oxide coverage in a proton exchange membrane fuel cell. *Electrochemical and Solid-State Letters*, 13(1):B1–B3, 2010.

[34] A. Panchenko, M. T. M. Koper, T. E. Shubina, S. J. Mitchell, and E. Roduner. Ab-initio calculations of intermediates of oxygen reduction on low-index platinum surfaces. *Journal of The Electrochemical Society*, 151(12):A2016–A2027, 2004.

[35] V. Tripković, E. Skúlason, S. Siahrostami, J. K. Nørskov, and J. Rossmeisl. The oxygen reduction reaction mechanism on pt(111) from density functional theory calculations. *Electrochimica Acta*, 55(27):7975 – 7981, 2010.

[36] Vijay A. Sethuraman, John W. Weidner, Andrew T. Haug, Marianne Pemberton, and Lesia V. Protsailo. Importance of catalyst stability vis-à-vis hydrogen peroxide formation rates in pem fuel cell electrodes. *Electrochimica Acta*, 54:5571–5582, 2009.

[37] A.Damjanovic and V.Brusic. Electrode kinetics of oxygen reduction on oxide-free platinum electrodes. *Electrochimica Acta*, 12:615–628, 1967.

[38] Nenad M. MarkoviC, Hubert A. Gasteiger, and Jr Philip N. Ross. Oxygen reduction on platinum low-index single-crystal surfaces in sulfuric acid solution: Rotating ring-pt(hkl) disk studies. *The Journal of Physical Chemistry*, 99(11):3411 – 3415, 1995.

[39] D.B.Sepa and M.V. Vojnovic. Reaction intermediates as a controlling factor in the kinetics and mechanism of oxygen reduction at platinum electrodes. *Electrochimica Acta*, 26(6):781–793, 1980.

[40] Halina S. Wroblowa, Yen-Chin-Pan, and Gerardo Razumney. Electroreduction of oxygen. a new mechanism criterion. *J. Electroanal. Chem.*, 69:195 – 201, 1976.

[41] E. Yeager. Electrocatalysis for o2 reduction. *Electrochmica Acta*, 29(1):1527 – 1537, 1984.

[42] Ryosuke Jinnouchi, Kensaku Kodama, Tatsuya Hatanaka, and Yu Morimoto. Intermediate coverage in oxygen reduction reaction by first principles-based mean field model. *Meet. Abstr*, 2:854, 2011.

[43] J. K. Norskov, J. Rossmeisl, A. Logadottir, and L. Lindqvist. Origin of the overpotential for oxygen reduction at a fuel-cell cathode. *J. Phys. Chem*, 108:17886–17892, 2004.

[44] Jia X. Wang, Junliang Zhang, and Radoslav R. Adzic. Double-trap kinetic equation for the oxygen reduction reaction on pt(111) in acidic media. *J. Phys. Chem. A*, 207(111): 12702–12710, 2007.

[45] Hubert A. Gasteiger, Shyam S. Kocha, Bhaskar Sompalli, and Frederick T. Wagner. Activity benchmarks and requirements for pt, pt-alloy, and non-pt oxygen reduction catalysts for pemfcs. *Applied Catalysis B: Environmental*, 56:9–35, 2005.

[46] Zhen-Ming Huang, Ay Su, Che-Jung Hsu, and Ying-Chieh Liu. A high-efficiency, compact design of open-cathode type pemfcs with a hydrogen generation system. *Fuel*, 122: 76–81, 2014.

[47] Gregory Jerkiewicz, Gholamreza Vatankhah, Jean Lessard, Manuel P. Soriaga, and Yeon-Su Park. Surface-oxide growth at platinum electrodes in aqueous h2so4 reexamination of its mechanism through combined cyclic-voltammetry, electrochemical quartz-crystal nanobalance, and auger electron spectroscopy measurements. *Electrochimica Acta*, 49(1):1451–1459, 2004.

[48] Mohammad Alsabet, Michal Grden, and Gregory Jerkiewicz. Comprehensive study of the growth of thin oxide layers on pt electrodes under well-defined temperature, potential, and time conditions. *Journal of Electroanalytical Chemistry*, 589(1):120–127, 2006.

[49] V.I.Birss, M.Chang, and J.Segal. Platinum oxide film formation—reduction: an in-situ mass measurement study. *Journal of Electroanalytical Chemistry*, 355(1-2):181–191, 1993.

[50] N. Cabrera and N. F. Mott. Theory of the oxidation of metals. *Progress in Physics*, 12: 163–184, 1949.

[51] K.J.Vetter and J.W.Schultze. The kinetics of the electrochemical formation and reduction of monomolecular oxide layers on platinum in 0.5 m h2so4: Part i. potentiostatic pulse measurements. *Journal of Electroanalytical Chemistry and Interfacial Electrochemistry*, 34(1):131–139, 1972.

[52] C. H. Paik, T. D. Jarvi, and W. E. O'Grady. Extent of pemfc cathode surface oxidation by oxygen and water measured by cv. *Electrochemical and Solid-State Letters*, 7(4): A82–A84, 2004.

[53] Chul Goo Chung, Lim Kim, Yong Wook Sung, Jinwoo Lee, and Jong Shik Chung. Degradation mechanism of electrocatalyst during long-term operation of pemfc. *Hydrogen Energy*, 34:8974–8981, 2009.

[54] N.M. Markovic, H.A. Gasteiger, B.N. Grgur, and P.N. Ross. Oxygen reduction reaction on pt(111): effects of bromide. *Journal of Electroanalytical Chemistry*, 467:57 – 163, 1999.

[55] Francisco A. Uribe, Thomas E. Springer, and Shimshon Gottesfeld. A microelectrode study of oxygen reduction at the platinum/recast-nafion film interface. *Journal of The Electrochemical Society*, 139(3):765–773, 1992.

[56] Matthew Markiewicz, Christopher Zalitis, and Anthony Kucernak. Performance measurements and modelling of the orr on fuel cell electrocatalysts – the modified double trap model. *Electrochimica Acta*, 179(1):126–136, 2015.

[57] M. Moore, A. Putz, and M. Secanell. Investigation of the orr using the double-trap intrinsic kinetic model. *Journal of The Electrochemical Society*, 160(6):F670–F681, 2013.

[58] Heather A. Baroody, Gregory Jerkiewicz, and Michael H. Eikerling. Modelling oxide formation and growth on platinum. *J. Chem. Phys.*, 146:144102, 2017.

[59] J. O'M. Bockris and L. F. Oldfield. The oxidation-reduction reactions of hydrogen peroxide at inert metal electrodes and mercury cathodes. *Transactions of the Faraday Society*, 51:249–259, 1955.

[60] Arvind Parthasarathy, Supramaniam Srinivasan, and A. John Appleby. Temperature dependence of the electrode kinetics of oxygen reduction at the platinum/nation interface– a microelectrode investigation. *Journal of Electrochemical Society*, 139(10):2856–2862, 1992.

[61] D. E. Ramaker, A. Korovina, V. Croze, J. Melke, and C. Roth. Following orr intermediates adsorbed on a pt cathode catalyst during break-in of a pem fuel cell by in operando x-ray absorption spectroscopy. *Phys. Chem. Chem. Phys.*, 16:13645–13653, 2014.

[62] Hernan Sanchez Casalongue, Sarp Kaya, Venkatasubramanian Viswanathan, Daniel J. Miller, Daniel Friebel, Heine A. Hansen, Jens K. Nørskov, Anders Nilsson, and Hirohito

Ogasawara. Direct observation of the oxygenated species during oxygen reduction on a platinum fuel cell cathode. *Nature Communications*, 4(2817), 2013.

[63] Mitsuru Wakisaka, Hirokazu Suzuki, Satoshi Mitsui, Hiroyuki Uchida, and Masahiro Watanabe. Identification and quantification of oxygen species adsorbed on pt(111) single-crystal and polycrystalline pt electrodes by photoelectron spectroscopy. *Langmuir*, 25:1897–1900, 2009.

[64] Jun Huang, Jianbo Zhang, and Michael Eikerling. Unifying theoretical framework for deciphering the oxygen reduction reaction on platinum. *Phys. Chem. Chem. Phys*, 20: 11776–11786, 2018.

[65] Colleen Jackson, Xiaoqian Lin, Pieter B. J. Levecque, and Anthony R. J. Kucernak. Toward understanding the utilization of oxygen reduction electrocatalysts under high mass transport conditions and high overpotentials. *ACS Catalysis*, 12:200–211, 2022.

[66] D. V. Savinova, E. B. Molodkina, A. I. Danilov, and Yu. M. Polukarov. Surface and subsurface oxygen on platinum in a perchloric acid solution. *Russian Journal of Electrochemistry*, 40(7):683–686, 2004.